A RESPONSE THEORY OF TOPOLOGICAL INSULATORS

BY WING FUNG LEUNG

A dissertation submitted to the

Graduate School—New Brunswick

Rutgers, The State University of New Jersey

in partial fulfillment of the requirements

for the degree of

Doctor of Philosophy

Graduate Program in Physics and Astronomy

Written under the direction of

Piers Coleman

and approved by

_____

_____

_____

_____

_____

New Brunswick, New Jersey

October, 2013

ABSTRACT OF THE DISSERTATION

A Response Theory of Topological Insulators

by Wing Fung Leung

Dissertation Director: Piers Coleman

A time-reversal invariant topological insulator is defined by its topological magnetoelectric response that is robust against disorder. The response formula, defined on a Brillouin torus, defines a $\mathbb{Z}_2$ invariant and classifies the topological phase. However, in the presence of disorder or the magnetic field, the notion of Brillouin torus is destroyed and the response formula is no longer well-defined. This has been a challenging open problem, and it is essental in defining a topological insulator. This thesis proposes a topological response theory that is free from this fundamental deficiency. We derived the magnetoelectric response formula in position space for a generic three dimensional model under disorder and finite magnetic field. For time-reversal invariant systems, we connected the result to the 2nd Chern number in Noncommutative Geometry. We developed the noncommutative theory of Chern numbers and showed that the quantization of the magnetoelectric response is robust against disorder. Numerical studies on serveral disodered topological models in 1D and 3D are presented.

Acknowledgements

First and foremost, I have had great fortune to have Emil Prodan as my thesis advisor and collaborator. I am very grateful for his encouragements and supports throughout the past two years. He has given me a lot of freedom in exploring my research interests. Interacting with him helped me think like a scientist. Without him, no part of this thesis will be possible. I would like to thank Piers Coleman and David Vanderbilt for keeping me on track in my PhD progress and more importantly in my understading of physics. I would also like to thank Mark Croft and Joel Shapiro for being my committee members.

My research could not be accomplished without my collobaborators, I am indebted to them. I am grateful for the collaborations with Jean Bellissard, Taylor Hughes, Ian Mondragon-Shem and Juntao Song. Interactions with them helped me grow as a physicist.

The past five years have been an interesting journey for me. I have met lots of amazing friends in physics and they have all helped sharp on my way of thinking one way or the other. I would like to thank Victor Alexandrov, Mohammad Ramezanali, Dima Krotov, Camille Aron, Lisa Carbone, Matthew Brahlek, Sinisa Coh, Christian and Emmanuel Contreras-Campana, Matthew Foster, Yanan Geng, Jose Juknevich, Simon Knapen, August Krueger, Jianpeng Liu, Mike Park, Sebastian Reyes-Lillo, Rob Schabinger, Alexey Soluyanov, Wenhu Xu, Jan Tomczak, Tahir Yusufaly, Yue Zhao and Yi Zhang. Special thanks goes to Sergey Artyukhin and Victor for allowing me to crash on their couch while this thesis is being written.

Graduate school has been a very confusing period of my life. I am very lucky

to share this period with my wonderful friends in New York. I would love to thank Ali Al-Qadhi, Eduardo Alves, Hannah Cao, Isabella Fraenkel Glaser, Tom Lagatta, Lian Lin, Min Ong, Matthew Wade, and Anna Djup for teaching me how to take the $\hbar$ goes to zero limit. They have opened a new window of my universe.

As someone once famously said that a physicist is a machine for turning coffee into equations and theories. Certainly, 88 Orchard, Think Coffee, Toby's Estate and El Beit have played an important part in providing me fuel and creative spaces to formulate the theory in this thesis.

The greatest thing that ever happened for my PhD education is attending the trimester program at the Institut Henri Poincare in 2012. Spending the entire summer by Jadin du Luxemburg has been a very fruitful and inspiring experience. I also have the luck to attend great schools and conferences in Jerusalem, Princeton and Boston, etc. They have provided stimulating enviornments for me to interact with other students.

To get to where I am at now, I could not do it if it were not for my teachers and friends at UC Berkeley. The time I spent at Berkeley is the best I have ever had. I was surrounded by the best and most creative minds. My professors and classmates have always believed in me and inspired me deeply. They have taught me the most valuable lesson in life: how to think. Berkeley has defined who I am.

Last, nothing I can say to show how much I appreciate the unconditional love from my parents and my brother. Even though my parents may never understand what an atom means and the implication of it, they have always been very supportive during my entire time in college and graduate school. Action speaks louder than words, the only thing I will do is to pass on their unconditional love to the future generations.

The most important lesson I have learned in the past five years is that beside the trophy at the end of a long journey, perusing something I truly believe in is

even more important. It is along this journey, I discovered and got to know more about myself. It is a tremendous gift in life to be given the opportunity to spend the past years just thinking about physics. Now, I am so excited to begin the rest of my life.

Dedication

To my family

Table of Contents

List of Tables

List of Figures

Chapter 1

Introduction

There is a theory which states that if ever anybody discovers exactly what the Universe is for and why it is here, it will instantly disappear and be replaced by something even more bizarre and inexplicable. There is another theory which states that this has already happened.

Douglas Adams

Time-reversal invariant topological insulators represent a new class of materials where the topology of the bulk electronic structure induces non-trivial characters [10, 27, 35, 42, 44, 45, 50, 60]. These materials have been theoretically predicted and then observed in laboratories. Many additional topological materials have been discovered since then [5, 37, 38, 81]. An up-to-date topological materials are summarized on Table 1.1. This thesis mainly studies the 3D time-reversal invariant strong topological insulators, and we will refer to them simply as topological insulators.

The defining character of topological insulators is their topological magneto-electric responses in the bulk [21, 79]. Metallic states exist on the surface of the insulators, as a manifestation of the non-trivial bulk topology [37, 38, 81]. The topological response is believed to be protected against disorder by time-reversal symmetry, provided the spectral gap remains open. The robustness is at the heart of many proposed technological applications, including quantum computation [37, 81]. Understanding the effect of disorder is also necessary since the topological materials are "dirty" in the laboratory. As shown in Table 1.1, most topological materials have a metallic bulk in the experiments, most probably due

Type	Material	Band gap	Bulk transport	Remark
2D	CdTe/HgTe/CdTe	< 10 meV	insulating	high mobility
2D	AlSb/InAs/GaSb/AlSb	∼4 meV	weakly insulating	gap is too small
3D	$Bi_{1-x}Sb_x$	< 30 meV	weakly insulating	complex S.S.
3D	Sb	semimetal	metallic	complex S.S.
3D	Bi_2Se_3	0.3 eV	metallic	simple S.S.
3D	Bi_2Te_3	0.17 eV	metallic	distorted S.S.
3D	Sb_2Te_3	0.3 eV	metallic	heavily p-type
3D	Bi_2Te_2Se	∼0.2 eV	reasonably insulating	ρ_{xx} up to 6 Ωcm
3D	$(Bi,Sb)_2Te_3$	< 0.2 eV	moderately insulating	mostly thin films
3D	$Bi_{2-x}Sb_xTe_{3-y}Se_y$	< 0.3 eV	reasonably insulating	Dirac-cone engineering
3D	$Bi_2Te_{1.6}S_{1.4}$	0.2 eV	metallic	n-type
3D	$Bi_{1.1}Sb_{0.9}Te_2S$	0.2 eV	moderately insulating	ρ_{xx} up to 0.1 Ωcm
3D	Sb_2Te_2Se	?	metallic	heavily p-type
3D	$Bi_2(Te,Se)_2(Se,S)$	0.3 eV	semi-metallic	natural Kawazulite
3D	$TlBiSe_2$	∼0.35 eV	metallic	simple S.S., large gap
3D	$TlBiTe_2$	∼0.2 eV	metallic	distorted S.S.
3D	$TlBi(S,Se)_2$	< 0.35 eV	metallic	topological P.T.
3D	$PbBi_2Te_4$	∼0.2 eV	metallic	S.S. nearly parabolic
3D	$PbSb_2Te_4$	?	metallic	p-type
3D	$GeBi_2Te_4$	0.18 eV	metallic	n-type
3D	$PbBi_4Te_7$	0.2 eV	metallic	heavily n-type
3D	$GeBi_{4-x}Sb_xTe_7$	0.1–0.2 eV	metallic	n (p) type at $x = 0$ (1)
3D	$(PbSe)_5(Bi_2Se_3)_6$	0.5 eV	metallic	natural heterostructure
3D	$(Bi_2)(Bi_2Se_{2.6}S_{0.4})$	semimetal	metallic	$(Bi_2)_n(Bi_2Se_3)_m$ series
3D	$(Bi_2)(Bi_2Te_3)_2$	?	?	no data published yet
3D TCI	SnTe	0.3 eV (4.2 K)	metallic	Mirror TCI, $n_{\mathcal{M}} = -2$
3D TCI	$Pb_{1-x}Sn_xTe$	< 0.3 eV	metallic	Mirror TCI, $n_{\mathcal{M}} = -2$
3D TCI	$Pb_{0.77}Sn_{0.23}Se$	invert with T	metallic	Mirror TCI, $n_{\mathcal{M}} = -2$
2D?	Bi bilayer	∼0.1 eV	?	not stable by itself
3D?	Ag_2Te	?	metallic	famous for linear MR
3D?	SmB_6	20 meV	insulating	possible Kondo TI
3D?	$Bi_{14}Rh_3I_9$	0.27 eV	metallic	possible weak 3D TI
3D?	RBiPt (R = Lu, Dy, Gd)	zero gap	metallic	evidence negative
Weyl SM?	$Nd_2(Ir_{1-x}Rh_x)_2O_7$	zero gap	metallic	too preliminary

Table 1.1: Summary of 2D and 3D topological insulator materials that have be experimentally addressed (reviewed in Ref. [5]). (S.S., P.T., and SM stand for surface state, phase transition, and semimetal, respectively.)

to disorder. A great deal of effort has been dedicated to understanding the behavior of the topological materials in the presence of disorder [20, 32–34, 43, 55, 64–66, 73, 75, 77, 94, 110].

For a clean crystalline insulator, the topological properties is protected by its spectral gap. It cannot go through a topological phase transition without closing its spectral gap. It is well known that disorder can lead to electron localization. When disorder is strong enough, the spectral gap is closed and filled with a dense localized spectrum. The spectral gap is then replaced by a mobility gap. The

conventional theory of robustness, which depends on a spectral gap, breaks down. One important open question for topological insulators is if the robustness extends to this regime.

The theory of topological magnetoelectric response was first developed for prefectly perodic crystals [22, 79]. The topological response formula, defined on a Brillouin torus, is robust against continuous deformations of the parameters of the crystalline insulators. However, as soon as disorder or the magnetic field is turned on, the perodicity is lost and the response formula "disappears." Since the defining character of a topological insulator is its robustness against disorder, it is important to search for an alternative theory. The main result of this thesis is a theory of topological magnetoelectric response using Noncommutative Geometry. We obtain a magnetoelectric formula in the presence of disorder and magnetic field. We show that the change in the magnetoelectric response can be connected to the noncommutative 2nd Chern number. The latter is shown to be quantized and invariant as long as the Fermi level lies in a mobility gap.

On the numerical side, an accurate and efficient method for computing topological invariants for disordered systems will be very valuable. Disorder can induce topological phases in 2D and 3D [32, 34, 55] and strongly deform the topological phase digram [43, 75, 110]. We investigate this issue numerically using a 3D $\mathbb{Z}_2$ topological index [74] with twisted boundary conditions. Beside being a well-defined disordered topological invariant, the noncommutative Chern formulae have been proven to be numerically effective. Their computations were successfully done for topological models that have significantly larger lattice sizes, compared to the twisting boundary method [73, 75, 77, 108].

The main Chapters of this thesis develop the noncommutative response theory of topological insulators and Chern numbers. Chapter 1 reviews the conventional theory of topological responses. To include disorder and magnetic field, aperiodic

crystals and covariant observables are defined in Chapter 2. We review an important formalism developed by Bellissard to extend Brillouin torus to aperiodic crystals. This is known as the noncommutative Brillouin torus [7].

Chapter 3 develops the noncommutative theory of magnetoelectric response [54]. To understand the strong disorder effect, we develop the noncommutative theory of Chern numbers in chapter 4 [78]. The physical meaning of the Chern numbers is also discussed.

Chapter 5 studies the physical implications of the noncommutative polarization formula [91], numerical studies are presented [98]. Chapter 6 covers the numerical studies of strong disorder effect in a topological insulator model. A projector formulation of $\mathbb{Z}_2$ invariant [74] is computed for disordered model with twisted boundary conditions, and the topological phase diagram is constructed [53]. Together with the level statistics analysis, the results suggest the robustness of the topological index remains in the strong disorder regime.

1.1 Topological responses

What is a topological insulator? A topological insulator is characterized by its topological magnetoelectric response that is robust against disorder. The topological response defines a $\mathbb{Z}_2$ classification, distinguishing a topological insulator from a trivial insulator.

The canonical picture of topological theory begins with a lattice model with translational symmetry: a periodic crystal. In the absence of a magnetic field and disorder, a periodic lattice Hamiltonian takes the form:

$$H_0 = \sum_{\boldsymbol{x},\alpha} \sum_{\boldsymbol{y},\beta} t^{\alpha\beta}_{\boldsymbol{x}-\boldsymbol{y}} |\boldsymbol{x},\alpha\rangle\langle\boldsymbol{y},\beta|. \tag{1.1}$$

where $\boldsymbol{x} \in \mathbb{Z}^D$ is a site of the lattice and $\alpha = 1, \ldots, Q$ labels the atomic or molecular orbitals associated with that site. We will assume that $t_{\boldsymbol{x}-\boldsymbol{y}} \neq 0$ only if

$|\boldsymbol{x} - \boldsymbol{y}| < R$ (finite hopping range), with R arbitrarily large but finite and fixed. It is convenient to fix the Fermi level at zero by introducing an additive constant to the Hamiltonian. We will label Fermi level with E_F throughout the thesis. A material-specific lattice model can be generated from *ab-initio* computations using Wannier function representations or simply by fitting the measured band structure [57].

Because of the translation symmetry, Bloch theory allows us to compute the band structure of the crystals in $\boldsymbol{k}$-space. Using Bloch transformation, we can define the model over a Brillouin torus $\mathcal{T}^D = \mathcal{S}_1 \times \ldots \times \mathcal{S}_1$, where the Hamiltonian is represented by a family of $Q \times Q$ Bloch Hamiltonian $H_{\boldsymbol{k}}$. If H_0 has a spectral gap at the Fermi level, and consequently we can define an analytical $\boldsymbol{k}$-dependent projector $\tilde{P}_{\boldsymbol{k}} = \chi_{(-\infty, E_F]}(H_{\boldsymbol{k}})$ on the Brillouin torus $\mathcal{T}^D$. The analytic family of projectors $\{\tilde{P}_{\boldsymbol{k}}\}_{\boldsymbol{k} \in \mathcal{T}^D}$ defines the Berry curvature for the occupied Bloch states:

$$\mathcal{F} = \tilde{P}_{\boldsymbol{k}} \, d\tilde{P}_{\boldsymbol{k}} \wedge d\tilde{P}_{\boldsymbol{k}}. \tag{1.2}$$

The classical nth Chern number over a Brillouin $2n$-torus is then defined by the formula [6]:

$$Ch_n := \frac{(-1)^n}{(2\pi i)^n n!} \int_{\mathcal{T}^{2n}} \mathrm{tr}\{\mathcal{F}^n\}. \tag{1.3}$$

where $\mathrm{tr}\{\}$ represents a trace over the orbital index α and $i = \sqrt{-1}$. It is a standard result in differential topology that, as long as $\tilde{P}_{\boldsymbol{k}}$ remains globally smooth in $\boldsymbol{k}$, the Chern numbers take integer values and remain constant under smooth deformations of the $\{\tilde{P}_{\boldsymbol{k}}\}_{\boldsymbol{k} \in \mathcal{T}^{2n}}$ family [61]. In the present context, the smoothness of $\tilde{P}_{\boldsymbol{k}}$ is protected by the spectral gap of H_0.

Bloch theory has been a canonical tool for understanding the physical propertites of crystalline solids. In particular, Chern numbers sets the fundation for

our understanding of physical responses and the classification for topological matters. In two dimensions, the 1st Chern number reveals the topological origin of the integer quantized Hall effect. TKNN showed that the Hall conductivity can be expressed as the 1st Chern number [103]:

$$\sigma_{xy} = -\frac{e^2}{h}\frac{1}{2\pi i}\int_{\mathcal{T}^2} \text{tr}\{\mathcal{F}\}. \tag{1.4}$$

As a topology consequence, the right hand side is always an integer multiple of e^2/h, given that a finite spectral gap exists. This quantization allows us to distinguish the topologically distinct phases of this system. The robustness of the Chern number ensures that the value of Hall response remains unchanged upon continuous deformations of the parameters of the crystal, unless the system goes through a transition by closing the insulating gap.

The topological magnetoelectric response in a topological insulator describes the induced quantized polarization (magnetization) by an external magnetic (electric) field. As we shall see, the magnetoelectric response connects to the 2nd Chern number. For an adiabatic path $\gamma(t)$ connecting a trivial phase ($t = 0$) and a topologically non-trivial phase ($t = \pi$), the topological magnetoelectric response can be computed using [21, 79]:

$$\alpha = \frac{e^2}{h}\frac{1}{16\pi^2}\int_{\mathcal{T}^3\times\gamma} \text{tr}\{\mathcal{F}_t^2\}. \tag{1.5}$$

where $\mathcal{F}_t := \tilde{P}_{\boldsymbol{k}}(t)d\tilde{P}_{\boldsymbol{k}}(t) \wedge d\tilde{P}_{\boldsymbol{k}}(t)$ and the spectral gap is maintained along the adiabatic path. For a time-reversal system, the expression is equal to half of the second Chern number. Just like in the integer quantum Hall effect, a change in the Chern number for the system cannot happen without closing the spectral gap and crossing a metallic region. As a result, the magnetoelectric coupling Eq. 1.5 is quantized as a half-integer multiples of e^2/h for topological insulators, and the quantization is topologically protected for bulk insulating systems.

The main challenge of the topological response theory is that Bloch theory fails in the presence of some physical effects. For example, both magnetic field and disorder break translational symmetry, and no Brillouin torus can be constructed. The conventional formulae presented in this section are no longer well-defined. Since both effects are fundamental in our understanding of quantized Hall and magnetoelectric responses, the response theory of periodic crystals cannot be the end of the story. This points us to the main theme of this thesis: a topological reponse theory of aperiodic crystals.

Chapter 2

Noncommutative Brillouin Torus

We introduce the aperiodic lattice models which are used throughout the thesis. We define the covariant Hamiltonians and noncommutative Brillouin torus. The formalism was first introduced by Bellissard to generalize Bloch theory to aperiodic crystals in the 80s. The classical theory of Chern numbers can also be extended to this framework. It provides a natural language to describe topological responses and to classify the topological phases in the presense of disorder and an arbitrary magnetic field.

2.1 Aperiodic crystals

In this section, we consider aperiodic lattice models that include disorder and an uniform magnetic field. Traditionally, an on-site random disorder potential is added to study disorder effect, but we also include the disorder that couples between two sites and different orbitals. This could represent a disordered displacement of the atomic positions in a crystal, which introduces a random component in the hopping amplitudes. A D-dimentional disordered lattice Hamiltonian is of the form:

$$H_{\boldsymbol{\omega}} = \sum_{\boldsymbol{x},\alpha} \sum_{\boldsymbol{y},\beta} t_{\boldsymbol{x},\boldsymbol{y}}^{\alpha\beta}(\boldsymbol{\omega}) |\boldsymbol{x},\alpha\rangle\langle\boldsymbol{y},\beta|. \tag{2.1}$$

with

$$t_{\boldsymbol{x},\boldsymbol{y}}^{\alpha\beta}(\boldsymbol{\omega}) = t_{\boldsymbol{x}-\boldsymbol{y}}^{\alpha\beta} + \lambda\omega_{\boldsymbol{x},\boldsymbol{y}}^{\alpha\beta}, \tag{2.2}$$

where $\omega_{\boldsymbol{x},\boldsymbol{y}}^{\alpha\beta}$ are independent random variables, uniformly distributed in the interval $[-\frac{1}{2}, \frac{1}{2}]$. The collection of all random variables $\boldsymbol{\omega} = \{\omega_{\boldsymbol{x},\boldsymbol{y}}^{\alpha\beta}\}$ can be viewed as a point in an infinite dimensional disorder configuration space:

$$\Omega = \bigotimes_{\boldsymbol{x},\alpha;\boldsymbol{y},\beta} [-\frac{1}{2}, \frac{1}{2}], \tag{2.3}$$

which is metrizable and can be viewed as a probability space. It is equipped with the probability measure:

$$dP(\boldsymbol{\omega}) = \prod_{\boldsymbol{x},\boldsymbol{y}} \prod_{\alpha\beta} d\omega_{\boldsymbol{x},\boldsymbol{y}}^{\alpha\beta}. \tag{2.4}$$

Furthermore, there is a natural action of the discrete $\mathbb{Z}^D$ additive group on Ω:

$$(\mathsf{t}_{\boldsymbol{a}}\omega)_{\boldsymbol{x},\boldsymbol{y}}^{\alpha\beta} = \omega_{\boldsymbol{x}-\boldsymbol{a},\boldsymbol{y}-\boldsymbol{a}}^{\alpha\beta}, \ a \in \mathbb{Z}^D, \tag{2.5}$$

acts ergodically and leaves $dP(\boldsymbol{\omega})$ invariant. The ergodicity assumption implies the Birkhoff's ergodic theorem. For an ergodic translation t_n, it states that:

$$\lim_{N\to\infty} \frac{1}{N} \sum_{n=0}^{N-1} f(t_n^{-1}\boldsymbol{\omega}) = \int_\Omega dP(\boldsymbol{\omega}) \ f(\boldsymbol{\omega}) \tag{2.6}$$

where f is a function depending on the configuration $\boldsymbol{\omega}$. It means that averaging over the infinite successive lattice translations is equivalent to the ensemble average over the entire configuration space. For a covariant observable F_ω, we can translate it to the following:

$$\lim_{\mathcal{V} \to \infty} \frac{1}{|\mathcal{V}|} \sum_{x \in \mathcal{V}} \langle 0|F_{t_x^{-1}\boldsymbol{\omega}}|0\rangle = \int_{\Omega} dP(\boldsymbol{\omega}) \, \langle 0|F_{\boldsymbol{\omega}}|0\rangle \qquad (2.7)$$

where $\mathcal{V}$ is a box and $|\mathcal{V}|$ is its volume. The physical meaning of this quantity will be clear after we introduced the noncommutative trace in the next section.

Now, we will include the effect of the magnetic field. For a 2D lattice model under an uniform magnetic field, the effect can be included using Peierls substitution [68]:

$$t_{\boldsymbol{x},\boldsymbol{y}}^{\alpha\beta}(\boldsymbol{\omega}) \to e^{-i\int_{\boldsymbol{R}_y}^{\boldsymbol{R}_x} d\boldsymbol{l}\cdot\boldsymbol{A}} t_{\boldsymbol{x},\boldsymbol{y}}^{\alpha\beta}(\boldsymbol{\omega}) = e^{\frac{i}{2}\boldsymbol{B}\cdot(\boldsymbol{x}\wedge\boldsymbol{y})} t_{\boldsymbol{x},\boldsymbol{y}}^{\alpha\beta}(\boldsymbol{\omega}), \qquad (2.8)$$

where $\hbar = e = 1$ is set and the area of unit cell is set to 1. We can generalize this to higher dimensions. For example in three dimensions, the Peierls phase is $e^{\frac{i}{2}B_1(x_2y_3-x_3y_2)}e^{\frac{i}{2}B_2(x_3y_1-x_1y_3)}e^{\frac{i}{2}B_3(x_1y_2-x_2y_1)}$. The magnetic field can be parametrized as a 3×3 antisymmetric tensor B_{ij}:

$$B_{ij} = \begin{pmatrix} 0 & B_3 & -B_2 \\ -B_3 & 0 & B_1 \\ B_2 & -B_1 & 0 \end{pmatrix}. \qquad (2.9)$$

and the phase factor can be written as $e^{\frac{i}{2}x_i B_{ij} y_j}$. In general, under a fixed magnetic field and disorder, our D-dimensional aperiodic model takes the form:

$$H_{\boldsymbol{\omega}} = \sum_{\boldsymbol{x},\alpha} \sum_{\boldsymbol{y},\beta} e^{\frac{i}{2}x_i B_{ij} y_j} t_{\boldsymbol{x},\boldsymbol{y}}^{\alpha\beta}(\boldsymbol{\omega})|\boldsymbol{x},\alpha\rangle\langle\boldsymbol{y},\beta|. \qquad (2.10)$$

The magnetic translations by lattice $\boldsymbol{a}$ are given by $U_{\boldsymbol{a}}$:

$$U_{\boldsymbol{a}}|\boldsymbol{x},\alpha\rangle = e^{-\frac{i}{2}a_i B_{ij} x_j} T_{\boldsymbol{a}}|\boldsymbol{x},\alpha\rangle = e^{-\frac{i}{2}a_i B_{ij} x_j}|\boldsymbol{x}+\boldsymbol{a},\alpha\rangle, \qquad (2.11)$$

where T_a is lattice translation by a. It is straightforwards to show that Eq. 2.10 satisfies the following relation:

$$
\begin{aligned}
U_{\boldsymbol{a}} H_{\boldsymbol{\omega}} U_{\boldsymbol{a}}^{-1} &= \sum_{\boldsymbol{x},\alpha} \sum_{\boldsymbol{y},\beta} e^{\frac{i}{2}(x_i+a_i)B_{ij}(y_j+a_j)} t_{\boldsymbol{x},\boldsymbol{y}}^{\alpha\beta}(\boldsymbol{\omega})|\boldsymbol{x}+\boldsymbol{a},\alpha\rangle\langle\boldsymbol{y}+\boldsymbol{a},\beta| \\
&= \sum_{\boldsymbol{x},\alpha} \sum_{\boldsymbol{y},\beta} e^{\frac{i}{2}x_i B_{ij} y_j} t_{\boldsymbol{x}-\boldsymbol{a},\boldsymbol{y}-\boldsymbol{a}}^{\alpha\beta}(\boldsymbol{\omega})|\boldsymbol{x},\alpha\rangle\langle\boldsymbol{y},\beta| \\
&= \sum_{\boldsymbol{x},\alpha} \sum_{\boldsymbol{y},\beta} e^{\frac{i}{2}x_i B_{ij} y_j} t_{\boldsymbol{x},\boldsymbol{y}}^{\alpha\beta}(\boldsymbol{t_a}\boldsymbol{\omega})|\boldsymbol{x},\alpha\rangle\langle\boldsymbol{y},\beta| \\
&= H_{\boldsymbol{t_a}\boldsymbol{\omega}},
\end{aligned}
$$

where a change of coordinates and Eq. 2.5 are used. The equality $U_{\boldsymbol{a}} H_{\boldsymbol{\omega}} U_{\boldsymbol{a}}^{-1} = H_{\boldsymbol{t_a}\boldsymbol{\omega}}$ is called the covariant relation, and the Hamiltonian Eq. 2.10 forms a family of covariant operators $\{H_{\boldsymbol{\omega}}\}_{\boldsymbol{\omega}\in\Omega}$. The triplet $(\Omega, \boldsymbol{t}, \{H_{\boldsymbol{\omega}}\}_{\boldsymbol{\omega}\in\Omega})$ defines a homogenous system [7]. Taking the magnetic field and disorder to zero, the relation reduces to $T_{\boldsymbol{a}} H T_{\boldsymbol{a}}^{-1} = H$ which defines the translational invariant Hamiltonian for a periodic crystal.

For perfectly periodic systems we are primarily concerned with the translationally invariant Hamiltonians. The main difficulty in studying aperidoic crystals is the lack of transational symmetry, Bloch theory is then not applicable. However, the aperiodic crystals are still homogenous in space, macrosopically, and the physical properties are translationally invariant. The idea is that for such homogenous systems we consider all translates of the Hamiltonian, the covariant family of Hamiltonians.

2.2 Algebra of covariant observables

The basic idea of noncommutative geometry comes from the duality between algebra and geometry [15]. Our classical thinking of spaces relies on the notion of geometric manifolds. However, there is another half of the story: the algebraic

way. In its simplest form: the information about a classical space can be encoded in the commutative algebra of functions on that space. We can look at a classical space from two different but equivalent points of view: algebra or geometry. Noncommutative geometry relaxes the commutative restriction and extends the duality to noncommutative algebra, i.e. the C*-algebra of functions on the noncommutative space.

The conventional theory of topological insulators begins by going into momentum space, defining topological invariants on the Brillouin torus. As emphazied before, this preassumes the existence of the Brillouin manifold, hence translational symmetry in the system. We will follow the noncommutative approach and study the algebra of covariant observables. Such algebra, together with calculus tools, defines the noncommutative Brillouin torus [7]. It provides a natural theoretical framework for the study of aperiodic crystals. The response and thermodynamic functions for a homogeneous model can be computed within the algebra generated by the covariant families of operators.

For a covariant family of operators $\{F_{\boldsymbol{\omega}}\}_{\boldsymbol{\omega} \in \Omega}$, all the information is encoded in the matrix elements:

$$f_{\alpha,\beta}(\boldsymbol{\omega}, \boldsymbol{x}) = \langle \mathbf{0}, \alpha | F_{\boldsymbol{\omega}} | \boldsymbol{x}, \beta \rangle, \qquad (2.12)$$

All the other matrix elements can be obtained from $f_{\alpha,\beta}(\boldsymbol{\omega}, \boldsymbol{x})$ using magnetic translations. As such, the entire family of covariant operators can be described using a single function:

$$f : \Omega \times \mathbb{Z}^D \to \mathcal{M}_{Q \times Q}, \qquad (2.13)$$

where $\mathcal{M}_{Q \times Q}$ is the space of $Q \times Q$ complex matrices. This definition leads to the following addition and multiplication algebraic operations:

$$(f+g)(\boldsymbol{\omega}, \boldsymbol{x}) = \langle 0, \alpha | F_{\boldsymbol{\omega}} + G_{\boldsymbol{\omega}} | x, \beta \rangle \tag{2.14}$$

$$= f(\boldsymbol{\omega}, \boldsymbol{x}) + g(\boldsymbol{\omega}, \boldsymbol{x}),$$

$$(f*g)(\boldsymbol{\omega}, \boldsymbol{x}) = \langle 0, \alpha | F_{\boldsymbol{\omega}} G_{\boldsymbol{\omega}} | x, \beta \rangle \tag{2.15}$$

$$= \sum_{\boldsymbol{y} \in \mathbb{Z}^D} e^{\frac{i}{2} x_i B_{ij} y_j} f(\boldsymbol{\omega}, \boldsymbol{y}) g(\mathsf{t}_{\boldsymbol{y}}^{-1} \boldsymbol{\omega}, \boldsymbol{x} - \boldsymbol{y}).$$

Each element from the algebra $\mathcal{A}_0$ defines a family of covariant bounded operators on $\ell^2(\mathbb{Z}^D, \mathbb{C}^Q)$, through the representation:

$$(\pi_{\boldsymbol{\omega}} f) | \boldsymbol{x}, \alpha \rangle = \sum_{\boldsymbol{y} \in \mathbb{Z}^D} \sum_{\beta=1}^{Q} e^{\frac{i}{2} x_i B_{ij} y_j} f_{\beta\alpha}(\mathsf{t}_{\boldsymbol{y}}^{-1} \boldsymbol{\omega}, \boldsymbol{x} - \boldsymbol{y}) | \boldsymbol{y}, \beta \rangle. \tag{2.16}$$

A direct calculation using the definition shows that the representation $\pi_{\boldsymbol{\omega}} F$ is just the covariant operator $F_{\boldsymbol{\omega}}$. For example, it is easy to show that the element

$$h^{\alpha\beta}(\boldsymbol{\omega}, \boldsymbol{x}) = t_{0, \boldsymbol{x}}^{\alpha\beta}(\omega) = t_{0-x}^{\alpha\beta} + \lambda \omega_{0, x}^{\alpha\beta} \tag{2.17}$$

generates the covariant Hamiltonian Eq. 2.10. If we furthur introduce the following norm on $\mathcal{A}_0$:

$$\|f\| = \sup_{\boldsymbol{\omega} \in \Omega} \|\pi_{\boldsymbol{\omega}} f\|, \tag{2.18}$$

and the $*$-operation:

$$f^*(\boldsymbol{\omega}, \boldsymbol{x}) = f(\mathsf{t}_{\boldsymbol{x}}^{-1} \boldsymbol{\omega}, -\boldsymbol{x})^{\dagger}, \tag{2.19}$$

then the completion of $\mathcal{A}_0$ under the norm of Eq. 2.18 becomes a C^*-algebra, which will be denoted by $\mathcal{A}$. The advantage of the algebraic approach is that it remains a valid description even when the translational symmetry is absence. With defined noncommutative calculus, the algebra generalized the Brillouin torus, and is called the noncommutative Brillouin torus [7].

2.3 Noncommutative calculus

The classical differential manifolds are completely determined by the algebra of smooth functions defined over the manifold and by the differential calculus with these functions. In the noncommutative setting, we replace the commutative algebra of smooth functions over the classic Brillouin torus with the noncommutative algebra $\mathcal{A}$, and then build a noncommutative differential calculus over $\mathcal{A}$. The k-derivations are given by linear automorphisms of algebra $\mathcal{A}$:

$$(\partial_j f)(\boldsymbol{\omega}, \boldsymbol{x}) = i x_j f(\boldsymbol{\omega}, \boldsymbol{x}), \tag{2.20}$$

where $j = 1, \ldots, D$, and the classical integration on a Brillouin torus is replaced by a trace over $\mathcal{A}$:

$$\mathcal{T}(f) = \int_\Omega dP(\boldsymbol{\omega}) \ \mathrm{tr}\{f(\boldsymbol{\omega}, \mathbf{0})\}, \tag{2.21}$$

where tr is trace over $\mathcal{M}_{D \times D}$ space, and 0 is the origin of the lattice. Together with the algebra, the triplet $(\mathcal{A}, \mathcal{T}, \partial)$ defines the noncommutative Brillouin torus.

The derivations are not defined over the entire algebra $\mathcal{A}$ but only over the subalgebra of "differentiable" functions:

$$\mathcal{C}^1(\mathcal{A}) = \{f \in \mathcal{A}, \ \|\partial_j f\| < \infty, \ j = 1, \ldots, D\}. \tag{2.22}$$

More general, the subalgebra of Nth differentiable functions is defined as:

$$\mathcal{C}^N(\mathcal{A}) = \{f \in \mathcal{A}, \ \|\partial_1^{\alpha_1} \partial_2^{\alpha_2} \partial_3^{\alpha_3} f\| < \infty, \ \alpha_1 + \alpha_2 + \alpha_3 = N\}. \tag{2.23}$$

We will only work with $\mathcal{C}^\infty(\mathcal{A})$ elements, so from now all elements will be assumed to be part of this subalgebra. The operator representations of the derivations can

be derived by using the Eq. 2.16 and 2.20:

$$\pi_{\boldsymbol{\omega}}(\partial_j f) = -i[X_j, \pi_\omega f] = -i[X_j, F_{\boldsymbol{\omega}}], \tag{2.24}$$

where $\boldsymbol{X} = (X_1, \ldots, X_D)$ is the position operator. For homogenous systems, the physical meaning of $\mathcal{T}$ can be understood in the operator representation:

$$
\begin{aligned}
\mathcal{T}(f) &= \int_\Omega dP(\boldsymbol{\omega}) \ \mathrm{tr}\langle 0|F_{\boldsymbol{\omega}}|0\rangle \\
&= \lim_{\mathcal{V}\to\infty} \frac{1}{\mathcal{V}} \mathrm{tr} \sum_{\boldsymbol{x}\in\mathcal{V}} \langle 0|F_{t_{-x}\boldsymbol{\omega}}|0\rangle \\
&= \lim_{\mathcal{V}\to\infty} \frac{1}{\mathcal{V}} \mathrm{tr} \sum_{\boldsymbol{x}\in\mathcal{V}} \langle x|F_\omega|x\rangle,
\end{aligned}
\tag{2.25}
$$

where the ergodic theorem and covariant relation are used in the second and third line respectively. It means that moving through the infinite sample is equivalent to moving through the entire disorder configuration space. In general, we can show that:

$$\mathcal{T}(f * g \ldots) = \int_\Omega dP(\boldsymbol{\omega}) \ \mathrm{tr}\langle 0|F_{\boldsymbol{\omega}} G_{\boldsymbol{\omega}} \ldots |0\rangle, \tag{2.26}$$

and

$$\mathcal{T}(f * g \ldots) = \lim_{\mathcal{V}\to\infty} \frac{1}{\mathcal{V}} \mathrm{Tr}_\mathcal{V}\{F_{\boldsymbol{\omega}} G_{\boldsymbol{\omega}} \ldots\} := \tau(F_{\boldsymbol{\omega}} G_{\boldsymbol{\omega}} \ldots), \tag{2.27}$$

where the trace $\mathrm{Tr}_\mathcal{V}$ means the trace over the quantum states inside the box $\mathcal{V}$. Therefore, given a specific disorder realization, the trace of covariant operators per unit volume is equivalent to its disorder average at the origin:

$$\tau(F_\omega G_\omega \ldots) = \int_\Omega dP(\boldsymbol{\omega}) \ \mathrm{tr}\{f * g \ldots (\boldsymbol{\omega}, \boldsymbol{0})\} \tag{2.28}$$

which means the observables are self-averaging.

In the translational invariant limit, they both have natural correspondence to the classical $\boldsymbol{k}$-space calculus. For periodic crystals, a translational invariant operator F corresponds to a $\boldsymbol{k}$-derivative on a Brillouin torus:

$$[X_j, F] \longrightarrow i \frac{\partial}{\partial k^j} \tilde{F}_{\boldsymbol{k}}, \tag{2.29}$$

and only a single unit cell is needed for consideration due to translational symmetry. Due to translational symmetry, the trace per volume is equivalent to "trace per Brillouin torus":

$$
\begin{aligned}
\tau(FG\ldots) &= \lim_{\mathcal{V} \to \infty} \frac{1}{\mathcal{V}} \mathrm{Tr}_\mathcal{V}\{F_{\boldsymbol{\omega}} G_{\boldsymbol{\omega}} \ldots\} \\
&= \frac{1}{(2\pi)^D} \int_{\mathcal{T}^D} d^D\boldsymbol{k} \ \mathrm{tr}\{\tilde{F}_{\boldsymbol{k}} \tilde{G}_{\boldsymbol{k}} \ldots\}.
\end{aligned} \tag{2.30}
$$

And we conclude the correspondence for the traces:

$$\mathcal{T}(f * g \ldots) \longrightarrow \frac{1}{(2\pi)^D} \int_{\mathcal{T}^D} d^D\boldsymbol{k} \ \mathrm{tr}(\tilde{F}_{\boldsymbol{k}} \tilde{G}_{\boldsymbol{k}} \ldots). \tag{2.31}$$

Next, we collect below a list of well-known calculus rules ($j, k = 1, 2, 3$):

1. The derivations commute:

$$\partial_j \partial_k f = \partial_k \partial_j f. \tag{2.32}$$

2. The derivations are *-derivations:

$$\partial_j(f^*) = (\partial_j f)^*. \tag{2.33}$$

3. The derivations satisfy the Leibniz rule:

$$\partial_j(f * g) = (\partial_j f) * g + f * (\partial_j g). \tag{2.34}$$

4. For f invertible in $\mathcal{A}$, then:

$$\partial_j f^{-1} = -f^{-1} * (\partial_j f) * f^{-1}. \tag{2.35}$$

5. The trace satisfies positivity:

$$\mathcal{T}(f * f^*) \geq 0. \tag{2.36}$$

6. The trace are cyclic:

$$\mathcal{T}(f * g) = \mathcal{T}(g * f). \tag{2.37}$$

7. The boundary vanishes:

$$\mathcal{T}(\partial_j f) = \int_\Omega dP(\boldsymbol{\omega}) \sum_\alpha \langle 0, \alpha | i[X_j, F_{\boldsymbol{\omega}}] | 0, \alpha \rangle = 0. \tag{2.38}$$

8. Combining with the Leibnitz rule, we get the partial integration rule:

$$\mathcal{T}(\partial_j f * g) = -\mathcal{T}(f * \partial_j g). \tag{2.39}$$

In addition, we need to define the following notions of norm. For $1 \leq s < \infty$, the following equation:

$$\|f\|_{L^s} = \mathcal{T}\left(\{f * f^*\}^{\frac{s}{2}}\right)^{\frac{1}{s}} \tag{2.40}$$

defines a norm on $\mathcal{A}_0$. The completion of $\mathcal{A}_0$ under this norm is called the noncommutative L^s-space and is denoted by $L^s(\mathcal{A}, \mathcal{T})$. Let $\alpha = (\alpha_1, \ldots, \alpha_D)$ be

a multi-index, $|\alpha| = \alpha_1 + \ldots \alpha_D$, and $\partial^\alpha = \partial_1^{\alpha_1} \ldots \partial_D^{\alpha_D}$. Then, for $1 \leq s < \infty$ and k a positive integer, the following equation:

$$\|f\|_{W^{s,k}} = \sum_{0 \leq |\alpha| \leq k} \|\partial^\alpha f\|_{L^s} \tag{2.41}$$

defines a norm on $\mathcal{A}_0$. The completion of $\mathcal{A}_0$ under this norm is called non-commutative Sobolev space and is denoted by $W^{s,k}(\mathcal{A}, \mathcal{T})$. The noncommutative Sobolev space $W^{D,1}(\mathcal{A}, \mathcal{T})$ will play a special role in what follows. Since this is the only Sobolev space used in this thesis, we will use the simplified notation $W(\mathcal{A}, \mathcal{T})$ for it. It is useful to explicitly write its norm:

$$\|f\|_W = \mathcal{T}\left(|f|^D\right)^{\frac{1}{D}} + \sum_{i=1}^{D} \mathcal{T}\left(|\partial_i f|^D\right)^{\frac{1}{D}}, \tag{2.42}$$

where $|f| = (f * f^*)^{\frac{1}{2}}$.

2.4 Magnetic derivative

The traditional linear response calculus with respect to the magnetic field can also be extended to this formulism [7, 82]. It allows us to take derivatives with respect to the magnetic field in the algebra $\mathcal{A}$. It has been successfully used to derive Streda formula [91] and magnetoelectric response [54]. The derivatives acting on $f \in \mathcal{A}$ can be computed using:

$$\partial_{B_j} \mathcal{T}(f) = \mathcal{T}(\delta_j f), \tag{2.43}$$

where δ_j's, $j = 1, \ldots, D$ are the algebraic derivatives with respect to the magnetic field. For 3D, they satisfy the following algebraic relationships (with j taken mod 3):

α.) $\delta_j \partial_i f = \partial_i \delta_j f$

$\beta.)\ \delta_j f^* = (\delta_j f)^*$

$\gamma.)\ \delta_j(f*g) = (\delta_j f)*g + f*(\delta_j g) + \frac{i}{2}(\partial_{j+1}f*\partial_{j+2}g - \partial_{j+2}f*\partial_{j+1}g)$

$\delta.)\ \delta_j[f,g] = [\delta_j f, g] + [f, \delta_j g] + \frac{i}{2}([\partial_{j+1}f, \partial_{j+2}g] - [\partial_{j+2}f, \partial_{j+1}g]$

$\epsilon.)\ \delta_j(f^{-1}) = -f^{-1}*\delta_j f*f^{-1} + \frac{i}{2}f^{-1}*[\partial_{j+1}f*f^{-1}, \partial_{j+2}f*f^{-1}]$

They can be checked using the relations in the previous section. $\alpha.)$ follows directly by applying Eq. 2.20 and 2.43. To be explicit:

$$
\begin{aligned}
(\delta_j \partial_i f)(\boldsymbol{B}, \boldsymbol{\omega}, \boldsymbol{x}) &= ix_i(\delta_j f)(\boldsymbol{B}, \boldsymbol{\omega}, \boldsymbol{x}) \\
&= ix_i \frac{\partial}{\partial B^j} f(\boldsymbol{B}, \boldsymbol{\omega}, \boldsymbol{x}) \\
&= (\partial_i \delta_j f)(\boldsymbol{B}, \boldsymbol{\omega}, \boldsymbol{x})
\end{aligned}
$$

While $\beta.)$ follows from the fact that $\boldsymbol{B}$ is real, $\gamma.)$ can be shown by first applying ∂_{B_3} to the right hand side of Eq. 2.15:

$$
\begin{aligned}
\delta_3(f*g) &= \frac{\partial}{\partial B^3}\left(\sum_{\boldsymbol{y}\in\mathbb{Z}^3} f(\boldsymbol{\omega}, \boldsymbol{y})g(t_{\boldsymbol{y}}^{-1}\boldsymbol{\omega}, \boldsymbol{x}-\boldsymbol{y})e^{\frac{i}{2}x_i B_{ij}y_j}\right) \\
&= \sum_{\boldsymbol{y}\in\mathbb{Z}^3}\left(\frac{\partial}{\partial B^3}f(\boldsymbol{\omega}, \boldsymbol{y})\right)g(t_{\boldsymbol{y}}^{-1}\boldsymbol{\omega}, \boldsymbol{x}-\boldsymbol{y})e^{\frac{i}{2}x_i B_{ij}y_j} \\
&\quad + \sum_{\boldsymbol{y}\in\mathbb{Z}^3} f(\boldsymbol{\omega}, \boldsymbol{y})\left(\frac{\partial}{\partial B^3}g(t_{\boldsymbol{y}}^{-1}\boldsymbol{\omega}, \boldsymbol{x}-\boldsymbol{y})\right)e^{\frac{i}{2}x_i B_{ij}y_j} \\
&\quad + \frac{i}{2}\sum_{\boldsymbol{y}\in\mathbb{Z}^3} f(\boldsymbol{\omega}, \boldsymbol{y})g(t_{\boldsymbol{y}}^{-1}\boldsymbol{\omega}, \boldsymbol{x}-\boldsymbol{y})(x_1y_2 - x_2y_1)e^{\frac{i}{2}x_i B_{ij}y_j} \\
&= (\delta_3 f)*g + f*(\delta_3 g) + \frac{i}{2}(x_1y_2 - x_2y_1)f*g \\
&= (\delta_3 f)*g + f*(\delta_3 g) + \frac{i}{2}(\partial_2 f*\partial_1 g - \partial_1 f*\partial_2 g)
\end{aligned}
$$

where the last line is reached by observating $(x_1y_2 - x_2y_1) = (x_1 - y_1)y_2 - (x_2 - y_2)y_1$ and applying Eq. 2.20. Permutating on x, y, z, $\gamma.)$ is concluded. Next, $\delta.)$ immediately follows from $\gamma.)$. Finally, $\epsilon.)$ can be shown directly using $\delta_j(f^{-1}*f) =$

0, γ.) and Eq. 2.35. These rules of calculus allow us to compute any response function involving magnetic field.

Chapter 3

Topological Magnetoelectric Response

Here, the magnetoelectric response in position space is derived in the framework of noncommutative Brillouin torus. The formula is well-defined for an arbitrary magnetic field and disorder. The connection between the quantization of the magnetoelectric response and second noncommutaive Chern number are shown for three dimensional time-reversal topological insulators.

3.1 Introduction

The magnetoelectric effect in insulating materials consists in the appearance of a finite electric bulk polarization $\boldsymbol{P}$ when a sample is subjected to an external magnetic field $\boldsymbol{B}$, and in the appearance of a finite bulk magnetization $\boldsymbol{M}$ when the sample is subjected to an external electric field $\boldsymbol{E}$. It is described by the magnetoelectric response tensor:

$$\alpha_{ij} = \frac{\partial P_i}{\partial B^j} = \frac{\partial M_j}{\partial E^i}, \tag{3.1}$$

where the derivatives are not necessarily taken at zero $\boldsymbol{B}$ or $\boldsymbol{E}$ fields. The last equality only holds in the absence of dissipation and dispersion. Therefore, they are only valid for a low frequency, low temperature response of an insulator. The effect has been observed in a variety of materials and its technological applications can be tremendous [25, 99].

Originally, the effect was sought in materials with broken time-reversal and

inversion symmetries, but recently it was also shown that topological insulators can display large magnetoelectric responses [79, 104] due to topological characteristics of their electronic structures. It was shown that the three dimensional topological insulators can be classified by their magnetoelectric response.

For perfectly periodic, time-reversal invariant insulators, the magnetoelectric response induces a $\mathbb{Z}_2$ topological classification [79] and the topological part of the magnetoelectric tensor, which defines an invariant for this classification, was shown [106] to equal the previously introduced [28, 60, 88] $\mathbb{Z}_2$ invariants. This was an important development in the field because it provided a measurable bulk effect which sets apart the trivial and topological three dimensional time-reversal invariant insulators [56].

The magnetoelectric response has ionic, spin and orbital contributions. Here we discuss only the orbital component, which can be decomposed into isotropic and traceless parts. Both components are experimentally measurable quantities but we will focus exclusively on the isotropic component:

$$\alpha = \frac{1}{3} \sum_{j=1}^{3} \alpha_{jj}, \tag{3.2}$$

for it contains the topological response. For perfectly periodic, time-reversal or inversion invariant crystals in the absence of external fields, α was derived and explicitly computed in Refs. [21, 41, 79] for several insulator models, showing that indeed α can take non-trivial quantized values. For perfectly periodic systems without time-reversal and inversion symmetries, Refs. [22, 59] showed that α has additional contributions besides the topological component.

Our goal here is to extend the above mentioned works to the case when disorder and magnetic field are present, maintaining the assumption of a gap in the energy spectrum at the Fermi level. The main challenges arising in this more general setup are the breaking of the translational symmetry and the tedious

linear response calculus with respect to the magnetic field. Both challenges are overcome using noncommutative geometry [15].

The starting point for our work is Ref. [91] where noncommutative formulae for $\boldsymbol{P}$ and $\boldsymbol{M}$ have been reported. Given these results, we could have proceeded along two routes, one relying on the variation of $\boldsymbol{P}$ with $\boldsymbol{B}$ and the other one relying on the variation of $\boldsymbol{M}$ with $\boldsymbol{E}$. We chose the first route because computing the variation of $\boldsymbol{P}$ with $\boldsymbol{B}$ fits better into the noncommutative geometry of the Brillouin torus [7], which provides us a tool to compute the derivatives with respect to the magnetic field (see Chapter 2).

3.2   Isotropic magnetoelectric response

The modern polarization begins with the realization that it is the change of polarization that is a well-defined bulk property and an experimental observable [46, 83]. Instead of polarization itself, we should define the difference in polariation between two states that can be connected via an adiabatic change of the Hamiltonian $H(t)$, where the parameter t is the adabatic parameter. While keeping the spectral gap opens, the differnce in polarization can be computed by the integrated bulk current density $j(t)$ in the j direction as the system evolves from $t = 0$ to $t = T$ adabatically:

$$\Delta P_j = P_j(T) - P_j(0) = \int_0^T dt \; j(t) \tag{3.3}$$

Ref. [91] proved the following result: The change of the electric polarization during an adiabatic variation of the Hamiltonian at a fixed magnetic field is given by:

$$\Delta P_j = i \int_\gamma dt \; \mathcal{T}\big(p * [\partial_t p, \partial_j p]\big), \tag{3.4}$$

where $p := p(t) = \chi_{(-\infty, E_F]}(h(t))$ is the projector onto the occupied states. The noncommutative formula for polarization can be thought of as a generalization of the King-Smith and Vanderbilt formula [46]. It shows that the polarization formula is well-defined even in the presense of a magnetic field and disorder.

It was noted by Thouless, that for a T-periodic Hamiltonian, the polarization is in fact, a topological quantity [102]. Physically, this implies the quantization of charge transported during a cyclic deformation of the Hamiltonian. This reasoning suggests a connection between Eq. 3.4 to the noncommutative 1st Chern number. It implies that the quantization is stable in the presense of disorder, provided the spectral gap remains open.

The key observation is that applying the algebraic magnetic derivative to Eq. 3.4 leads to the topological magnetoelectric response [54]. The magnetoelectric tensor is well-defined only when referenced from a "standard" system. We will denote the reference system by h_0 and we will consider adiabatic time variations of the Hamiltonian $h(t)$ which originate at this h_0. The main assumption is that the Fermi level is always in a spectral gap during the adiabatic variation. For a 3D homogenous lattice Hamiltonian Eq. 2.10, the variation in isotropic magnetoelectric response can be computed as:

$$\Delta\alpha = \frac{1}{3}\sum_{j=1}^{3}\frac{\partial \Delta P_j}{\partial B^j} = i\int_{\gamma} dt \; \frac{1}{3}\sum_{j=1}^{3}\mathcal{T}\big(\delta_j(p * [\partial_t p, \partial_j p])\big), \qquad (3.5)$$

Our main task is to compute:

$$\sum_{j=1}^{3}\mathcal{T}\big(\delta_j(p * [\partial_t p, \partial_j p])\big). \qquad (3.6)$$

Using the rule of calculus from Sec. 2.4, we have:

$$\delta_j(p * [\partial_t p, \partial_j p]) = \delta_j p * [\partial p, \partial_j p] + p * \delta_j[\partial_t p, \partial_j p]$$
$$+ \frac{i}{2}\partial_{j+1}p * \partial_{j+2}[\partial_t p, \partial_j p] - \frac{i}{2}\partial_{j+2}p * \partial_{j+1}[\partial_t p, \partial_j p]. \quad (3.7)$$

The contributions to $\Delta\alpha$ from the last two terms above identically cancel out, as it can be easily seen by using an integration by parts. The magnetic derivative of the commutator is:

$$\delta_j[\partial_t p, \partial_j p] = [\delta_j \partial_t p, \partial_j p] + [\partial_t p, \delta_j \partial_j p]$$
$$+ \frac{i}{2}\big([\partial_{j+1}\partial_t p, \partial_{j+2}\partial_j p] - [\partial_{j+2}\partial_t p, \partial_{j+1}\partial_j p]\big). \quad (3.8)$$

The contribution to the integrant in Eq. 3.5 from the last two terms of Eq. 3.8 is zero while the first from the first two terms of Eq. 3.8 gives:

$$\sum_{j=1}^{3}\mathcal{T}\big(p * ([\delta_j\partial_t p, \partial_j p] + [\partial_t p, \delta_j\partial_j p])\big) = 2\sum_{j=1}^{3}\mathcal{T}\big([\partial_t p, \partial_j p] * \delta p_j\big)$$
$$+ \frac{d}{dt}\sum_{j=1}^{3}\mathcal{T}\big(\chi(h - E_F) * \partial_j p * \delta_j p\big). \quad (3.9)$$

So far the calculation stands as:

$$\sum_{j=1}^{3}\mathcal{T}\big(\delta_j(p * [\partial_t p, \partial_j p])\big) = 3\sum_{j=1}^{3}\mathcal{T}\big([\partial_t p, \partial_j p] * \delta_j p\big)$$
$$+ \frac{d}{dt}\sum_{j=1}^{3}\mathcal{T}\big(\chi(h - E_F) * \partial_j p * \delta_j p\big). \quad (3.10)$$

Now:

$$\mathcal{T}\big([\partial_t p, \partial_j p] * \delta_j p\big) = \mathcal{T}\big([\partial_t p, \partial_j p] * \delta_j p * p\big) + \mathcal{T}\big([\partial_t p, \partial_j p] * \delta_j p * (1-p)\big)$$

$$= \mathcal{T}\big(p * [\partial_t p, \partial_j p] * \delta_j p * p\big)$$

$$+ \mathcal{T}\big((1-p) * [\partial_t p, \partial_j p] * \delta_j p * (1-p)\big),$$

where in the last line we used the cyclicity of the trace and the idempotency of p and $1 - p$. Given the fact that p and $(1 - p)$ commute with $[\partial_t p, \partial_j p]$, we can continue as:

$$\ldots = \mathcal{T}\big([\partial_t p, \partial_j p] * (p * \delta_j p * p + (1-p) * \delta_j p * (1-p))\big) \qquad (3.11)$$

$$= \frac{1}{2i}\mathcal{T}\big((2p-1) * [\partial_t p, \partial_j p] * [\partial_t p, \partial_j p]\big)$$

$$= \frac{1}{i}\mathcal{T}\big(p * [\partial_t p, \partial_j p] * [\partial_t p, \partial_j p]\big), \qquad (3.12)$$

where in the second line we used the following identites for projectors [91]:

$$p * (\delta_j p) * p = -\frac{i}{2} p * [\partial_{j+1} p, \partial_{j+2} p] * p \qquad (3.13)$$

and

$$(1-p) * (\delta_j p) * (1-p) = \frac{i}{2}(1-p) * [\partial_{j+1} p, \partial_{j+2} p] * (1-p). \qquad (3.14)$$

We conclude:

$$\frac{i}{3}\sum_{j=1}^{3}\mathcal{T}\big(\delta_j(p*[\partial_t p, \partial_j p])\big) = \sum_{j=1}^{3}\mathcal{T}\big(p*[\partial_t p, \partial_j p]*[\partial_{j+1}p, \partial_{j+2}p]\big)$$

$$+\frac{i}{3}\frac{d}{dt}\sum_{j=1}^{3}\mathcal{T}\big(\chi(h-E_F)*\partial_j p*\delta_j p\big), \qquad (3.15)$$

and the first term on the left side can be anti-symmetrized and brought to the desired form:

$$\Delta\alpha = \frac{1}{2}\int_{\gamma} dt\; \varepsilon^{\alpha\beta\gamma\delta}\mathcal{T}\big(p*\partial_\alpha p*\partial_\beta p*\partial_\gamma p*\partial_\delta p\big)$$

$$+\frac{i}{3}\mathcal{T}\big(\chi(h-\epsilon_F)*\partial_j p*\delta_j p\big)\Big|_{\text{initial}}^{\text{final}}, \qquad (3.16)$$

where summation over the repeating indices is assumed. The indices $\alpha,\ldots,\delta$ run through t and $j = 1, 2, 3$, and ε is the signature of the permutation. The first (second) term on the right hand side of Eq. 3.16 is called topological (non-topological) for reasons to be discussed shortly. Just like the polarization formula, the change in magnetoelectric response for T-periodic Hamiltonian will be protected against disorder [91]. We would like to point out that the computation of this section remains valid even in the regime of strong disorder where the insulating gap is closed and is replaced by a mobility gap (provided we accept the formula Eq. 3.4 for the electric polarization).

3.3   Quantization and invariance

For the purpose of this discussion, it is more convenient to view the adiabatic time evolution from an initial to a final configuration as an adiabatic interpolation between two points in the parameter space of the model. The adiabatic
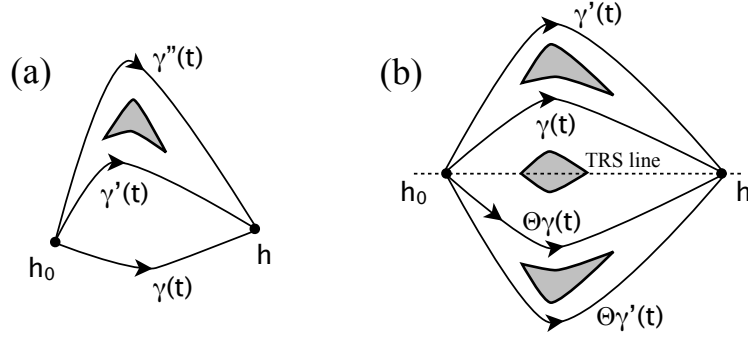
Figure 3.1: (a) Various adiabatic interpolations between the initial (h_0) and final (h) systems. (b) Here h_0 and h are time-reversal symmetric (TRS), but they are adiabatically interpolated via paths that are not necessarily time-reversal symmetric ($\Theta\gamma \neq \gamma$). The shaded regions represents regions in the model's parameter space where the spectral gap closes. The TRS line is invariant to the time-reversal operation.

interpolations will be represented as curves in this parameter space and the time-integral can be viewed as an integral along such curve. We automatically assume that the spectral gap at the Fermi level remains open during the adiabatic interpolations. We will use the notations $\gamma + \gamma'$ to denote the interpolation path obtained by joining the interpolation paths γ and γ', $-\gamma$ to denote the interpolation path γ when taken in reverse, and $\Delta\alpha[\gamma]$ to indicate that the variation in the magnetoelectric response depends on the interpolation path γ.

The first question we want to address is what happens to the variation of the isotropic magnetoelectric response when we consider different interpolation paths, $\gamma(t)$ and $\gamma'(t)$, between the reference and the final systems. Since:

$$\Delta\alpha[\gamma] - \Delta\alpha[\gamma'] = \Delta\alpha[\gamma - \gamma'], \tag{3.17}$$

we can write:

$$\Delta\alpha[\gamma] - \Delta\alpha[\gamma'] = \frac{1}{2} \oint_{\gamma-\gamma'} dt \; \varepsilon_{\alpha\beta\gamma\delta} \mathcal{T}\left(p * \partial_\alpha p * \partial_\beta p * \partial_\gamma p * \partial_\delta p\right), \tag{3.18}$$

and the important observation here is that the t-integral is now taken over a closed loop. We can then recognize on the right-hand side the expression of the second Chern number Ch_2 over the space $(\gamma - \gamma') \times$ noncommutative Brillouin torus, written in the position space rather than in the k-space. Because of the finite gap assumption, the second Chern number is quantized, due to a general argument by Connes [14], which says that the pairing between the projectors and cyclic cocycles is a homotopy invariant. Hence the quantization occurring in the clean limit persists when the disorder is turned on, at least as long as the spectral gap remains open.

Therefore, the answer to our first question is that the difference in $\Delta\alpha[\gamma]$, when computed along different adiabatic evolutions, is always an integer number (we recall that our units were taken such that $e = \hbar = 1$). We illustrate in Fig. 1(a) various possible situations. For example, if the interpolating paths $\gamma(t)$ and $\gamma'(t)$ can be deformed into each other without closing the spectral gap, then Ch_2 is necessarily zero and $\Delta\alpha[\gamma]$ is identical for the two interpolation paths. But, if the interpolating paths cannot be deformed into each other without closing the spectral gap, such as it happens for $\gamma(t)$ and $\gamma''(t)$ in Fig. 1(a), then Ch_2 may take non-trivial integer values so $\Delta\alpha[\gamma]$ and $\Delta\alpha[\gamma'']$ cannot be expected to be identical, but we know that the difference between the two will be an integer number.

We now turn our attention to adiabatic interpolations between time-reversal invariant systems, in which case we need to turn the magnetic field off. Symmetry considerations can be used to show that only the topological part of $\Delta\alpha$ survives for such such systems [22, 59]. The time-reversal operation is given by the map:

$$\Theta : \mathcal{A}|_{\boldsymbol{B}=0} \to \mathcal{A}|_{\boldsymbol{B}=0}, \quad (\Theta f)(\boldsymbol{\omega}, \boldsymbol{x}) = e^{i\pi s_y}\overline{f(\boldsymbol{\omega}, \boldsymbol{x})}e^{-i\pi s_y}, \qquad (3.19)$$

where s_y is a matrix from $\mathcal{M}_{D \times D}$ representing the y-component of the spin operator, and the line at the top represents complex conjugation. Some immediate

properties of time-reversal map Θ are:

$$\Theta(f * g) = (\Theta f) * (\Theta g), \tag{3.20}$$

and

$$\partial_j \Theta f = -\Theta(\partial_j f). \tag{3.21}$$

Now, let h_0 and h be two time-reversal invariant Hamiltonians, $\Theta h_0 = h_0$ and $\Theta h = h$. The key observation is that, if $\gamma(t)$ is an adiabatic interpolation between h_0 and h, then $\Theta \gamma$ is also an adiabatic interpolation between h_0 and h (with a strictly positive spectral gap), and furthermore:

$$\Delta \alpha[\gamma] = \Delta \alpha[-\Theta \gamma]. \tag{3.22}$$

This can be seen from the explicit formula of Eq. 3.16 and the properties of the time-reversal map stated in Eqs. 3.20 and 3.21. We already established that:

$$\Delta \alpha[\gamma] - \Delta \alpha[\Theta \gamma] = Ch_2[\gamma - \Theta \gamma], \tag{3.23}$$

and this together with Eq. 3.22 leads to an important conclusion for this section:

$$\Delta \alpha[\gamma] = \frac{1}{2} Ch_2[\gamma - \Theta \gamma]. \tag{3.24}$$

This shows the quantization of topological magnetoelectric response is robust against disorder.

In Fig. 3.1(b) we illustrate several possible situations. If γ can be deformed to a time-reversal invariant path, $\Theta \gamma = \gamma$, then $Ch_2 = 0$ and $\Delta \alpha[\gamma]$ is necessary zero. But if h_0 and h cannot be connected with a time-reversal invariant path

without closing the spectral gap at the Fermi level, then γ must be taken as in Fig. 3.1(b) so that to avoid the closing of the spectral gap. In this case, $Ch_2[\gamma - \Theta\gamma]$ can take non-trivial integer values and consequently $\Delta\alpha[\gamma]$ can take non-trivial values, which are either integer or half-integer numbers. If we take a different interpolation path, such as γ' in Fig. 3.1(b), then $\Delta\alpha[\gamma']$ may change but only by an integer number, as it was already established above. As such, for all possible adiabatic interpolation paths, $\Delta\alpha[\gamma]$ is either an integer number or a half-integer number. In other words, the integer or half-integer character of $\Delta\alpha[\gamma]$ is topologically stable.

3.4 $\mathbb{Z}_2$ classification

The results of the last section can be further developed into a $\mathbb{Z}_2$ classification of three dimensional disordered time-reversal invariant insulators. We can take the reference systems to be the insulators with zero hopping amplitudes between different lattice sites. These systems can be called "trivial" since they do not display any magnetoelectric response as there are no Peierls factors when a magnetic field is turned on. As such, we can postulate $\alpha = 0$ for the trivial systems. Then, the time-reversal invariant insulators fall into two classes (here we assume that all time-reversal symmetric insulators can be adiabatically connected to a representative from the trivial class): one for which $\alpha = $ integer and another for which $\alpha = $ half-integer, and we can be sure that an insulator from the first class and an insulator from the second class cannot be connected by a time-reversal invariant interpolation path without closing the insulating gap.

An insulator from a given symmetry class is generally called topological [41] if it cannot be adiabatically connected with its atomic limit (obtained by turning off the hopping terms between distinct lattice sites) via an interpolation path that respects the symmetry of the class and without closing the insulating gap. If we

follow this definition, then the class of three dimensional disordered time-reversal invariant insulators with α = half-integer contains only topological insulators. Of course, our analysis does not rule out additional, more refined topological sub-classifications of either α = integer or α = half-integer classes.

A $\mathbb{Z}_2$ classification of the disordered inversion symmetric insulators is also possible via similar arguments. This is the case because the inversion operation satisfies the properties written in Eqs. 3.20 and 3.21, which are at the core of the $\mathbb{Z}_2$ classification of time-reversal insulators. However, for inversion symmetric insulators, it is explicitly known [41] that the $\mathbb{Z}_2$ classification is not the end of the story as it can be furtherly refined.

3.5   Position formulae

The physical meaning of the algebraic formulae becomes the transparent in Hilbert space, where its connection to the $\boldsymbol{k}$-space formula can be estisbalished. Using the operator representations, the algebraic polarization formula Eq. 3.4 can be translated to:

$$\Delta P_j = e \int_\gamma dt \; \tau\big(P_{\boldsymbol{\omega}}[\partial_t P_{\boldsymbol{\omega}}, [X_j, P_{\boldsymbol{\omega}}]]\big), \qquad (3.25)$$

where $P_{\boldsymbol{\omega}} := \chi_{(-\infty, E_F]}(H_{\boldsymbol{\omega(t)}})$ is the "global" projector and the physcial constant e is recovered. This is simply a position formula for the polarization. For a translational symmetric system, using the correspondences for translational invariant operators F and G:

$$[X_j, F] \to i\frac{\partial \tilde{F}_{\boldsymbol{k}}}{\partial k^j} \qquad (3.26)$$

and

$$\tau(FG) \rightarrow \frac{1}{(2\pi)^D} \int_{\mathcal{T}^D} d^D k \ \text{tr}\{\tilde{F}_{\boldsymbol{k}}\tilde{G}_{\boldsymbol{k}}\}, \tag{3.27}$$

we can recover the King-Smith and Vanderbilt in $\boldsymbol{k}$-space [46]:

$$\Delta P_j = ie \int_\gamma dt \int_{\mathcal{T}^1} \frac{dk}{2\pi} \ \text{tr}\big(\tilde{P}_{\boldsymbol{k}}[\partial_t \tilde{P}_{\boldsymbol{k}}, \partial_{k^j} \tilde{P}_{\boldsymbol{k}}])\big), \tag{3.28}$$

Similarly, we can write down the position representation for our magnetoelectric formula,

$$\Delta\alpha = \frac{e^2 4\pi i}{h} \int_\gamma dt \ \varepsilon^{ijk} \tau\big(P_{\boldsymbol{\omega}}[\partial_t P_{\boldsymbol{\omega}}, [X_i, P_{\boldsymbol{\omega}}]][[X_j, P_{\boldsymbol{\omega}}], [X_k, P_{\boldsymbol{\omega}}]]\big), \tag{3.29}$$

where repeated indices are summed over the spatial direction and the physical constants are recovered. In addition, if we assume the reference Hamiltonian to be trivial insulator and take the "$\boldsymbol{k}$-space limit":

$$\begin{aligned}
\alpha &= \frac{e^2}{h} \int_\gamma dt \int_{\mathcal{T}^3} \frac{d^3 k}{2\pi^2} \ \varepsilon^{ijk} \text{tr}\big(\tilde{P}_{\boldsymbol{k}}[\partial_t \tilde{P}_{\boldsymbol{k}}, \partial_{k^i} \tilde{P}_{\boldsymbol{k}}][\partial_{k^j} \tilde{P}_{\boldsymbol{k}}, \partial_{k^k} \tilde{P}_{\boldsymbol{k}}]\big) \tag{3.30} \\
&= \frac{e^2}{h} \int_\gamma dt \int_{\mathcal{T}^3} \frac{d^3 k}{8\pi^2} \ \varepsilon^{\alpha\beta\gamma\delta} \text{tr}\big(\mathcal{F}_{\alpha\beta}\mathcal{F}_{\gamma\delta}\big).
\end{aligned}$$

where in the last line we used the definiton of the Berry curvature for Bloch states, $\mathcal{F}_{ij} = \langle u_{\boldsymbol{k}}|\tilde{P}_{\boldsymbol{k}}[\partial_{k^i} \tilde{P}_{\boldsymbol{k}}, \partial_{k^j} \tilde{P}_{\boldsymbol{k}}]|u_{\boldsymbol{k}}\rangle$, and the identity $\varepsilon^{ijk}\mathcal{F}_{ti}\mathcal{F}_{jk} = \frac{1}{8}\varepsilon^{\alpha\beta\gamma\delta}\mathcal{F}_{\alpha\beta}\mathcal{F}_{\gamma\delta}$. This shows that the position space formula reduces to the 2nd Chern number [6] for peridoic crystals. Integrating out the adabatic parameter, the magnetoelectric coupling can be reduced to the Chern-Simons integral [21, 61, 79]:

$$
\begin{aligned}
\alpha &= \frac{e^2}{h} \int_\gamma dt \int_{\mathcal{T}^3} \frac{d^3k}{8\pi^2} \, \varepsilon^{\alpha\beta\gamma\delta} \mathrm{tr}\big(\mathcal{F}_{\alpha\beta}\mathcal{F}_{\gamma\delta}\big) \\
&= \frac{e^2}{h} \int_\gamma dt \int_{\mathcal{T}^3} \frac{d^3k}{2\pi^2} \, \varepsilon^{\alpha\beta\gamma\delta} \partial_\alpha \mathrm{tr}\big(\mathcal{A}_\beta \partial_\gamma \mathcal{A}_\delta + \frac{2}{3}\mathcal{A}_\beta \mathcal{A}_\gamma \mathcal{A}_\delta\big), \\
&= \frac{e^2}{h} \int_{\mathcal{T}^3} \frac{d^3k}{2\pi^2} \, \varepsilon^{ijk} \mathrm{tr}\big(\mathcal{A}_i \partial_j \mathcal{A}_k + \frac{2}{3}\mathcal{A}_i \mathcal{A}_j \mathcal{A}_k\big).
\end{aligned}
\tag{3.31}
$$

where $\mathcal{A}_i = \langle u_{\boldsymbol{k}}|\partial_{k^i}|u_{\boldsymbol{k}}\rangle$ is the Berry connection defined in $\boldsymbol{k}$ space. Eq. 3.31 is directly connected to the theta term [79] via:

$$
\alpha = \frac{e^2}{h}\frac{\theta}{2\pi},
\tag{3.32}
$$

where θ is quantized to be 0 and π for trivial and topologicla insulators respectively.

An important observation is that the position formulation is independent of the existence of Brillouin torus, in contrast to the $\boldsymbol{k}$-space formula. When we turn on disorder, the formula Eq. 3.29 and its topological stability remains valid. In general, it assure us that, given a finite spectral gap along t, any random disorder configuration cannot change the physical response. Therefore, the topological magnetoelectric is independent of any disorder configurations.

3.6 Numerical computation

In this section, we compute the topological magnetoelectric coupling for a three dimensional time-reversal symmetric topological insulator model. We consider the Fu-Kane-Mele model on a diamond lattice with a staggered Zeeman term [21, 28] and on-site disorder potential:
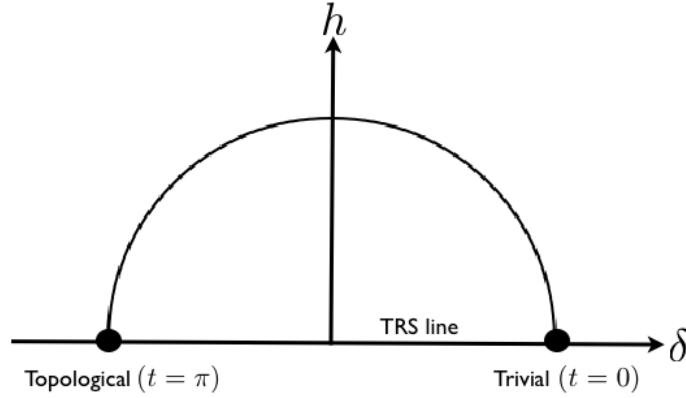
Figure 3.2: For the following parameters: $W = 0, \gamma = 1, \lambda_{SO} = 0.125, h = sin(t)$ and $\delta = cos(t)$, the adiabatic parameter t connects the trivial phase $(t = 0)$ and the topological phase $(t = \pi)$ of the model Eq. 3.33. On the time-reversal symmetric (TRS) line, the gap closes and a topological phase transition occurs at the orgin. The time reversal symmetry is broken and a spectral gap is ensured along the adiabatic path.

$$
\begin{aligned}
H_\omega &= \sum_{\langle \boldsymbol{x}, \boldsymbol{y} \rangle} t_{\boldsymbol{xy}} |\boldsymbol{x}\rangle\langle\boldsymbol{y}| + i\frac{4\lambda_{SO}}{a^2} \sum_{\langle\langle \boldsymbol{x}, \boldsymbol{y} \rangle\rangle} \boldsymbol{\sigma} \cdot (\boldsymbol{d}^1_{\boldsymbol{xy}} \times \boldsymbol{d}^2_{\boldsymbol{xy}}) |\boldsymbol{x}\rangle\langle\boldsymbol{y}| \\
&+ \boldsymbol{h} \cdot \left(\sum_{\boldsymbol{x} \in A} \boldsymbol{\sigma} |\boldsymbol{x}\rangle\langle\boldsymbol{x}| - \sum_{\boldsymbol{x} \in B} \boldsymbol{\sigma} |\boldsymbol{x}\rangle\langle\boldsymbol{x}| \right) \\
&+ W \sum_{\boldsymbol{x}} \omega_{\boldsymbol{x}} |\boldsymbol{x}\rangle\langle\boldsymbol{x}|,
\end{aligned}
\tag{3.33}
$$

The first term is the first neighbors hopping where its amplitude depends on the bond direction. We take $t_{\boldsymbol{xy}} = 3\gamma + \delta$ for direction [111] (in the conventional fcc unit cell of size a) and $t_{\boldsymbol{xy}} = \gamma$ for the other three bonds. The spin-orbit interaction connects pairs of second neighbors, where $\boldsymbol{d}^1_{ij}$ and $\boldsymbol{d}^2_{ij}$ connects the first neighbor legs and $\sigma's$ are the Pauli spin matrices. The staggered Zeeman term is added to break time-reversal symmetry. It has opposite signs on the two fcc sublattices A and B, and $\boldsymbol{h}$ is chosen to be in the [111] direction. For
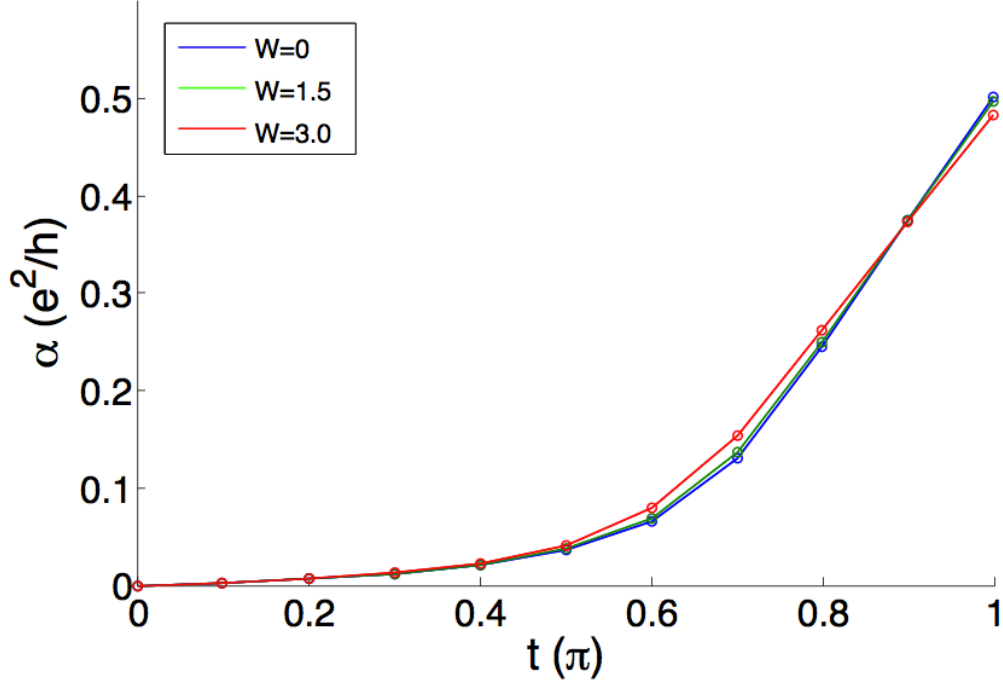
Figure 3.3: The topological magnetoelectric response is computed for Fu-Kane-Mele model with a lattice size $14 \times 14 \times 14$. The calculations are done for different disorder strengths W and the following parameters are chosen: $\gamma = 1, \lambda_{SO} = 0.125, \delta = cos(t)$ and $h = sin(t)$. The path γ is discretized using 10 points and the time derivative is computed using the 5-point finite difference formula. Only one disorder configuration is used for each calculation.

the calculations, we choose $\gamma = 1$ and $\lambda_{SO} = 0.125$. The computation shown in Fig. 3.3 are done using our magnetoelectric formula Eq. 3.29. δ is set to be $cos(t)$, so that in the absence of disorder, it connects the trivial $(t = 0)$ and the strong topological $(t = \pi)$ phase. The term $\boldsymbol{h}$ is chosen to be $sin(t)$ to keep the spectral gap open along the adiabatic interpolation.

In Fig. 3.3, the magnetoelectric response is computed for the model with and without disorder. In the clean limit, the energy gap is about 2 for the chosen parameters. As it can be seen in the figure, the magnetoelectric response is quantized to $e^2/2h$. This agrees with the calculation for the clean model using the $\boldsymbol{k}$-space formula in Ref. [21]. We have also done calculations for the model with

two different disorder strengths. Our results confirm that the topological magnetoelectric response remains quantized and robust in the presence of disorder.

3.7   Summary

We have obtained a formula for the topological magnetoelectric response in position space. The topological quantization of our formula, which is defined on a noncommutative Brillouin torus, is well-defined even in the presense of disorder. This result also produces a position-space formulation of the topological invariant.

The noncommutative magnetoelectric formula was numerically using the methods developed in Ref. [76]. The results confirmed that the topological magnetoelectric response is robust against disorder. As such, we now have a practical tool to explore the physics of disordered topological insulators. It is worth stressing that our calculation was carried out using a $14 \times 14 \times 14$ lattice model. This is significantly larger than previous disordered $\mathbb{Z}_2$ calculation which used twisted boundary conditions [53]. Our position space formula is self-averaging, hence only one disorder configuration is required for an accurate prediction.

Chapter 4

Noncommutative Chern numbers

Motivated by the connection between the noncommutative 2nd Chern number and the magnetoelectric response, we develop the noncommutative theory of Chern numbers. The quantization and robustness are shown by connecting it to a Fredholm index. What makes noncommutative Chern numbers fundamental is their generality, in particular their robustness against disorder and variations of the magnetic field. We will only focus on the results and their physical meanings and present the mathematical details and proofs in the Appendix. Interested readers can also refer to Ref. [9, 15, 78].

4.1   Introduction

The noncommutative 1st Chern number [9] can be viewed as a generalization of the TKNN invariant [103] to the the case of aperiodic systems. While the TKNN invariant is protected by a spectral gap and can be defined only for an uniform magnetic field satisfying the "rational-flux" condition, the noncommutative 1st Chern number is protected by a mobility gap and can be defined for an arbitrary uniform magnetic field. These special properties of the 1st Chern number played a decisive role in our understanding of the integer quantum Hall effect.

In the new field of topological insulators, the noncommutative 1st Chern number was successfully used to characterize and compute the phase diagram of strongly disordered two dimensional Chern insulators [73, 77]. The noncommutative 1st Chern number also played an instrumental role in the definition of

the noncommutative spin Chern number [71]. The latter proved to be an effective tool in the characterization and computation of the phase diagram of strongly disordered two dimensional quantum spin Hall insulators [73, 75, 108].

The theory of topological insulators is on a rigorous footing for perfectly periodic crystals [28, 60, 88], but little progress has been made for strongly disordered crystals. Some of the important theoretical open questions for the latter case are: Do the topological invariants, defined for the periodic case, continue to make sense at strong disorder when the Fermi level is embedded in a dense localized spectrum? Do bulk extended states exist at strong disorder, like in the integer quantum Hall effect? Are the metallic surface states robust against strong disorder? Some of these open questions have been numerically investigated [53] and the available results hint to positive answers. On the analytical front, it was recently noted [54] that a rigorous theory of the noncommutative 2nd Chern number in four dimensions could provide an answer to the first two open question.

4.2   Topological insulators and Chern number

The second Chern number enters the picture in the following way. Let us consider first the perfectly periodic three dimensional insulators (see Eq. 1.1). Suppose a quantum system, described by a Hamiltonian $H_{\boldsymbol{\lambda}}$ which depends on a set of parameters $\boldsymbol{\lambda} = \{\lambda_1, \ldots\}$. The key physical property to consider is the isotropic part of the magnetoelectric response of the system:

$$\alpha = \frac{1}{3} \sum_{j=1}^{3} \frac{\partial P_j}{\partial B^j} = \frac{1}{3} \sum_{j=1}^{3} \frac{\partial M_j}{\partial E^j}, \tag{4.1}$$

where $\boldsymbol{P}$ and $\boldsymbol{M}$ are the vectors of electric polarization and magnetization, respectively, and $\boldsymbol{B}$ and $\boldsymbol{E}$ are the magnetic and electric fields, respectively. Let $\boldsymbol{\lambda}_1$ and $\boldsymbol{\lambda}_2$ be two points in the parameter space defining two Hamiltonians that are time-reversal symmetric, and consider a path γ, not necessarily time-reversal

invariant, connecting $\boldsymbol{\lambda}_1$ and $\boldsymbol{\lambda}_2$ such that the Fermi level of $H_{\boldsymbol{\lambda}}$ is in a spectral gap for all $\boldsymbol{\lambda} \in \gamma$. Under these conditions, the variation of the isotropic magnetoelectric response along γ is given by [21, 41, 79]:

$$\Delta \alpha[\gamma] = \frac{1}{2} Ch_2[\gamma - \theta \gamma]. \tag{4.2}$$

Here, $C_2(\gamma - \theta \gamma)$ is the 2nd Chern number (see Eq. 1.3) over the manifold generated by the closed path $\gamma - \theta \gamma$ times the three dimensional Brillouin torus. The symbol θ represents the time-reversal operation in the parameter space of the Hamiltonian. Choosing a standard reference system, it follows from Eq. 4.2 that the time-reversal insulators fall into two topologically distinct classes, according to the integer or half-integer character of α (a property that is path-independent). This is the well established $\boldsymbol{Z}_2$ classification of periodic, time-reversal symmetric insulators [28, 60, 79, 88]. Two systems from the two different classes cannot be connected by a time-reversal path (i.e. $\theta \gamma = \gamma$) without the continuum energy spectrum crossing the Fermi level.

In the previous Chapter, we have computed the topological magnetoelectric response in the presence of disorder and under the gap condition [54]. It can be shown that via an interpolation arguments similar to the periodic case, the result can be expressed as:

$$\Delta \alpha[\gamma] = \frac{1}{2} Ch_2[\gamma - \theta \gamma], \tag{4.3}$$

where $Ch_2[\gamma - \theta \gamma]$ is the noncommutative 2nd Chern number over a closed loop $\gamma - \theta \gamma$ times the noncommutative Brillouin torus of the three dimensional aperiodic crystal. Our hope is that the theory of noncommutative Chern numbers developed in this Chapter will enable new progress on the classification of the topological insulators in the presence of disorder, that goes beyond the limitations imposed by the spectral gap condition.

4.3 Fredholm module

To show the quantization of noncommutative Chern numbers, we need to first introduce the Fredholm module [15]. Let:

$$\mathcal{H} = \ell^2(\mathbb{Z}^{2n}, \mathbb{C}^D) \otimes \mathrm{Cliff}(2n). \tag{4.4}$$

The C^*-algebra $\mathcal{A}$ can be represented on $\mathcal{H}$ by $\pi_\omega \otimes \mathrm{id}$, $\omega \in \Omega$. We will denote these representations by the same symbols π_ω. We will also use the same symbol tr for the trace over the Hilbert space $\mathcal{H}$. Let $\gamma_1, \ldots, \gamma_{2n}$ be the generators of the Clifford algebra and:

$$\gamma_0 = i^n \gamma_1 \ldots \gamma_{2n}. \tag{4.5}$$

It is clear that $\pi_\omega(f)\gamma_0 = \gamma_0 \pi_\omega(f)$. Furthermore, let:

$$D = \sum_{i=1}^{2n} x^i \gamma_i \tag{4.6}$$

be the Dirac operator, acting by multiplication on $\mathcal{H}$. We will use the shorthands $\boldsymbol{x} \cdot \boldsymbol{\gamma} = \sum_{i=1}^{2n} x^i \gamma_i$ and $\hat{\boldsymbol{x}} = \boldsymbol{x}/|\boldsymbol{x}|$. Also,

$$D_{\boldsymbol{a}} = (\boldsymbol{x} + \boldsymbol{a}) \cdot \boldsymbol{\gamma} \tag{4.7}$$

will denote the translated of the Dirac operator.

Now, let $\boldsymbol{x}_0$ be a fixed point in $\mathbb{R}^{2n}$ such that $0 \leq x_0^i \leq 1$, $i = 1, \ldots, 2n$. If $\boldsymbol{x}_0 \notin \mathbb{Z}^{2n}$, we define:

$$\hat{D}_{\boldsymbol{x}_0} = \frac{D_{\boldsymbol{x}_0}}{|D_{\boldsymbol{x}_0}|}, \tag{4.8}$$

which acts on $\mathcal{H}$ by multiplication with $\widehat{\boldsymbol{x} + \boldsymbol{x}_0} \cdot \boldsymbol{\gamma}$. If $\boldsymbol{x}_0 \in \mathbb{Z}^{2n}$, we define:

$$\hat{D}_{\boldsymbol{x}_0} = \begin{cases} \widehat{\boldsymbol{x} + \boldsymbol{x}_0} \cdot \boldsymbol{\gamma}, \text{ if } \boldsymbol{x} \neq -\boldsymbol{x}_0 \\[2mm] \frac{1}{\sqrt{2n}} \sum_{i=1}^{2n} \gamma_i \text{ if } \boldsymbol{x} = -\boldsymbol{x}_0. \end{cases} \tag{4.9}$$

Clearly, for all cases, $\hat{D}_{\boldsymbol{x}_0}$ has the following properties:

$$(\hat{D}_{\boldsymbol{x}_0})^2 = 1, \ \hat{D}_{\boldsymbol{x}_0}\gamma_0 = -\gamma_0\hat{D}_{\boldsymbol{x}_0}. \tag{4.10}$$

The triple $(\mathcal{H}, \hat{D}_{\boldsymbol{x}_0}, \gamma_0)$ is an even Fredholm module over $\mathcal{A}$, as defined by Connes [15]. For $n = 1$, the index of the Fredholm module is equal to noncommutative first Chern number for the integer quantum Hall effect [9].

4.4 Noncommutative Chern numbers

In this section, we propose the definition of noncommutative Chern numbers. They are basically the algebraic way of defining Chern numbers, therefore a more appropriate name is algebraic Chern numbers. Discussions on its physical meaning will be given in Sec. 4.6. They allow an application for topological responses when a Brillouin manifold ceases to exit.

On the noncommutative Brillouin torus $(\mathcal{A}, \mathcal{T}, \partial)$ of the homogeneous lattice system Eq. 2.10. Let $p = \chi_{(-\infty, E_F]}(h)$ be the projection which generates the covariant family of the spectral projectors P_ω $(= \pi_\omega p)$ onto the occupied states. Based on the form of classical Chern numbers [6, 9, 54], we propose the following definition of the noncommutative nth Chern number:

$$Ch_n \overset{\text{def}}{=} \frac{(2\pi i)^n}{n!} \sum_\sigma (-1)^\sigma \mathcal{T} \left(p \prod_{i=1}^{2n} \partial_{\sigma_i} p \right). \tag{4.11}$$

We now post the main question of this section: Under what conditions does the quantity defined in Eq. 4.11 display quantization and homotopy invariance? The answer is given by using Fredholm index and techniques in noncommutative

geometry. We present the theorem here and leaves the index calculation in the Appendix A.1.

Theorem [9, 78] If:

$$\Lambda_n = \sum_{i=1}^{2n} \mathcal{T}\left(|\partial_i p|^{2n}\right)^{\frac{1}{2n}} < \infty, \tag{4.12}$$

then the operator $\pi_\omega^-(p)\hat{D}_{x_0}\pi_\omega^+(p)$ is a Fredholm operator. Its Fredholm index is independent of ω or x_0, and is equal to the algebraic nth Chern number:

$$\text{Index}\left(\pi_\omega^-(p)\hat{D}_{x_0}\pi_\omega^+(p)\right) = \frac{(2\pi i)^n}{n!}\sum_\sigma (-1)^\sigma \mathcal{T}\left(p\prod_{i=1}^{2n}\partial_{\sigma_i}p\right). \tag{4.13}$$

As a consequence, the algebraic nth Chern number stays quantized and constant under continuous homotopies of p, where the continuity is considered with respect to the Sobolev norm $\|\ \|_W$ of $W(\mathcal{A}, \mathcal{T})$ (see Eq. 2.42).

Remark. Λ_n has the unit of length and can be interpreted as a natural definition of the localization length. It will be further discussed later on.

The theorem states the conditions needed for topological quantization of nth Chern numbers to occur. For $n = 1$, it represents the celebrated result for the integer quantum Hall effect [9]. For $n = 2$, it represents the 2nd Chern number for topological insulators, which is our main interest [54, 78].

4.5   Localization and stability

Two remarkable facts about the integer quantum Hall effect are the integer quantization and its stability with respect to changes in the parameters. The first fact has a topological orign and the second is due to Anderson localization in the sample [9, 85]. It has been proven that on the parameter space (λ, E_F), the Hall conductance is constant whenever it is in the localization regime [85]. We

will generalize this result to all even dimensions. The main motivation is to provide physical conditions under which the noncommutative Chern numbers stay quantized.

The quantization and homotopy invariance of an noncommutative Chern number both hold for smooth deformations of the lattice model itself (as opposed to deformations of p), as long as the Fermi level is in a region of localized spectrum. This is characterized by the Aizenman-Molchanov bound on the fractional powers of the Green's function [4]:

$$\int_\Omega dP(\boldsymbol{\omega}) \; |(h - E_F)^{-1}(\boldsymbol{\omega}, \boldsymbol{x})|^s \leq C_s e^{-s\beta|\boldsymbol{x}|}. \tag{4.14}$$

Here, s is any positive number strictly smaller than one, β is a strictly positive parameter which generally depends on E_F, and C_s is a constant that generally depends on s. The symbol $|\cdot|$ on the left hand side, and throughout this section, denotes the matrix norm on $\mathcal{M}_{Q\times Q}$.

The technique based on the fractional powers of the Green's function is one of the most effective tools in the analysis of the localization problem. The bound of Eq. 4.14 has been established for all cases where the localization is known to occur [3], such as at large disorder strength [4] or at the edges of the energy spectrum [1]. Furthermore, the bound can be established algorithmically, in a finite number of steps [2]. This means we can use a computer [70] to explore the localization problem beyond the typical situations mentioned above. We mention that all the characteristics of the localization phenomenon, such as the dynamical localization of the time-evolution operator, spectral localization (i.e the pure point nature of the energy spectrum) or the exponential decay of the eigenstates and of the projector onto the occupied electron states, follow from the bound on the fractional powers of the Green's function [2]. Now, we state the main results in this section:

Proposition 1 [78, 85]. Let h be the random lattice Hamiltonian defined in Eq. 2.10.

1. Assume that the energy spectrum near and at the Fermi level is localized. Then $\|p\|_W < \infty$ and the localization length Λ_n defined in Eq. 4.12 is finite.

2. Let $h' = h + \delta h$ be a deformation of the Hamiltonian h induced by a continuous change of the hopping amplitudes of h_0, of the Fermi energy and of the disorder strength. If the spectrum near and at the Fermi level stays localized, then the deformation of the model generates a continuous homotopy between p and p' in the topology induced by the Sobolev norm $\| \ \|_W$.

The above proposition, combined with the theorem in previous section, immediately allows us to state the physical condition for when the topological quantization of noncommutative Chern numbers is guaranteed.

Corollary [9, 78, 85]. Whenever the Fermi level lies in a region of localized states, the localization length Λ_n (see Eq. 4.12) stays bounded. Then the nth noncommutative Chern number is an integer, its value coincides with the case when disorder and the magnetic field are absense. More, the integer character is robust under smooth deformations of the parameters of the Hamiltonian.

Another way to say this is that: A Noncommutative Chern number is quantized and robust against disorder and the variations of parameters of the Hamiltonian, i.e. B field, hopping terms, as long as the electron states are localized.

4.6 Operator representations

The noncommutative Chern numbers may look exotic, but they can be understood intuitively in the Hilbert space. To see that, we derive their operator representations. A direct use of Eq. 2.16, 2.24 and 2.27 shows that an nth noncommutative Chern number has an operator representation:

$$
\begin{aligned}
Ch_n &= \frac{(2\pi i)^n}{n!} \sum_\sigma (-1)^\sigma \tau \Big(P_\omega \prod_{i=1}^{2n} \big(i[X_{\sigma_i}, P_\omega] \big) \Big) \\
&= \frac{(-2\pi i)^n}{n!} \epsilon^{\sigma_1 \sigma_2 \ldots \sigma_{2n}} \tau \Big(P_\omega [X_{\sigma_1}, P_\omega][X_{\sigma_2}, P_\omega] \ldots [X_{\sigma_{2n}}, P_\omega] \Big),
\end{aligned}
\tag{4.15}
$$

where $P_\omega = \chi_{(-\infty,0]}(H_\omega)$ is the projector onto the occupied states of the Hamiltonian H_ω. The expression here gives us a clear physical picture of the noncommutative Chern numbers. They are nothing but the postion space formulation of the classical topological invariants. In the periodic limit, we see that the noncommutative Chern number reduces to (see Section 2.3):

$$
\begin{aligned}
Ch_n &= \frac{(-2\pi i)^n}{n!} \epsilon^{\sigma_1 \sigma_2 \ldots \sigma_{2n}} \int_{\mathcal{T}^{2n}} \frac{d^{2n} k}{(2\pi)^{2n}} \ \mathrm{tr} \Big\{ \tilde{P}_{\boldsymbol{k}} \frac{\partial \tilde{P}_{\boldsymbol{k}}}{\partial k^{\sigma_1}} \frac{\partial \tilde{P}_{\boldsymbol{k}}}{\partial k^{\sigma_2}} \cdots \frac{\partial \tilde{P}_{\boldsymbol{k}}}{\partial k^{\sigma_{2n}}} \Big\} \\
&= \frac{(-1)^n}{(2\pi i)^n n!} \epsilon^{\sigma_1 \sigma_2 \ldots \sigma_{2n}} \int_{\mathcal{T}^{2n}} d^{2n} k \ \mathrm{tr} \Big\{ \tilde{P}_{\boldsymbol{k}} \frac{\partial \tilde{P}_{\boldsymbol{k}}}{\partial k^{\sigma_1}} \frac{\partial \tilde{P}_{\boldsymbol{k}}}{\partial k^{\sigma_2}} \cdots \frac{\partial \tilde{P}_{\boldsymbol{k}}}{\partial k^{\sigma_{2n}}} \Big\},
\end{aligned}
\tag{4.16}
$$

which is exactly the classical Chern number on a Brillouin $2n$-torus [6] (See Sec. 1.1).

Unlike the $\boldsymbol{k}$-space experssions which can only be obtained from Bloch Hamiltonians, Eq. 4.15 can be computed directly using the real space Hamiltonians Eq. 2.10.

4.7 Summary

In this Chapter, we developed the theory of Chern numbers for aperiodic crystals. This allows us to write down topological invariants that are robust against disorder. They also allow a position operator formulation of Chern numbers. The topological responses can then be computed directly in position space, allowing classification of topological phases in the presense of disorder and an magnetic

field.

As mentioned in the begining of the Chapter, a goal is to understand topological robustness in the strong disorder regime and the existence of bulk extended states. The theory we developed provides the answer to these questions, but only to even dimensions. Since Chern numbers are even dimensional invariants, an interpolation argument between trivial and topological phases are needed to describe odd dimensional systems. For example, in the case of 1D and 3D, polarization and magnetoelectric response are described by 1st and 2nd Chern number via the adiabatic path method. An ambigurity exists in this method regarding to the mobility gap. While disorder can localize states in spatial dimensions, this mechanism is also needed along adiabatic path. This issue are disscussed in details for 1D sytem in next Chapter.

A noncommutative theory of odd dimensional invariants should provide the final answer to this issue. We suggest a way to obtain the Chern-Simons invariant in position space. We can start with the noncommutative magnetization of Schulz-Baldes and Teufel and apply the definition of magnetoelectric coupling $\partial M^j / \partial E_i$ [91]. Afterwards, developing the Freholm theory for odd dimensions would sheld light on the existence of 3D extended states in topological insulators.

The classical Chern numbers have been used to classify some topological phases in the classification table [47, 89, 90]. It is natural to expect that the noncommutative numbers could be used to classify these sytems in the presence of disorder. It will be interesting to work out the explicit connections and write down the noncommutative formulae for the corresponding classes in the table.

Chapter 5

Polarization

We discuss the noncommutative polarization formula of Schulz-Baldes and Teufel [91]. The formula was derived and proven for disordered lattice model under a finite magnetic field. It extends our understanding of polarization to aperiodic systems. In the presence of disorder, we show that the quantization of polarization for an inversion symmetric system can be protected. Numerical confirmations on our arguments are given.

5.1   Introduction

The electric polarization of an inversion-symmetric one dimensional insulator, when counted modulo 2π, can take the trivial value 0 or the non-trivial value π. These values cannot be changed as long as the insulating gap remains open. We demonstrate that the polarization of such system remains quantized and topological in the presence of a generic on-site disorder, which preserves the inversion symmetry only on the average. These topologically robust properties are shown to exist only as long as the spectral gap remains open. Furthermore, we demonstrate that a non-trivially quantized polarization does not require the presence of extended states. In fact, the numerical tests on the Rice-Mele model indicate that all the quantum states become localized immediately after the disorder is turned on, yet the non-trivially quantized polarization survives.

5.2 Settings

We consider a generic disordered one dimensional lattice model $H_{\boldsymbol{\omega}} = H_0 + V_{\boldsymbol{\omega}}$ described by Eq. 2.10, but in the absence of a magnetic field. The translational invariant piece of the Hamiltonian is assumed to depend on a set of N parameters $\boldsymbol{\xi} = (\xi_1, \ldots, \xi_N)$. When needed, we write this dependence explicitly as $H_0(\boldsymbol{\xi})$ or $H_{\boldsymbol{\omega}}(\boldsymbol{\xi})$. The random potential $V_{\boldsymbol{\omega}}$ depends on the disorder configuration $\boldsymbol{\omega}$, which is seen here as a point in a disorder configuration space Ω equipped with a probability measure $dP(\boldsymbol{\omega})$. The system is assumed to be homogeneous, that is, $T_{\boldsymbol{a}} H_{\boldsymbol{\omega}} T_{\boldsymbol{a}}^{-1} = H_{\mathsf{t}_{\boldsymbol{a}} \boldsymbol{\omega}}$ for any lattice translation $T_{\boldsymbol{a}}$. Recall $\mathsf{t}_{\boldsymbol{a}}$'s represent the action of the translations on Ω, assumed ergodic and probability preserving so that Birkhoff's ergodic theorem applies a function $f(\boldsymbol{\omega})$:

$$\lim_{\mathcal{V} \to \infty} \frac{1}{\mathcal{V}} \sum_{\boldsymbol{a} \in \mathcal{V}} f(\mathsf{t}_{\boldsymbol{a}} \boldsymbol{\omega}) = \int_{\Omega} dP(\boldsymbol{\omega}) \, f(\boldsymbol{\omega}). \tag{5.1}$$

The inversion operation, which has the generic form:

$$\mathcal{I} |\boldsymbol{x}, \alpha\rangle = \sum_{\alpha'} R_{\alpha\alpha'} |-\boldsymbol{x}, \alpha'\rangle, \tag{5.2}$$

$$\mathcal{I}^2 = 1, \tag{5.3}$$

generates an action on the parameter space: $\mathcal{I} H_0(\boldsymbol{\xi}) \mathcal{I}^{-1} = H_0(\mathcal{I}\boldsymbol{\xi})$, and an action on the disorder configuration space: $\mathcal{I} V_{\boldsymbol{\omega}} \mathcal{I}^{-1} = V_{\mathcal{I}\boldsymbol{\omega}}$. It is assumed that the latter is probability preserving: $dP(\boldsymbol{\omega}) = dP(\mathcal{I}\boldsymbol{\omega})$. As such, the total Hamiltonian obeys:

$$\mathcal{I} H_{\boldsymbol{\omega}}(\boldsymbol{\xi}) \mathcal{I}^{-1} = H_{\mathcal{I}\boldsymbol{\omega}}(\mathcal{I}\boldsymbol{\xi}). \tag{5.4}$$

These are the generic settings for our studies on polarization. The crucial detail

here is that at the inversion-symmetric points $\boldsymbol{\xi} = \mathcal{I}\boldsymbol{\xi}$, $H_{\boldsymbol{\omega}}(\boldsymbol{\xi})$ is not inversion-symmetric. However, the disorder average of $H_{\boldsymbol{\omega}}(\boldsymbol{\xi})$ and of any function of $H_{\boldsymbol{\omega}}(\boldsymbol{\xi})$ will be inversion symmetric, as it can be formally seen from:

$$\mathcal{I}\left(\int_{\Omega} dP(\boldsymbol{\omega})\, \chi\big(H_{\boldsymbol{\omega}}(\boldsymbol{\xi})\big)\right)\mathcal{I}^{-1} = \int_{\Omega} dP(\boldsymbol{\omega})\, \chi\big(H_{\mathcal{I}\boldsymbol{\omega}}(\boldsymbol{\xi})\big), \tag{5.5}$$

where a change of variable $\mathcal{I}\boldsymbol{\omega} \to \boldsymbol{\omega}$ leads to:

$$\ldots = \int_{\Omega} dP(\mathcal{I}^{-1}\boldsymbol{\omega})\, \chi\big(H_{\boldsymbol{\omega}}(\boldsymbol{\xi})\big) = \int_{\Omega} dP(\boldsymbol{\omega})\, \chi\big(H_{\boldsymbol{\omega}}(\boldsymbol{\xi})\big). \tag{5.6}$$

An explicit yet very general model (see Chapter 2.1) which satisfies all the above conditions is:

$$H_{\boldsymbol{\omega}} = \sum_{\boldsymbol{x},\alpha;\boldsymbol{y},\beta} (t_{\boldsymbol{x}-\boldsymbol{y}}^{\alpha\beta}(\boldsymbol{\xi}) + W\omega_{\boldsymbol{x},\boldsymbol{y}}^{\alpha\beta})|\boldsymbol{x},\alpha\rangle\langle\boldsymbol{y},\beta|, \tag{5.7}$$

where $\omega_{\boldsymbol{x},\boldsymbol{y}}^{\alpha\beta}$ are independent random variables, uniformly distributed in the interval $[-\frac{1}{2}, \frac{1}{2}]$. The collection of all random variables $\boldsymbol{\omega} = \{\omega_{\boldsymbol{x},\boldsymbol{y}}^{\alpha\beta}\}$ can be viewed as a point in an infinite dimensional configuration space Ω, which can be equipped with the probability measure: $dP(\boldsymbol{\omega}) = \prod d\omega_{\boldsymbol{x},\boldsymbol{y}}^{\alpha\beta}$. There is a natural action of the lattice translations on Ω:

$$(\mathsf{t}_{\boldsymbol{a}}\omega)_{\boldsymbol{x},\boldsymbol{y}}^{\alpha\beta} = \omega_{\boldsymbol{x}-\boldsymbol{a},\boldsymbol{y}-\boldsymbol{a}}^{\alpha\beta}, \quad a \in \mathbb{Z}^D, \tag{5.8}$$

which acts ergodically and leaves $dP(\boldsymbol{\omega})$ invariant. The inversion operation induces the action:

$$(\mathcal{I}\boldsymbol{\omega})_{\boldsymbol{xy}}^{\alpha\beta} = \sum_{\alpha'\beta'} \omega_{-\boldsymbol{x},-\boldsymbol{y}}^{\alpha'\beta'} R_{\alpha'\alpha} R_{\beta\beta'}^*, \tag{5.9}$$

and we can verify explicitly that:

$$dP(\mathcal{I}\boldsymbol{\omega}) = dP(\boldsymbol{\omega}). \tag{5.10}$$

5.3 Quantization

By definition, the change in the electric polarization of an adiabatic deformation $H_{\boldsymbol{\omega}}(\boldsymbol{\xi}_t)$ of the Hamiltonian is [46, 83]:

$$\Delta\boldsymbol{\mathcal{P}}_{\boldsymbol{\omega}} = \int_0^T dt \; \boldsymbol{j}_{\boldsymbol{\omega}}(t), \tag{5.11}$$

where $\boldsymbol{j}_{\boldsymbol{\omega}}(t)$ is the density of the charge-current:

$$\boldsymbol{j}_{\boldsymbol{\omega}}(t) = \lim_{\mathcal{V}\to\infty} \frac{1}{\mathcal{V}} \mathrm{Tr}_{\mathcal{V}}\{\rho_{\boldsymbol{\omega}}(t)\boldsymbol{J}_{\boldsymbol{\omega}}(t)\}. \tag{5.12}$$

Assuming that the adiabatic deformation starts from the thermodynamic equilibrium state, the density of states operator at time t is $\rho_{\boldsymbol{\omega}}(t) = U_t \chi_{\mathrm{FD}}(H_{\boldsymbol{\omega}}(\boldsymbol{\xi}_0))U_t^{-1}$, with U_t being the unitary time evolution generated by $H_{\boldsymbol{\omega}}(\boldsymbol{\xi}_t)$ and χ_{FD} being the Fermi-Dirac distribution. Note that, because the fundamental formula in Eq. 5.11 involves the density of the current, a trace over volume appears in Eq. 5.12. This is an important observation because we are going to use Birkhoff's ergodic theorem to demonstrate that $\Delta\boldsymbol{\mathcal{P}}_{\boldsymbol{\omega}}$ is independent of the disorder configuration $\boldsymbol{\omega}$.

Recall for any covariant operator F_{ω} satisfies $T_{\boldsymbol{a}}F_{\boldsymbol{\omega}}T_{\boldsymbol{a}}^{-1} = F_{t_a\boldsymbol{\omega}}$, where T_a is any lattice translation. Then,

$$\begin{aligned}
\lim_{\mathcal{V}\to\infty} \frac{1}{\mathcal{V}} \sum_{\boldsymbol{x}\in\mathcal{V}} \langle\boldsymbol{x}|F_{\boldsymbol{\omega}}|\boldsymbol{x}\rangle &= \lim_{\mathcal{V}\to\infty} \frac{1}{\mathcal{V}} \sum_{\boldsymbol{x}\in\mathcal{V}} \langle 0|F_{t_{\boldsymbol{x}}^{-1}\boldsymbol{\omega}}|0\rangle \tag{5.13} \\
&= \int_{\Omega} dP(\boldsymbol{\omega}) \; \langle 0|F_{\boldsymbol{\omega}}|0\rangle.
\end{aligned}$$

The conclusion is that $\Delta\mathcal{P}_{\boldsymbol{\omega}}$ is self-averaging, and its macroscopic value is equivalent to an average over the disorder configuration space. As such, we can drop the subscript $\boldsymbol{\omega}$ in $\Delta\mathcal{P}_{\boldsymbol{\omega}}$.

We consider now infinitely slow deformations, which are better visualized as paths γ in the parameter space, parametrized as $\{\boldsymbol{\xi}_t\}_{t\in[0,1]}$. By employing the adiabatic theorem, Ref. [91] showed that in the extreme adiabatic limit and when temperature goes to zero:

$$\Delta\boldsymbol{\mathcal{P}}[\gamma] = i \int_0^1 dt \int_\Omega dP(\boldsymbol{\omega}) \ \langle 0|P_{\boldsymbol{\omega}}(\boldsymbol{\xi}_t)[\partial_t P_{\boldsymbol{\omega}}(\boldsymbol{\xi}_t), [\boldsymbol{X}, P_{\boldsymbol{\omega}}(\boldsymbol{\xi}_t)]]|0\rangle, \tag{5.14}$$

where the sum over α is implicit and $P_{\boldsymbol{\omega}}(\boldsymbol{\xi}) = \chi_{(-\infty, E_F]}(H_{\boldsymbol{\omega}}(\boldsymbol{\xi}))$ is the projector onto the occupied states, and $\boldsymbol{X}$ is the position operator. Above, we assumed that the spectral gap of $H_{\boldsymbol{\omega}}(\boldsymbol{\xi}_t)$ remains open for all $t \in [0,1]$. Based on this formula, we can demonstrate that the change in the electric polarization along the path $\mathcal{I}\gamma$ is:

$$\Delta\boldsymbol{\mathcal{P}}[\mathcal{I}\gamma] = -\Delta\boldsymbol{\mathcal{P}}[\gamma]. \tag{5.15}$$

This equality is remarkable because the computation is done at an arbitrary disorder configuration. The proof goes as follows:

$$\Delta\boldsymbol{\mathcal{P}}[\mathcal{I}\gamma] = i \int_0^1 dt \int_\Omega dP(\boldsymbol{\omega}) \ \langle 0|P_{\boldsymbol{\omega}}(\mathcal{I}\boldsymbol{\xi}_t)[\partial_t P_{\boldsymbol{\omega}}(\mathcal{I}\boldsymbol{\xi}_t), [\boldsymbol{X}, P_{\boldsymbol{\omega}}(\mathcal{I}\boldsymbol{\xi}_t)]]|0\rangle, \tag{5.16}$$

and observe that $P_{\boldsymbol{\omega}}(\mathcal{I}\boldsymbol{\xi}_t) = \mathcal{I}P_{\mathcal{I}^{-1}\boldsymbol{\omega}}(\boldsymbol{\xi}_t)\mathcal{I}^{-1}$. Then a change of variable $\mathcal{I}^{-1}\boldsymbol{\omega} \to \boldsymbol{\omega}$ and some manipulations lead to:

$$\Delta\boldsymbol{\mathcal{P}}[\mathcal{I}\gamma] = i \int_0^1 dt \int_\Omega dP(\mathcal{I}\boldsymbol{\omega}) \ \langle 0|\mathcal{I}P_{\boldsymbol{\omega}}(\boldsymbol{\xi_t})[\partial_t P_{\boldsymbol{\omega}}(\boldsymbol{\xi_t}), [-\boldsymbol{X}, P_{\boldsymbol{\omega}}(\boldsymbol{\xi_t})]]\mathcal{I}^{-1}|0\rangle. \quad (5.17)$$

The probability measure is invariant: $dP(\boldsymbol{\omega}) = dP(\mathcal{I}\boldsymbol{\omega})$, and, since the trace is over the orbital degrees of freedom, the action of the remaining $\mathcal{I}$ operators have no effect. Then Eq. 5.15 follows.

We are now ready to assemble the final piece of the argument. Assume that the initial and final Hamiltonians are inversion symmetric. Then any path γ joining the two Hamiltonians can be closed by augmenting it by $-\mathcal{I}\gamma$, where the minus sign imply that the path is walked in reverse. Using Eq. 5.15, we see:

$$\Delta\boldsymbol{\mathcal{P}}[\gamma] = \frac{1}{2}\big(\Delta\boldsymbol{\mathcal{P}}[\gamma] + \Delta\boldsymbol{\mathcal{P}}[-\mathcal{I}\gamma]\big) = \frac{1}{2}\Delta\boldsymbol{\mathcal{P}}[\gamma - \mathcal{I}\gamma]. \quad (5.18)$$

But as already noted in [91], the change in the polarization along a closed loop leads to the noncommutative Chern number [9]. The conclusion is:

$$\Delta P_j[\gamma] = \frac{1}{2}Ch_1[(\gamma - \mathcal{I}\gamma) \times \mathcal{T}_j], \ j = 1, \ldots, D, \quad (5.19)$$

where $Ch_1[(\gamma - \mathcal{I}\gamma) \times \mathcal{T}_j]$ is the Chern number over the space $(\gamma - \mathcal{I}\gamma)$ times the section of the noncommutative Brillouin torus along the jth direction. This proves the quantization of the electric polarization in our general settings. Similarly, we can immediately see that charge transported in one cycle ΔQ is quntized without the use of symmetry [91, 101]:

$$\Delta Q_j = Ch_1[\mathcal{S}_1 \times \mathcal{T}_j] \quad (5.20)$$

5.4 Invariance

In two dimensional models, the quantization and the homotopy invariance of the noncommutative Chern number is protected by the mobility gap [9]. This means the Ch_1 can take non-fluctuating integer values even after the spectral gap was closed and the Fermi level is buried in a dense localized spectrum. Does this imply that the quantization and the homotopy invariance of the electric polarization holds as long as a mobility gap stays open? Then, a standard argument will show that extended states must exist whenever a $\mathcal{P}_j$ is half-integer.

Unfortunately, a simple but mostly overlooked fact prevents this to happen. The Chern number appearing in Eq. 5.19 is that of a fictitious two dimensional system, described by the Hamiltonian $H_{2d} = H_{\boldsymbol{\omega}}(\boldsymbol{\xi}_t)$, acting on wave-functions $\psi(t, n_j)$. The crucial observation is that the disorder is only on the n_j variable, while the t variable is smooth. This imply that, regardless of the disorder strength in the physical system, the spectrum of H_{2d} will always be continuous. As a result, if the Fermi level touches the spectrum of the physical system, it will be automatically in the continuous spectrum of the the two dimensional fictitious system and Ch_1 will loose its topological properties. This leads us to two conclusions:

1. The polarization cannot be expected to stay quantized once the spectral gap of the physical system closes.

2. Non-trivial quantized values of the polarization can occur even if all the states of the physical model are localized.

5.5 Numerical confirmation

For a one dimensional topological system, it is associated with the existence of end states or a zero energy mode. Here we consider a disordered Rice-Mele model [84]:
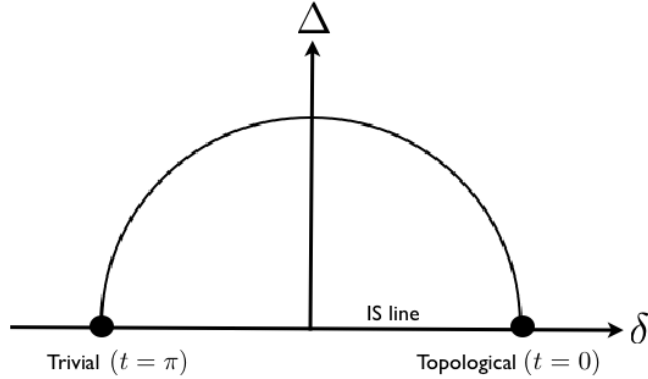
Figure 5.1: For the following parameters: $\delta = 0.1cos(t)$ and $\Delta = 0.1sin(t)$, the adiabatic parameter t connects the topological phase $(t = 0)$ and the trivial phase $(t = \pi)$ of the model Eq. 5.21. IS line represent the inversion symmetric line where the Hamiltonians are inversion symmetric. Along the axis, the gap closes at the orgin where a topological phase transition occurs. The inversion symmetry is broken and a finite spectral gap is ensured by Δ along the adiabatic path.

$$H = \sum_j \left(\frac{1}{2} + (-1)^j \frac{\delta}{2}\right)(|j\rangle\langle j+1| + h.c.) + \left(\Delta(-1)^j + W\omega_j\right)|j\rangle\langle j|, \quad (5.21)$$

where j is a lattice site, δ is the dimerization order and Δ is a staggered sublattice potential. ω_j represents a random number belonging to $[-\frac{1}{2}, \frac{1}{2}]$ and W denote the disorder strength. Note that when $\Delta = 0$ this Hamiltonian reduces to the Su-Shrieffer-Heeger model [100].

In Fig. 5.2, the Chern number, polarization and the spectral gap are mapped as function of disorder strength. Note that the Chern number is obtained by an adiabatic deformation where the spectral gap is kept open and the polarization is in fact the polarization difference between a topological phase and a trivial phase (see Fig. 5.1). In Fig. 5.2(a), in the case of lattice size $N = 100$ the Chern number and polarization present clear quantum plateaus at the weak disorder, which are 1 and π, respectively. By increasing the disorder strength, both the

Chern number and polarization plateaus begin to get worse at $W = 0.6$ and deviate from the quantized value. It is worth noting that the quantization of the Chern number and polarization is destroyed exactly when the spectral gap is closing in Fig. 5.2(b), which is fully computed along the adiabatic loop of the parameter t. In Fig. 5.2(c), the varying range of the spectrum gap along the t parameter from 0 to 2π is also given.
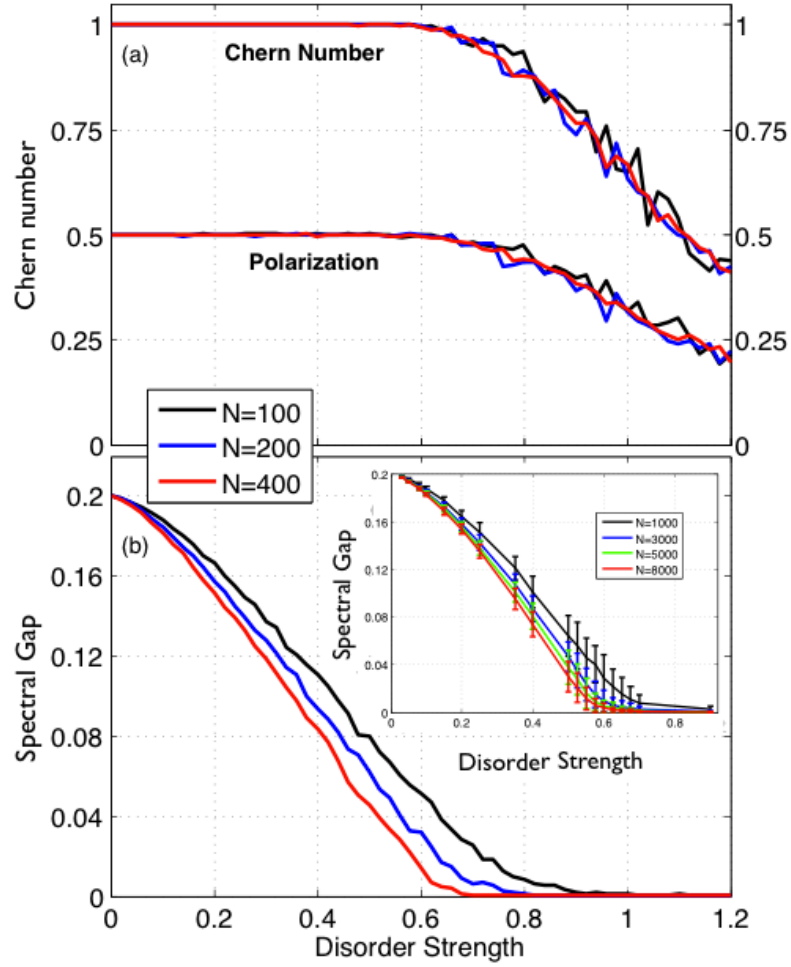
Figure 5.2: (a) Computation of the Chern number and polarization, and (b) of the spectral gap in the space of the t parameter, (c) represents the variation of the gap with changing t from 0 to 2π in the case of the lattice size $N = 400$. The other parameters are set as: $\delta_0 = -0.10$, $\Delta_0 = 0.10$, $\delta = \delta_0 \cos t$, $\Delta = \Delta_0 \sin t$, and the gap is averaged over 100 disorder configurations.

A general concept is that a topological quantized number in a 2D system is always accompanied by the extended bulk states and disappears when the mobility gap closes at strong disorder. A intriguing question is whether or not we can forward this conclusion to 1D system. To find the answer, in Fig. 5.3 we studied the variance of the energy level statistics (EnS) due to disorder, which has been prove to be an effective tool to characterize the extended state.

More importantly, as shown in Fig. 5.2(a), the quantized plateau of the Chern number and polarization do not change when increasing the lattice site from $N = 100$ to 400. Moreover, the spectral gap closing point or the transition point gradually approaches $W = 0.6$ with increasing the lattice size to $N = 400$. This scaling simulation illustrates that in the thermodynamic limit a topological phase transition will happen and the phase transition point is fixed at about $W = 0.6$.

As show in Fig. 5.3(a) with $N = 1000$, the variance of EnS at a weak disorder $W = 0.03$ almost touches the ideal value of 0.178 (the dotted line) at about $E_F = -1(1)$ which is nearby the bottom (top) of the valence (conduction) band. By increasing the disorder strength further, this touching point moves gradually toward the spectral gap. However at the disorder strength $W = 0.15$ the variance of EnS begins to move away from the dotted line of 0.178 and this deviation becomes more obvious for $W = 0.20$ and 0.25. A subsequent question is why the levitation and annihilation between the 'extended states' of valence and conduction bands never happens like in 2D case.

More intriguingly, the variance of EnS exhibits obvious changes when increasing the lattice size to 3000 (b) and 8000 (c). In particular, the variance of EnS deviates from the ideal value of 0.178 for the stronger disorder beyond $W = 0.08$ in Fig. 5.3(b) with $N = 3000$. Furthermore, this critical disorder strength is decreased to $W = 0.05$ when changing the lattice size to $N = 8000$. Comparing all corresponding lines in the cases of $N = 1000$, 3000 and 8000, it is not difficult to get a conclusion: In the thermodynamic limit the entire variance of Ens will

move away from the ideal line of 0.178, which exactly implies that no extended state exists in this 1D disordered Hamiltonian.

In Fig. 5.4, we study the variance of the level statistics for different δ. Based on the simple discussion above, the topological property of the Su-Shrieffer-Heeger model is completely determined by the sign of δ. In principle, the variance of EnS should behave differently in the two cases, namely with a negative and positive δ. Unexpectedly, when changing δ from -0.1 to 0.1 and meanwhile keeping $W = 0.5$ in Fig. 5.4, the variance of EnS keeps almost invariant. Moreover, this result holds true even increasing the lattice size from $N = 1000$ to 8000. It is worth noting that the Chern number and polarization are still quantized at the disorder strength $W = 0.5$ in Fig. 1. Fig. 5.3 and Fig. 5.4 demonstrates that there are indeed no extended states in the present 1D model, when the Chern number and polarization manifest a nonzero quantized value.

5.6   Summary

In summary, we studied the disordered Rice-Mele model numerically. We found that by increasing the disorder strength, the Chern number and polarization gradually change from a quantized value to zero. It exhibits a clear phase transition from the topological phase to the trivial phase. In sharp contrast to what is believed that a quantized topological number is always carried by extended states, no such bulk states appears in our model Eq. 5.21. All quantum states become localized immediately after the disorder is turned on, yet the non-trivial quantized polarization remains.
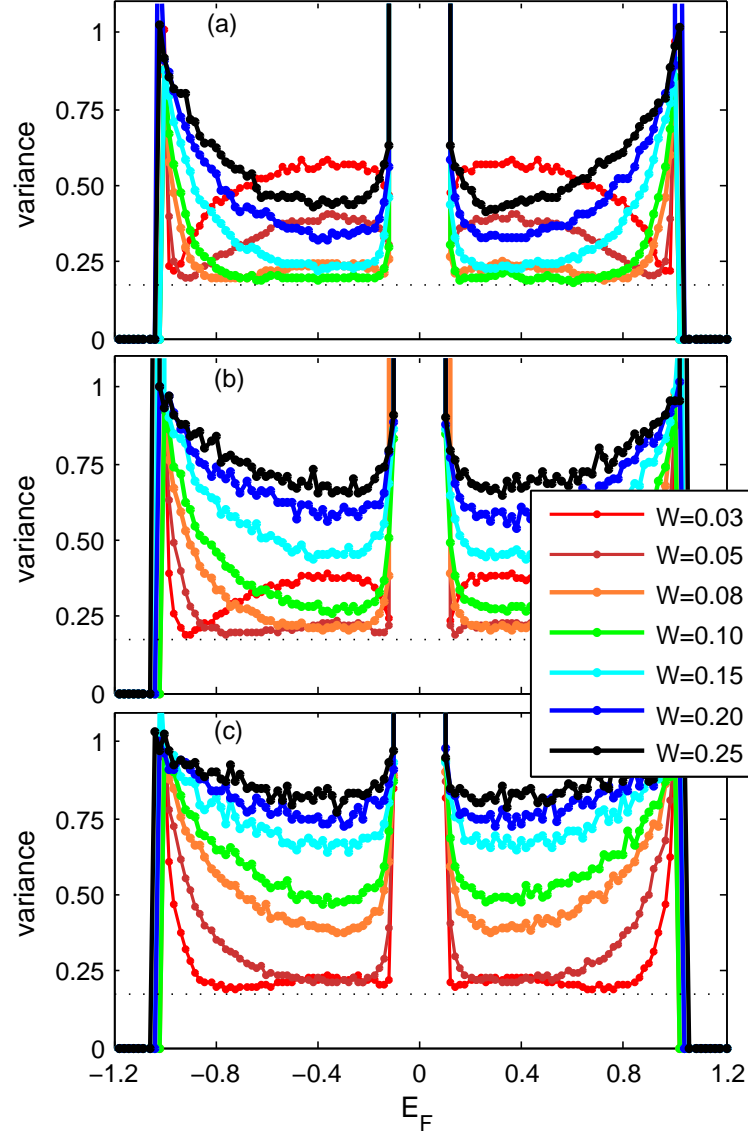
Figure 5.3: The variance of energy level spacing are given in three cases: (a) $N = 1000$, (b) $N = 3000$, and (c) 8000, respectively. The parameters are set as: $\delta = -0.1$, $\Delta = 0$, and the average is over 100 disorder configurations.
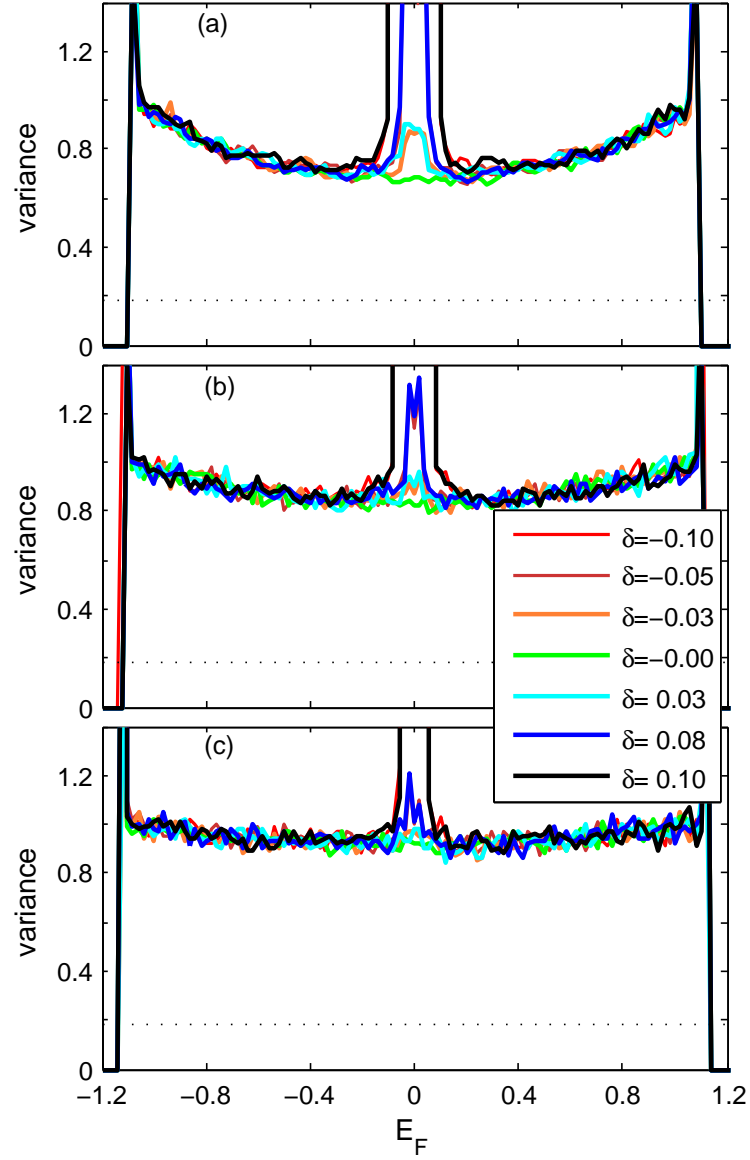
Figure 5.4: The variance of energy level spacing are given in three cases: (a) $N = 1000$, (b) $N = 3000$, and (c) 8000, respectively. The parameters are set as: $W = 0.5$, $\Delta = 0$, and the average is over 100 disorder configurations.

Chapter 6

Robustness of $\mathbb{Z}_2$ invariant

We study the effect of strong disorder in a three dimensional topological insulators with time-reversal symmetry and broken inversion symmetry. First, using level statistics analysis, we demonstrate the persistence of delocalized bulk states even at large disorder. The delocalized spectrum is seen to display the levitation and pair annihilation effect, indicating that the delocalized states continue to carry the $\mathbb{Z}_2$ invariant after the onset of disorder. Second, the $\mathbb{Z}_2$ invariant is computed via twisted boundary conditions using an efficient numerical algorithm. We demonstrate that the $\mathbb{Z}_2$ invariant remains quantized and non-fluctuating even after the spectral gap becomes filled with dense localized states. Our results indicate that the $\mathbb{Z}_2$ invariant remains quantized until the mobility gap closes or until the Fermi level touches the mobility edges. Based on such data, we compute the phase diagram of the Bi_2Se_3 topological material as function of disorder strength and position of the Fermi level.

6.1 Introduction

In the presence of time-reversal symmetry, topological insulators follow a $\mathbb{Z}_2$ topological classification. The strong $\mathbb{Z}_2$ invariant that renders an insulator as either trivial or topological was computed in various ways, but in general the computations were quite demanding because they had to be carried out with special

smooth gauges. The difficulty introduced by this requirement has been documented in Ref. [74]. For example, the original expressions of the $\mathbb{Z}_2$ invariant [26–28, 45], require special smooth gauges and were computed only for analytically solvable band models. These expressions have been reformulated in an almost gauge invariant fashion by Fukui and his collaborators [29, 40]. The method still requires a time-reversal adapted gauge at the boundary of half of the Brillouin zone, but nevertheless it became the method of choice when computing the $\mathbb{Z}_2$ invariant [20, 23, 24, 97, 105, 107]. An application of the method to the disordered case exists only in 2D [20]. The Chern-Simons integral of the quantized magnetoelectric polarization also requires a globally smooth gauge [79]. The difficulties introduced by this requirement were highlighted in Ref. [13].

The issue was recently reconsidered and gauge-independent formulations of the weak and strong $\mathbb{Z}_2$ invariants are now available [74, 86, 96, 97, 112]. Here we will follow Ref. [74] and argue here that this new formulations bring certain numerical advantages which open the possibility of directly computing the $\mathbb{Z}_2$ invariants for systems with large unit cells, particularly for disordered samples. We present a numerical analysis of the strong $\mathbb{Z}_2$ invariant for a system without inversion symmetry, computed in the weak and strong disorder regimes via the twisted boundary conditions technique combined with the new formulation of the invariant. The use of the twisted boundary conditions was advocated by Kane and Mele in their original discussion of the 2D $\mathbb{Z}_2$ invariant as an effective procedure for tackling the effect of disorder and electron-electron interaction [45]. Numerically, this method is equivalent to computing the $\mathbb{Z}_2$ invariant for a periodic system with a very large unit cell, leading to thousands of occupied energy bands. Finding smooth special gauges for such complex band structures is prohibitively difficult, which is why computing the $\mathbb{Z}_2$ invariant is notoriously difficult for disordered 3D topological insulators (the parity analysis was done for a system and disorder with inversion symmetry [33]).

Working with a tight-binding model for the 3D topological material Bi_2Se_3, we provide compelling evidence that the strong $\mathbb{Z}_2$ invariant remains well-defined and quantized even after the insulating gap becomes filled with a dense localized spectrum. Our various mappings of the $\mathbb{Z}_2$ invariant indicate that the quantization holds as long as the Fermi level remains in the mobility gap. Furthermore, we use level statistics analysis to map the localized or extended character of the energy spectrum for a wide range of disorder strength. The results show compelling evidence that there are bulk metallic states that persist even at strong disorder and we derive the phase diagram of the 3D model as function of Fermi level and disorder strength. The phase diagram consists of the strong topological phase, which is completely surrounded by a metallic phase, which is again surrounded by the trivial insulating phase. Computations of the $\mathbb{Z}_2$ invariant along paths that cross from the topological into the trivial insulating phase reveal strict quantization of the invariant to ± 1 values in the topological/trivial insulating phases, respectively, and strong fluctuations between ± 1 inside the metallic phase.

The motivation behind the present study was three-fold. First, there is no theory of the $\mathbb{Z}_2$ invariant for aperiodic systems (except for the trivial case when the Fermi level is in a spectral gap, i.e. a region that is void of any energy spectrum). For example, for Chern and spin Chern invariants we have theories that provide explicit and specific conditions, which can be written in one line, that tells us when these invariants take quantized values even if the Fermi level is not in a spectral gap [9, 73]. Furthermore, we have position formulations of these two invariants [73, 77], which allows us to compute them in "one shot" without involving twisted boundary conditions. Nothing like that exists for the strong $\mathbb{Z}_2$ invariant, despite some sustained efforts. This makes us to question that the strong $\mathbb{Z}_2$ invariant does indeed remain quantized once the spectral gap is closed. Our numerical study provides the first direct evidence that the strong $\mathbb{Z}_2$ invariant behaves similarly with these other two invariants, which can be a

strong motivation for people to continue searching for a theory of the strong $\mathbb{Z}_2$ invariant for aperiodic systems.

Second, it is known that disorder can strongly deform the phase boundary of the topological state [32, 34, 55, 75]. It is highly desired to devise quantitative methods that can accurately pinpoint the extent of the topological phases. Previously, the strong topological phase was identified by probing the metallic character of the surface states via transport calculations in a long bar geometry [34]. For the special case when the system and the disorder have inversion symmetry, the topological phase was identified using the parities of the states [33]. Ideally, it will be to directly map the strong $\mathbb{Z}_2$ invariant and our study demonstrates that this is indeed possible for 3D materials.

Last, we want to state that our numerical simulations probe uncharted territories. Our method, and for that matter all the established methods, are easily seen to produce quantized and non-fluctuating $\mathbb{Z}_2$ values, if a spectral gap between the occupied and non-occupied levels remains open at all times while twisting of the boundary conditions. However, at strong disorder, the spectral gap not only closes but the levels can change their ordering when twisting the boundary conditions. Thus, levels that once were occupied become unoccupied and vice-versa. Different disorder configurations can no longer be connected adiabatically. While our numerical procedure can still be applied in these situations, the available theoretical arguments can no longer assure us that the output remains the same from one disorder configuration to another (this also applies to the Bott index of Refs. [39, 58]).

6.2 $\mathbb{Z}_2$ invariant

We start our discussion with a review of the $\mathbb{Z}_2$ invariant [74]. The connection between this formulation and the existing ones can be found in the reference.
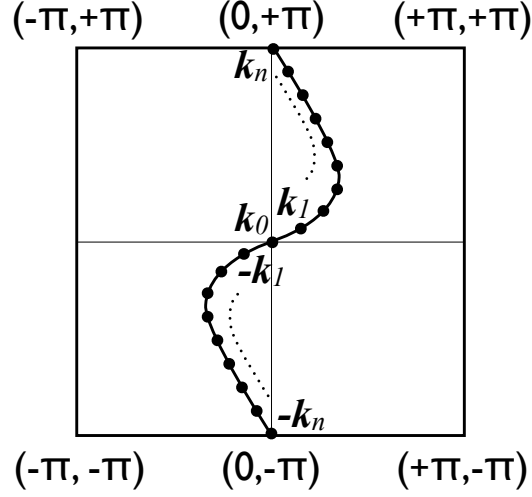
Figure 6.1: Example of a time-reversal invariant path in the Brillouin torus and its discretization.

Instead, we will give a detailed discussion of the numerical advantages brought in by this new method.

The method goes as follows. Let $P_{\boldsymbol{k}}$ denote the projector on to the states of $H_{\boldsymbol{\omega}}(\boldsymbol{k})$ below the Fermi level E_F, and let θ denote the time-reversal operation and assume the time-reversal invariance:

$$\theta H_{\boldsymbol{\omega}}(\boldsymbol{k})\theta^{-1} = H_{\boldsymbol{\omega}}(-\boldsymbol{k}). \tag{6.1}$$

We consider a closed, time-reversal invariant path (i.e. a path which is mapped into itself by θ) on the Brillouin torus,

$$[-\pi, \pi] \ni k \to \boldsymbol{k}(k), \tag{6.2}$$

parametrized by the variable k (we chose the notation on purpose because in practice this variable will often be k_z for example). Then we integrate the differential equation (with the initial condition $U_{k',k'} = P_{\boldsymbol{k}(k')}$):

$$i\tfrac{d}{dk}U_{k,k'} = i[P_{\boldsymbol{k}(k)}, \partial_k P_{\boldsymbol{k}(k)}]U_{k,k'}. \tag{6.3}$$

We will use the simplified notation: $P_{\boldsymbol{k}(k)} = P_k$. The result of the integration gives the unitary time evolution operator $U_{k,k'}$ corresponding to the process of adiabatically changing the $\boldsymbol{k}$-vector along the chosen path in the Brillouin torus. It is assumed that the path starts ($k = -\pi$) and closes ($k = \pi$) at a time-reversal invariant $\boldsymbol{k}$-point. Necessarily, the path will cross another time-reversal invariant point at midway $k = 0$ (see Fig. 3.1). Next, we consider arbitrary bases $\{e_\alpha^0\}$ and $\{e_\alpha^\pi\}$ for the occupied spaces at the time-reversal invariant points $k = 0$ and $k = \pi$, respectively, and we define the following matrices:

$$\hat{U}_{\alpha\beta} = \langle e_\alpha^\pi | U_{\pi,0} | e_\beta^0 \rangle,$$

$$\hat{\theta}^0_{\alpha\beta} = \langle e_\alpha^0 | \theta | e_\beta^0 \rangle, \tag{6.4}$$

$$\hat{\theta}^\pi_{\alpha\beta} = \langle e_\alpha^\pi | \theta | e_\beta^\pi \rangle.$$

These matrices satisfy the following fundamental relation [74]:

$$\frac{\mathrm{Pf}\{\hat{\theta}_\pi\}^{-1} \det\{\hat{U}\} \mathrm{Pf}\{\hat{\theta}_0\}}{\sqrt{\det\{U_{\pi,-\pi}\}}} = \pm 1. \tag{6.5}$$

The left hand side of Eq. 6.5 will be called a pseudo $\mathbb{Z}_2$ invariant for the following reasons. The left hand side is gauge independent. Given the transformation properties of the Pfaffians and determinants under the conjugation with unitary matrices, we can easily see that the numerator is independent of the bases $\{e_\alpha^0\}$ and $\{e_\alpha^\pi\}$ [74]. At the denominator, inside the square root, $U_{\pi,-\pi}$ maps the $k = \pm\pi$ occupied space into itself, so at a change of $\{e_\alpha^\pi\}$ basis we have $U_{\pi,-\pi} \to EU_{\pi,-\pi}E^{-1}$, with E a unitary matrix, so the determinant remains unchanged. However, the sign in Eq. 6.5 depends on which branch of the square root is used, but once a choice is made the value of the left-hand side cannot

be changed by smooth deformations of the Bloch Hamiltonians that keep the insulating gap opens.

The adiabatic evolution operators is computed by discretizing the paths and taking the product of projectors onto the occupied spaces at these discrete k-points. Since the path is time-reversal invariant, we can choose the discretization points so as $\boldsymbol{k}_0$, $\boldsymbol{k}_1$, ..., $\boldsymbol{k}_n$ discretizes the path from $k = 0$ to $k = \pi$, while $-\boldsymbol{k}_n$, $-\boldsymbol{k}_{n-1},\ldots,\boldsymbol{k}_0$ discretizes the path from $k = -\pi$ to $k = 0$. In this case:

$$U_{\pi,-\pi} = \lim_{n\to\infty} P_{\boldsymbol{k}_n} P_{\boldsymbol{k}_{n-1}} \ldots P_{\boldsymbol{k}_0} \ldots P_{-\boldsymbol{k}_{n-1}} P_{-\boldsymbol{k}_n}. \tag{6.6}$$

In practice, we have to stop limit at some $n = \bar{n}$ and work with an approximation:

$$U_{\pi,-\pi} = P_{\boldsymbol{k}_{\bar{n}}} P_{\boldsymbol{k}_{\bar{n}-1}} \ldots P_{\boldsymbol{k}_0} \ldots P_{-\boldsymbol{k}_{\bar{n}-1}} P_{-\boldsymbol{k}_{\bar{n}}}, \tag{6.7}$$

and similar for $U_{\pi,0}$:

$$U_{\pi,0} = P_{\boldsymbol{k}_{\bar{n}}} P_{\boldsymbol{k}_{\bar{n}-1}} \ldots P_{\boldsymbol{k}_0}. \tag{6.8}$$

We are going to show in the following that the quantization in Eq. 6.5 remains exact even for finite $\bar{n}$'s.

Using the elementary fact that $\theta P_{\boldsymbol{k}_j} \theta^{-1} = P_{-\boldsymbol{k}_j}$, we have:

$$U_{\pi,-\pi} = P_{\boldsymbol{k}_{\bar{n}}} P_{\boldsymbol{k}_{\bar{n}-1}} \ldots P_{\boldsymbol{k}_0} \theta P_{\boldsymbol{k}_0} \ldots P_{\boldsymbol{k}_{\bar{n}-1}} P_{\boldsymbol{k}_{\bar{n}}} \theta^{-1} \tag{6.9}$$

Inserting the identity operator $\sum_\alpha |e_\alpha^0\rangle\langle e_\alpha^0|$ at the appropriate places, we obtain:

$$\begin{aligned}
\langle e_\alpha^\pi | U_{\pi,-\pi} | e_\beta^\pi \rangle &= \langle e_\alpha^\pi | P_{\boldsymbol{k}_{\bar{n}}} P_{\boldsymbol{k}_{\bar{n}-1}} \ldots P_{\boldsymbol{k}_0} | e_\delta^0 \rangle \langle e_\delta^0 | \theta | e_\gamma^0 \rangle \\
&\quad \times \overline{\langle e_\gamma^0 | P_{\boldsymbol{k}_0} \ldots P_{\boldsymbol{k}_{\bar{n}-1}} P_{\boldsymbol{k}_{\bar{n}}} | e_\xi^\pi \rangle \langle e_\xi^\pi | \theta^{-1} | e_\beta^\pi \rangle} \\
&= \langle e_\alpha^\pi | P_{\boldsymbol{k}_{\bar{n}}} P_{\boldsymbol{k}_{\bar{n}-1}} \ldots P_{\boldsymbol{k}_0} | e_\delta^0 \rangle (\hat{\theta}_0)_{\delta\gamma} \\
&\quad \times \langle e_\xi^\pi | P_{\boldsymbol{k}_{\bar{n}}} P_{\boldsymbol{k}_{\bar{n}-1}} \ldots P_{\boldsymbol{k}_0} | e_\gamma^0 \rangle (\hat{\theta}_\pi^{-1})_{\xi\beta}.
\end{aligned} \tag{6.10}$$

Summation over repeating indices was assumed above. At this step, the conclusion is:

$$U_{\pi,-\pi} = \hat{U}\hat{\theta}_0\hat{U}^T\hat{\theta}_\pi^{-1}. \tag{6.11}$$

Taking the determinant and using the elementary properties of the determinants and pfaffians we obtain:

$$\det\{U_{\pi,-\pi}\} = [\mathrm{Pf}\{\hat{\theta}_\pi\}^{-1}\det\{\hat{U}\}\mathrm{Pf}\{\hat{\theta}_0\}]^2, \tag{6.12}$$

which is precisely Eq. 6.5.

The significance of the above conclusion for the numerical calculations is that it allows us to use relatively small number of discretization points when evaluating Eq. 6.5. One question that could be asked is if the result of such calculation, while indeed quantized, it really equals the result in the $\bar{n} \to \infty$ limit? To answer this question, we imagine a calculation with a dense number of discretization points and then adiabatically collapsing pairs of adjacent discretization points into a single discretization point. In this way we can adiabatically transform the original computation into a computation with half the number of discretized points. Repeating the same action we can adiabatically reduce the number of discretization points even further, by 4, 8 and so on. Since Eq. 6.5 is quantized, it cannot change its value during such adiabatic deformations, if all the quantities remain well-defined.

What can go wrong? In the $\bar{n} \to \infty$ limit, $U_{\pi,-\pi}$ is a true unitary operator so its determinant is a complex number on the unit circle. For finite $\bar{n}$, $U_{\pi,-\pi}$ is no longer unitary and its determinant moves inside the unit circle. As the number of discretization points is reduced, the determinant moves closer to the origin so there is the possibility that $\det\{U_{\pi,-\pi}\}$ actually becomes equal to zero. At such instance, the calculation breaks down and the quantized value of Eq. 6.5

can change. So the conclusion is that Eq. 6.5 can be indeed evaluated using a relatively small number of discretization points, as long as we make sure that $\det\{U_{\pi,-\pi}\}$ does not touches the origin. For our computation, we choose the number of discretized points so that $|\det\{U_{\pi,-\pi}\}| \approx 0.5$, which reduces the number of required k-points by an order of magnitude in our calculations, when compare with the case when $|\det\{U_{\pi,-\pi}\}| \approx 0.9$.

Eq. 6.5 cannot define a $\mathbb{Z}_2$ invariant by itself. That is because we don't have a canonical way to choose the branch of the square root at the denominator of Eq. 6.5. An important observation is that if we consider a pair of paths, then there is a canonical way to choose the same branch of the square root and genuine $\mathbb{Z}_2$ invariants can be defined. This has been detailed in Ref. [74]. The following lines explain how the procedures were explicitly implemented in our calculations.

For a 3D system, we consider 4 independent time-reversal invariant paths. If $\mathcal{P}_{k_x,k_y}$ denotes the path along k_z direction that intersects the plane $k_z = 0$ at (k_x, k_y), then we choose the following 4 paths:

$$
\begin{aligned}
\mathcal{P}_{0,0} &: \ (0, 0, -\pi) \rightarrow (0, 0, \pi) \\
\mathcal{P}_{0,\pi} &: \ (0, \pi, -\pi) \rightarrow (0, \pi, \pi) \\
\mathcal{P}_{\pi,0} &: \ (\pi, 0, -\pi) \rightarrow (\pi, 0, \pi) \\
\mathcal{P}_{\pi,\pi} &: \ (\pi, \pi, -\pi) \rightarrow (\pi, \pi, \pi),
\end{aligned}
\tag{6.13}
$$

We interpolated between the paths $\mathcal{P}_{0,0}$ and $\mathcal{P}_{0,\pi}$ using the process:

$$
[0, \pi] \ni k_y \rightarrow \mathcal{P}_{0,k_y}.
\tag{6.14}
$$

By computing the adiabatic evolution

$$
U_{(0,k_y,-\pi)\rightarrow(0,k_y,\pi)}
\tag{6.15}
$$

for the path $\mathcal{P}_{0,k_y}$, we continuously interpolate between the determinants

$$\det\{U_{(0,0,-\pi)\to(0,0,\pi)}\} \quad \leftrightarrow \quad \det\{U_{(0,\pi,-\pi)\to(0,\pi,\pi)}\}, \tag{6.16}$$

using the process:

$$[0,\pi] \ni k_y \to \det\{U_{(0,k_y,-\pi)\to(0,k_y,\pi)}\}. \tag{6.17}$$

This allows us to monitor how the determinant moves on the Riemann surface of the square root function, and to determine the location of $\det\{U_{(0,\pi,-\pi)\to(0,\pi,\pi)}\}$ relative to the location of $\det\{U_{(0,0,-\pi)\to(0,0,\pi)}\}$ on the Riemann surface. If the semi-axis $(-\infty,0)$ is crossed by the $\det\{U_{(0,k_y,-\pi)\to(0,k_y,\pi)}\}$ an odd number of times, then the determinants are located on opposite Riemann sheets and we have to use different branches of the square root, that is, we will have to use $\pm\sqrt{z}$ for one determinant and $\mp\sqrt{z}$ for the other determinant in Eq. 6.16 when we evaluate the denominator of Eq. 6.5. If $\det\{U_{(0,k_y,-\pi)\to(0,k_y,\pi)}\}$ crosses the semi-axis $(-\infty,0)$ an even number of times, then the determinants are located on the same Riemann sheet and we have to use $\pm\sqrt{z}$ for one determinant and same $\pm\sqrt{z}$ for the other determinant. There is still a sign ambiguity remaining (originally we had two sign ambiguities) but that becomes irrelevant if we form the product of two pseudo-invariants. Indeed, the following quantity:

$$\begin{aligned}
\Xi_0 &= \frac{\mathrm{Pf}\{\hat{\theta}_{(0,0,\pi)}\}^{-1} \det\{\hat{U}_{(0,0,0)\to(0,0,\pi)}\}\mathrm{Pf}\{\hat{\theta}_{(0,0,0)}\}}{\sqrt{\det\{U_{(0,0,-\pi)\to(0,0,\pi)}\}}} \\
&\quad \times \frac{\mathrm{Pf}\{\hat{\theta}_{(0,\pi,\pi)}\}^{-1} \det\{\hat{U}_{(0,\pi,0)\to(0,\pi,\pi)}\}\mathrm{Pf}\{\hat{\theta}_{(0,\pi,0)}\}}{\sqrt{\det\{U_{(0,\pi,-\pi)\to(0,\pi,\pi)}\}}}
\end{aligned}$$

is a genuine invariant taking the quantized values ± 1, which are independent of the branch of the square roots used in the calculation, as long as they are chosen consistently using the interpolating procedure described above. We can repeat

the same construction for the pair of paths $\mathcal{P}_{\pi,0}$ and $\mathcal{P}_{\pi,\pi}$ and define the invariant:

$$
\begin{aligned}
\Xi_\pi = & \frac{\mathrm{Pf}\{\hat{\theta}_{(\pi,0,\pi)}\}^{-1}\det\{\hat{U}_{(\pi,0,0)\to(\pi,0,\pi)}\}\mathrm{Pf}\{\hat{\theta}_{(\pi,0,0)}\}}{\sqrt{\det\{U_{(\pi,0,-\pi)\to(\pi,0,\pi)}\}}} \\
& \times \frac{\mathrm{Pf}\{\hat{\theta}_{(\pi,\pi,\pi)}\}^{-1}\det\{\hat{U}_{(\pi,\pi,0)\to(\pi,\pi,\pi)}\}\mathrm{Pf}\{\hat{\theta}_{(\pi,\pi,0)}\}}{\sqrt{\det\{U_{(\pi,\pi,-\pi)\to(\pi,\pi,\pi)}\}}}.
\end{aligned}
$$

The invariants Ξ_0 and Ξ_π are two of the four independent weak $\mathbb{Z}_2$ invariants. We can define two more weak invariants by pairing the paths in different ways, but that is not necessary because at this point we can define the strong $\mathbb{Z}_2$ invariant as:

$$
\Xi = \Xi_0\Xi_\pi \tag{6.18}
$$

If we count the strong $\mathbb{Z}_2$ invariant, then there are only 3 independent weak $\mathbb{Z}_2$ invariants remaining. We will concentrate entirely on the strong invariant.

We have already discussed the numerical aspects related to computing the $\mathbb{Z}_2$ pseudo-invariants for each of the four paths of Eq. 6.13. There is another important numerical aspect about determining the correct branch of the square roots. We should note that computing the pseudo-invariants involves one dimensional calculations, in the sense that we only need to integrate along the k_z direction and not on a surface as it is the case when applying, for example, the popular algorithm of Fukui et al from Ref. [40]. However, we still have to perform the interpolation along the k_y direction, so the calculations become two dimensional.

The key observation is that the number of k_y points required by a successful interpolation is usually an order of magnitude smaller than the number of k_z points needed in the computation of the pseudo-invariants. This is because all we need is to determine how the determinants wind around the origin during the interpolation and to trace these paths we can indeed use a relatively small number of k_y points. Therefore, our algorithm, while not strictly one dimensional, it can

be regarded as quasi-one dimensional.

To summarize, the application to the disordered system was possible because of the following numerical advantages of the present algorithm:

1. The algorithm is gauge independent. Finding a smooth gauge for a unit cell containing thousands of quantum states would have been practically impossible.

2. The quantization of the pseudo-invariants remain exact when the paths are discretized, allowing a drastic reduction of the number of the discretization points.

3. The interpolation between the different time-reversal invariant paths can be accomplished with a small number of k-points, transforming the algorithm into a quasi-one dimensional one.

6.3   The model

The model used in our numerical simulations is an effective lattice Hamiltonian fited to the topological material Bi_2Se_3. This H_0 was used in the previous studies of disordered Bi_2Se_3 in Refs. [33, 34]. The H_0 has inversion symmetry and, since we want to exemplify the algorithms for systems without such symmetry, we will include an additional term in the Hamiltonian that strongly breaks the inversion symmetry. This term can be thought as the effect of a mechanical strain applied along the z axis.

In the momentum space:

$$H_0(\boldsymbol{k}) = d_4(\boldsymbol{k}) + \begin{pmatrix} d_0(\boldsymbol{k}) & d_3(\boldsymbol{k}) & 0 & d_-(\boldsymbol{k}) \\ d_z(\boldsymbol{k}) & -d_0(\boldsymbol{k}) & d_-(\boldsymbol{k}) & 0 \\ 0 & d_+(\boldsymbol{k}) & d_0(\boldsymbol{k}) & -d_3(\boldsymbol{k}) \\ d_+(\boldsymbol{k}) & 0 & -d_3(\boldsymbol{k}) & -d_0(\boldsymbol{k}) \end{pmatrix} \tag{6.19}$$

where

$$d_0(\boldsymbol{k}) = \epsilon - 2t \sum_i \cos k_i,$$

$$d_i(\boldsymbol{k}) = -2\lambda \sin k_i, \quad i = 1, 2, 3 \tag{6.20}$$

$$d_4(\boldsymbol{k}) = 2\gamma \left(3 - \sum_i \cos k_i\right)$$

and

$$d_\pm(\boldsymbol{k}) = d_1(\boldsymbol{k}) \pm i d_2(\boldsymbol{k}). \tag{6.21}$$

The added term that preserves the time-reversal symmetry but breaks the inversion symmetry is:

$$V_{\mathcal{I}} = R \begin{pmatrix} 0 & 0 & 0 & e^{-ik_3} \\ 0 & 0 & -e^{ik_3} & 0 \\ 0 & -e^{-ik_3} & 0 & 0 \\ e^{ik_3} & 0 & 0 & 0 \end{pmatrix} \tag{6.22}$$

The following parameters will be fixed at these values throughout the Chapter: $\epsilon = 134$ meV, $\lambda = 30$ meV, $\gamma = 16$ meV, $R = 15$ meV. We will use $t = 40$ meV for the topological insulator and $t = 14$ meV for the trivial insulator (the two values lead to comparable insulating gaps). The insulating gap in our study is larger than the empirical insulating gap of the Bi_2Se_3 material, and the reason we chose to proceed this way was to be able to better showcase the behavior of the

strong $\mathbb{Z}_2$ invariant in the presence of disorder (the insulating and the mobility gaps would have closed too fast if the gap was fixed at the empirical value). This modification does not break the bridge with the experimental reality because it is known that a mechanical strain may increase the insulating gap of the material.

The real space representation of the translational invariant Hamiltonian can be constructed on cubic lattice where each vertex $\boldsymbol{n}$ carries four quantum states $|\boldsymbol{n}, \alpha, \sigma\rangle$. Here, $\alpha = \pm 1$ (= isospin) labels the s or the p angular momentum character of a state the bands and $\sigma = \pm 1$ the spin up and down configurations. On the Hilbert space spanned by $|\boldsymbol{n}, \alpha, \sigma\rangle$, we define $d_{i,j,k}$, $\hat{\sigma}$, $\hat{\alpha}$, r_α and r_σ as the translation, spin, isospin and flipping operators as follows:

$$\hat{d}_{i,j,k}|n_1, n_2, n_3, \alpha, \sigma\rangle = |n_1 + i, n_2 + j, n_3 + k, \alpha, \sigma\rangle$$

$$\hat{\sigma}|\boldsymbol{n}, \alpha, \sigma\rangle = \sigma|\boldsymbol{n}, \alpha, \sigma\rangle, \quad \hat{\alpha}|\boldsymbol{n}, \alpha, \sigma\rangle = \alpha|\boldsymbol{n}, \alpha, \sigma\rangle r \tag{6.23}$$

$$r_\sigma|\boldsymbol{n}, \alpha, \sigma\rangle = |\boldsymbol{n}, \alpha, -\sigma\rangle, \quad r_\alpha|\boldsymbol{n}, \alpha, \sigma\rangle = |\boldsymbol{n}, -\alpha, \sigma\rangle$$

Then, the real space representation of H_0 takes the form

$$H_0 = \epsilon\hat{\alpha} + 6\gamma + \lambda \sum_{s=\pm 1} s\hat{d}_{0,s,0} r_\alpha \hat{\sigma} r_\sigma$$

$$+ i\lambda \sum_{s=\pm 1} s(\hat{d}_{s,0,0} r_\alpha r_\sigma + \hat{d}_{0,0,s} r_\alpha \hat{\sigma}) \tag{6.24}$$

$$- t(\hat{\alpha} + \gamma) \sum_{s=\pm 1} (\hat{d}_{s,0,0} + \hat{d}_{0,s,0} + \hat{d}_{0,0,s})$$

and the inversion symmetry breaking term takes the form:

$$V_{\mathcal{I}} = \tfrac{R}{2}\hat{\sigma}(\hat{\alpha} - 1)(\hat{d}_{0,0,1} r_\alpha - \hat{d}_{0,0,-1}) r_\sigma. \tag{6.25}$$

As it is now well established, the topological properties of the clean model are revealed when restricting the total Hamiltonian $H_0 + V_{\mathcal{I}}$ on a slab: $0 < n_3 < N$, where N is taken large enough so that the tunneling between the two surfaces of
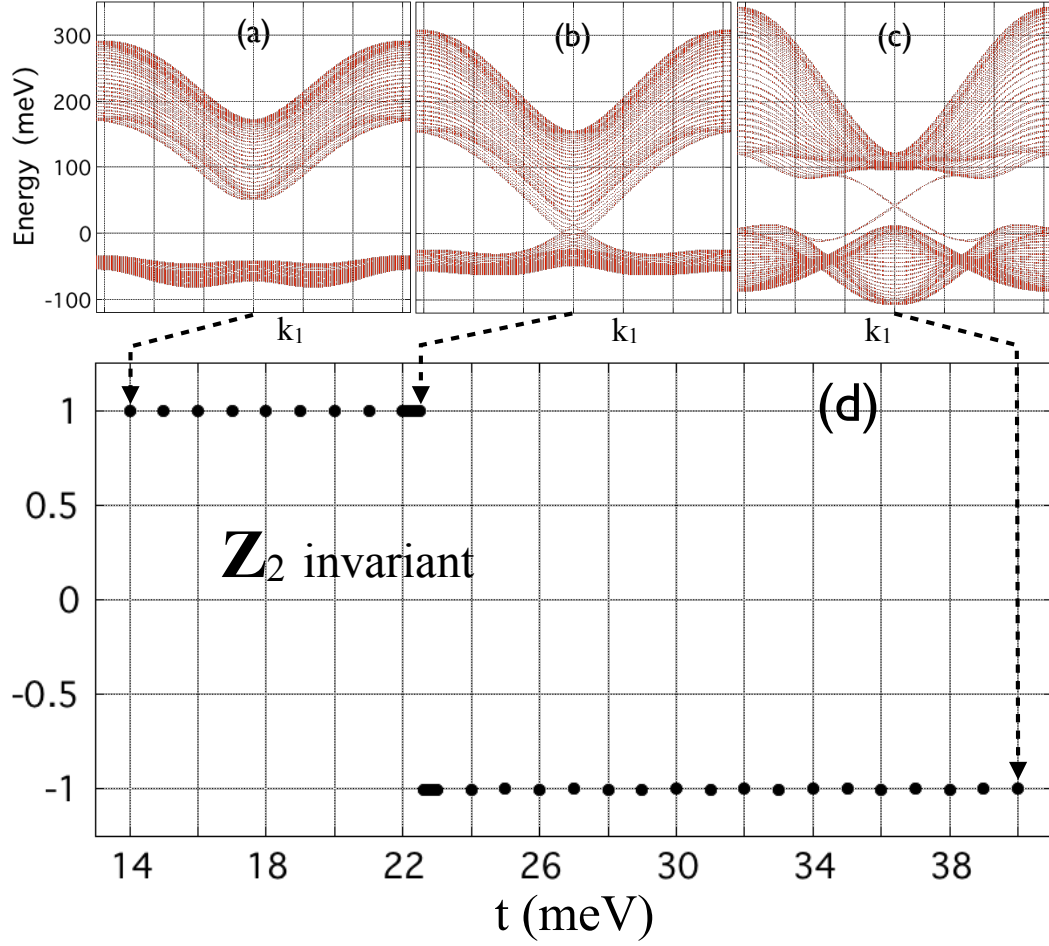
Figure 6.2: (a-c) The band structure of the model for a slab configuration $0 < n_3 < 30$, plotted as function of k_1 with k_2 fixed at $k_2 = 0$. The hopping parameter t takes the values $t = 14$ meV in panel (a), $t = 22.6$ meV in panel (b) and $t = 40$ meV in panel (c). Panel (d) reports a calculation of the strong $\mathbb{Z}_2$ invariant as t was varied from 14 to 40 meV.

the slab is negligible. The slab Hamiltonian takes the form:

$$H_0(k_1, k_2) = -t \sum_{s=\pm 1} \hat{d}_{00s}\hat{\alpha} + i\lambda \sum_{s=\pm 1} s\hat{d}_{00s}r_\alpha\hat{\sigma}$$

$$-\gamma \sum_{s=\pm 1} (\hat{d}_{00s}) + d_4'(k_1, k_2) + d_0'(k_1, k_2)\hat{\alpha} \tag{6.26}$$

$$+d_1(k_1)r_\alpha r_\sigma - id_2(k_2)r_\alpha\hat{\sigma}r_\sigma$$

where $d_4'(k_1, k_2) = 2\gamma\left(3 - \sum_{1,2} \cos(k_i)\right)$ and $d_0'(k_1, k_2) = \epsilon - 2t \sum_{1,2} \cos(k_i)$. For such configuration, the parallel component to the surfaces of the momentum is conserved, so we can plot the energy spectrum as function of k_1 and k_2. In Fig. 6.2(a-c) we show sections of such plots, by holding k_2 at $k_2 = 0$, for three different values of t. The dense band spectra seen in all three plots correspond to the bulk and we can see a bulk energy gap in panels (a) and (c). The bulk gap is closed in panel (b) and that marks the transition from the trivial to the topological insulator. Indeed, in panel (c) we can observe chiral bands connecting the valence and the conduction bands, and in panel (a) these bands are missing entirely. The chiral bands in panel (c), if plotted as function of k_1 and k_2, will give rise to a Dirac cone. The transition point between the phases is at $t = 22.6$ meV.

A straightforward test of the algorithm described in the previous section consists of computing the strong $\mathbb{Z}_2$ invariant for the clean system as function of parameter t, and comparing the output with the appearance or disappearance of the surface states in the slab calculations in Fig. 6.1. Fig. 6.1(d) shows these calculations, and both the $\mathbb{Z}_2$ invariant and the slab calculations predict a trivial insulator for $t < 22.6$ meV and a topological insulator for t above this value. The strong $\mathbb{Z}_2$ invariant was computed using the twisted boundary conditions on a 4×4×4 lattice. The size of the lattice is irrelevant for the clean systems, and we

just chose a convenient lattice size in order to test the twisted boundary conditions method. We used X number of k_z points to compute the pseudo-invariants, in which case $|\det\{U_{\pi,-\pi}\}| \approx ZZZ$, and Y number of k_y points to perform the interpolations.

6.4 Twisted boundary conditions

To include disorder, we consider a generic 3D quantum lattice model with quantum states α per site $\boldsymbol{n}$. The periodic Hamiltonian is given by:

$$H_0 = \sum_{\boldsymbol{n},\boldsymbol{p},\alpha,\alpha'} |\boldsymbol{n},\alpha\rangle h_{\boldsymbol{p}}^{\alpha\alpha'} \langle \boldsymbol{n}+\boldsymbol{p},\alpha'| = \sum_{\boldsymbol{n},\boldsymbol{p}} |\boldsymbol{n}\rangle \hat{h}_{\boldsymbol{p}} \langle \boldsymbol{n}+\boldsymbol{p}|, \qquad (6.27)$$

where $\boldsymbol{p}$ runs over first, second, etc., neighbors of the origin and the $\alpha's$ indices are suppressed in the last equality. For our disordered Hamiltonian $H_{\boldsymbol{\omega}} = H_0 + V_{\boldsymbol{\omega}}$, we consider an on-site random potential:

$$V_{\boldsymbol{\omega}} = W \sum_{\boldsymbol{n},\alpha} \omega_{\boldsymbol{n}\alpha} |\boldsymbol{n},\alpha\rangle \langle \boldsymbol{n},\alpha| = W \sum_{\boldsymbol{n}} |\boldsymbol{n}\rangle \hat{v}_{\boldsymbol{\omega}} \langle \boldsymbol{n}| \qquad (6.28)$$

where $\boldsymbol{\omega_{n\alpha}}$ are randomly independent amplitudes uniformly distributed in the interval $[-\frac{1}{2}, \frac{1}{2}]$.

The twisted boundary conditions technique was first introduced to compute Hall conductance for disordered system [63]. We apply this technique to compute our $\mathbb{Z}_2$ topological invariant. The method consists basically in a translation of the system size L_j by an additional phase factor $e^{i\phi_j}$, where ϕ_j is the twisting angle. We could then replace the Brillouin torus with the "twisting angles torus." On the finite size supercell with a size $L_x \times L_y \times L_z$, a physical phase boundary conditions is replaced by a phase twisting $\boldsymbol{\phi} = (\phi_x, \phi_y, \phi_z)$ on a single particle wave function $\psi(\boldsymbol{x})$:

$$\psi(n_i + L_i) = e^{i\phi_i}\psi(n_i) \tag{6.29}$$

where $i = x, y, z$. If we identify the opposite boundaries of the twisting space $[-\pi, \pi] \times [-\pi, \pi] \times [-\pi, \pi]$, the space is a 3-torus. For a supercell $\mathcal{S}$ with a size $\mathcal{N} \times \mathcal{N} \times \mathcal{N}$, the disordered Hamiltonian can be written as:

$$\begin{aligned} H_{\boldsymbol{\omega}}(\boldsymbol{\phi}) = \sum_{\boldsymbol{n} \in \mathcal{S}} \sum_{\boldsymbol{p}} |\boldsymbol{n}\rangle \; \hat{h}'_{\boldsymbol{np}}(\boldsymbol{\phi}) \; \langle(\boldsymbol{n} + \boldsymbol{p})\text{mod}\mathcal{N}| \\ + W \sum_{\boldsymbol{n} \in \mathcal{S}} |\boldsymbol{n}\rangle \hat{v}_{\boldsymbol{\omega}} \langle \boldsymbol{n}| \end{aligned} \tag{6.30}$$

with

$$\hat{h}'_{\boldsymbol{np}}(\boldsymbol{\phi}) = e^{-i\sum\limits_{\alpha=1}^{3} \phi_\alpha \left(\delta_{n_\alpha + p_\alpha, \mathcal{N}} - \delta_{n_\alpha + p_\alpha, -1}\right)} \hat{h}_{\boldsymbol{p}}. \tag{6.31}$$

The phase factor above occurs only for the lattice points $\boldsymbol{n}$ at the boundary. At this point we obtained a family of Bloch Hamiltonians indexed by a point on the 3-torus. The same construction can be achieved by wrapping the supercell $\mathcal{S}$ into a 3-torus and by threading magnetic fluxes through the 2D sections of this torus. The effect of such magnetic fluxes is captured by the same twisted boundary conditions.

It was argued that a bulk response may not be affected by the boundary conditions [63]. However, this method is probamatic since the boundary of the supercell is hard to define rigorously. We also note that the twisted boundary conditions method is defined for a finite volume, but we are really interested in an infinite bulk sample. Strictly speaking, we have to take the volume of the supercell to infinity.

6.5 Level statistics analysis

The total Hamiltonian will include a random potential:

$$H = H_0 + V_\mathcal{I} + V_{\boldsymbol{\omega}}, \tag{6.32}$$

where $V_{\boldsymbol{\omega}}$ is a non-magnetic random potential:

$$V_{\boldsymbol{\omega}} = W \sum_{\boldsymbol{n},\alpha,\sigma} \omega_{\boldsymbol{n}\alpha} |\boldsymbol{n}, \alpha, \sigma\rangle \langle \boldsymbol{n}, \alpha, \sigma| \tag{6.33}$$

with $\omega_{\boldsymbol{n}\alpha}$ random entries uniformly distributed in the interval $[-\frac{1}{2}, \frac{1}{2}]$.

For level statistics analysis, we diagonalized the disordered Hamiltonian on a $14\times14\times14$ lattice with periodic boundary conditions and for 500 random disorder configurations. We sampled the energy spectrum at 100 equally spaced energy levels E. For each such E, we identified, for each disorder configuration, the unique energy levels E_i and E_{i+1} satisfying: $E_i < E < E_{i+1}$, and we recorded the level spacings: $\Delta E = E_{i+j+1} - E_{i+j}$, letting j take consecutive values between -5 and 5. Note that j indexes the levels and that each level is doubly degenerate. In this way, we have generated ensembles containing 5500 level spacings for each energy E. Fig. 6.3 reports the variance $\langle s^2 \rangle / \langle s \rangle^2 - 1$ of these ensembles as function of energy E and disorder strength W. It also reports the integrated density of states (IDOS), which counts the number of eigenvalues below an energy E and normalizes this number by the dimension of the Hilbert space. When plotted as function of E, the IDOS remains flat in the spectral gaps, so it is a useful and effective tool for identifying the spectral gaps in the energy spectrum. We will be particularly interested to see when the insulating gap is closing.

The level spacings follow a Poisson distribution when E is in the localized spectrum and the localization length is smaller than the size of the system. The Poisson distribution has a variance equal to 1. In the spectral regions where the localization length exceeds the size of the system, the statistics of the level spacings coincides with that of a random Gaussian Symplectic Ensemble (GSE):[18, 19] $P_{\text{GSE}}(s) = \frac{2^{18}}{3^6 \pi^3} s^4 e^{-\frac{64}{9\pi} s^2}$. The variance of this distribution is 0.104. We can study
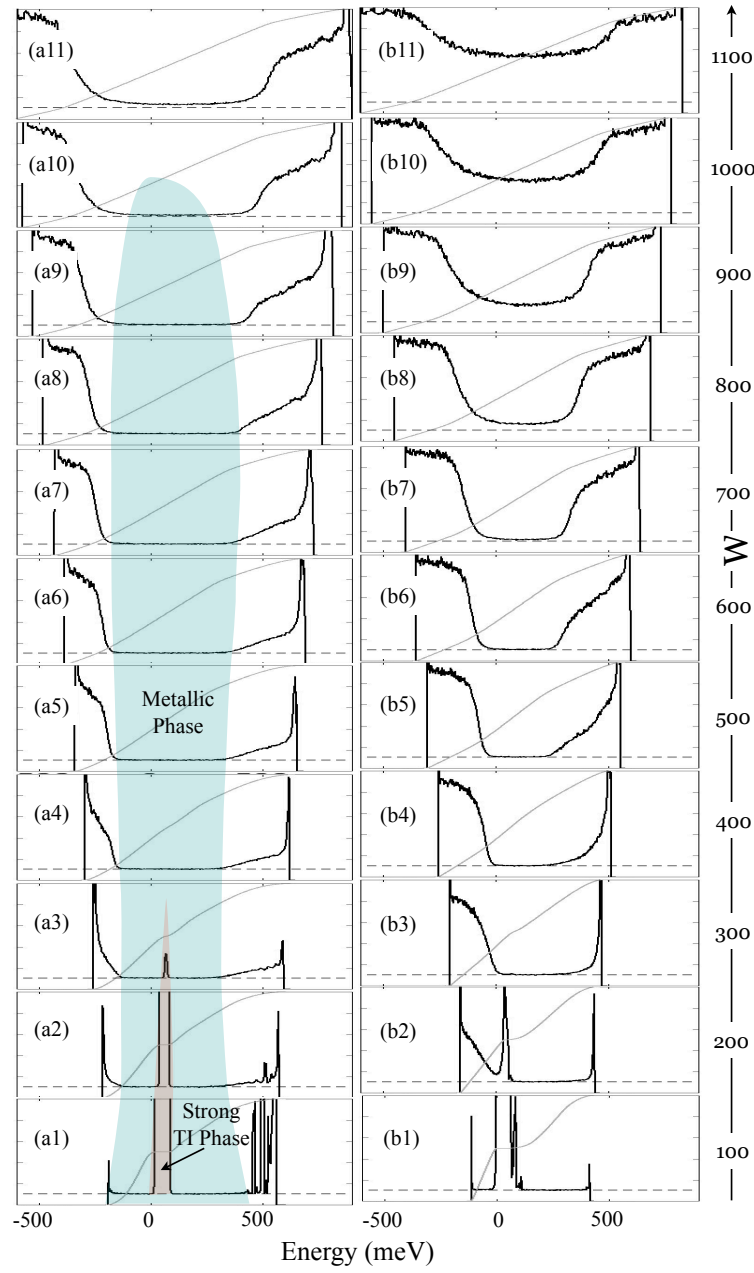
Figure 6.3: Level statistics analysis for (left column) the topological insulator $t = 40$ meV and (right column) the trivial insulator $t = 14$ meV. Each panel displays the variance of the level spacings ensembles as function of the energy where the level spacings were collected. The gray lines in each panels represent the integrated density of states (IDOS), which can be used to assess the evolution of the spectral gap, corresponding to the flat IDOS, and especially to determine when the gap is closing and becoming completely filled with localized states. The horizontal dash lines mark the value 0.104, the variance of the GSE ensemble. The vertical range in each panel goes from 0 to 1. The shaded regions represent the emerging phase diagram of the topological model.

the trends as the system size is increased, and if the size of the system reached a limit where the variance is seen to stabilize (which we have verified that it does), the level spacing analysis can be used quite effectively to identify the regions of localized and de-localized spectrum. This will be done after we discuss the qualitative behavior of the energy spectrum in response to disorder.

In three dimensions, extended states can exist even in trivial disordered models. The qualitative behavior of the spectrum in trivial models is as follows. Usually, the edges of the bands starts to localize the moment the disorder is turned on (for systems displaying large variations in the density of states, additional patches of localized spectrum can occur deep inside the band). At moderate disorder, extended states still survive deep within the bands. As such, there are usually two mobility edges forming per band, flanking the region of extended states, and these mobility edges moves towards each other when the disorder is increased until they merge and disappear. At that point, all the states become localized, as it should be the case at large disorder [4].

In a topological model, the behavior of the spectrum is markedly different. The edges of the bands are the first parts of the spectrum to become localized and the extended states are still located in the middle of the bands. But, if a band carries a nontrivial topological number that is robust against disorder, the two mobility edges flanking the extend states in a band cannot merge and disappear like in the trivial case because that will lead to a sudden change of the topological number carried by the bands, from a nontrivial to a trivial value. So what happens when increasing the disorder? The energy spectrum will eventually become entirely localized as the disorder is being steadily increased,[4] and the only way this can happen is through a scenario where the bands carrying topological numbers collide with each other and in the process they neutralize their topological numbers. This leads to one of the hallmarks of the topological models where, when increasing the disorder, the spectral regions of extended states are seen to drift towards each
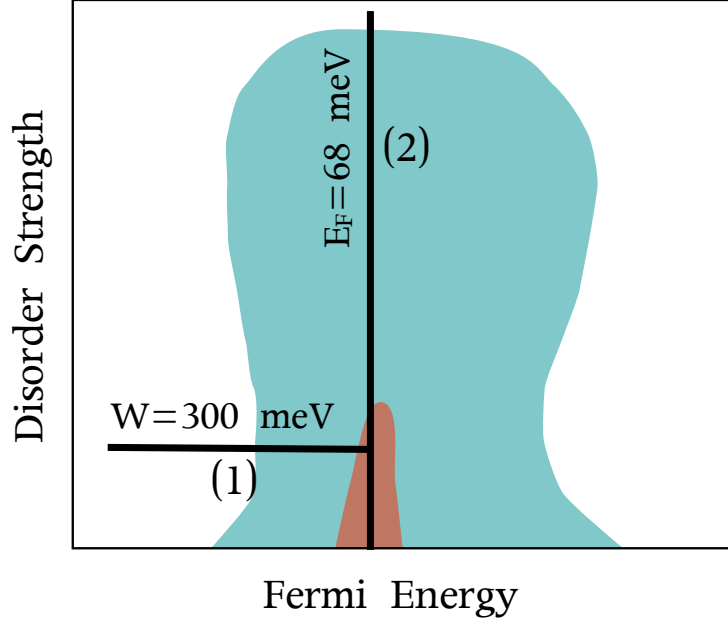
Figure 6.4: Illustration of the phase diagram of the model as derived in Fig. 6.3, and the two paths used in the mapping of the $\mathbb{Z}_2$ invariant.

other until they merge and disappear, usually at very large disorder strengths.

The levitation of the Chern-number carrying extended states in the integer quantum Hall effect is well known from the works of Halperin and Laughlin [36, 52], and the pair annihilations of the topological states in lattice models of quantum Hall effect was discussed in Refs. [87, 111]. The levitation and pair annihilation picture was instrumental for the understanding of the global phase diagram of integer quantum Hall effect [48], and that is also the case for our study.

In Fig. 6.3 we report the variance of the level spacings ensembles collected at various energies and for increasing disorder strengths. However, the level statistics have been exhaustively researched for topological models [12, 73, 77, 95], and the correlation between the histograms and the value of the variance has been already firmly established.

Examining the panels in Fig. 6.3, we can observe energy regions where the variance is large (and becomes unity at large disorder) but also energy regions

where the variance remains pinned at the 0.104 value. These later regions will be identified with the spectral regions of extended states, while the former ones with the spectral regions of localized states. In panels (a1)-(a11) we can clearly see the two extended states regions drifting and merging with each other as the disorder is increased. The extended states survive even at extreme values of disorder $W = 1000$ meV; this value is about twice the width of the entire clean energy spectrum. No such behavior is observed for the trivial case in panels (b1)-(b11), where the valance band is seen to become entirely localized already at W's as small as 200 meV, and the whole spectrum becomes localized before W reaches 700 meV.

Based on the results in Fig. 6.3(a1)-(a11), we can draw the phase diagram of the topological model in the (W, E_F) plane with quite accurate precision. It consists of a strong topological insulating phase surrounded by a metallic phase, which at its turn is surrounded by a trivial insulating phase (see Fig. 6.3). Examining the integrated density of states, we can see that the spectral gap is already closed at $W = 300$ meV but the topological phase extends beyond this W value. This phase diagram will be reconfirmed by a direct mapping of the $\mathbb{Z}_2$ invariant.

6.6 Maps of the $\mathbb{Z}_2$ invariant

The $\mathbb{Z}_2$ invariant will be mapped along the two paths shown in Fig. 6.4. Due to the computational costs of such calculations, we had to settle for a somewhat smaller lattice size of 8×8×8. We have used 400 k-points in the k_z direction to compute the monodromies, and 25 k-points in the k_y direction for the interpolation. As such, each $\mathbb{Z}_2$ invariant computation requires 20,000 exact diagonalizations of the disordered Hamiltonian. A number of 10 disorder configurations were considered for each point chosen along the paths shown in Fig. 6.4. We have also implemented the fortran routine PfaffianH [31] for our very large matrices calculations.
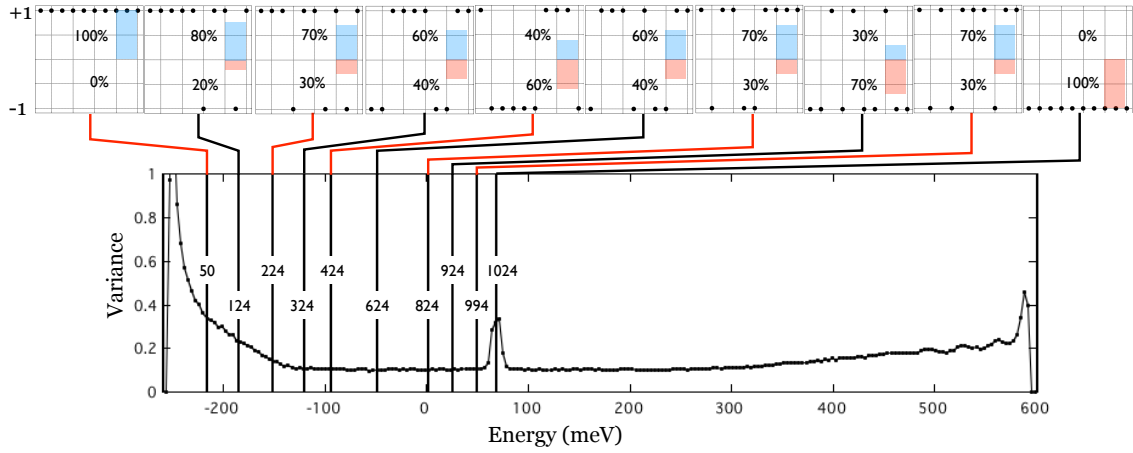
Figure 6.5: The upper panels show the $\mathbb{Z}_2$ invariant computed along the path (1) of Fig. 6.4, on a 8×8×8 unit cells lattice via twisted boundary conditions. The dimension of the occupied space was slowly reduced from 1024 to 124, as indicated in the figure. Each $\mathbb{Z}_2$ the calculation was repeated for 10 random disorder configurations and the output is shown by the full dots, exactly how it occur in the actual calculation. The percentages of the $\mathbb{Z}_2 = \pm 1$ occurrences is displayed in each panel. The lower panel shows the variance of the level spacings for $W = 300$ meV, and the averaged Fermi levels (see the vertical lines) corresponding to each $\mathbb{Z}_2$ calculation.

Fig. 6.5 reports the map of the $\mathbb{Z}_2$ invariant along the path (1). The calculations were performed with a fixed number of occupied states rather than a fixed Fermi level. By doing so, we ensured that all the projectors in the monodromy formula Eq. 6.7 have the same dimension but in this case the Fermi level displays small fluctuations which disappear in the thermodynamic limit. The dimension of the occupied states was slowly reduced from 1024 (half-filled) to 50, as illustrated in Fig. 6.5, and for each dimension we have computed the average Fermi level, defined as half between the last occupied and lowest unoccupied states. The averaged Fermi levels are shown as vertical lines, over-imposed on the variance plot at $W = 300$ meV. And the Fermi levels sample the entire spectrum below the gap.

We want to point out again that the spectral gap is already closed at $W = 300$ meV but, according to the level statistics analysis, there is still a mobility gap. We have verified this statement by direct check of the eigenvalue files. When the Fermi level was inside this mobility gap, we found absolute no fluctuations in the $\mathbb{Z}_2$ invariant, which turned out to be -1 for all 10 random configurations. As the Fermi level is lowered, it enters the region of extended states and here we observed large fluctuations. Even in this regime the $\mathbb{Z}_2$ continue to take quantized ± 1 but there is no way to tell which we will be so the output fluctuates between the two allowed values. This remains the case for as long as the Fermi level is in the region of extended states and, as soon as the Fermi level emerges back into the region of localized states, the $\mathbb{Z}_2$ invariant is seen to take a non-fluctuating quantized value of $+1$.

A similar behavior is observed when considering the path (2) of Fig. 6.4 for which the calculations are reported in Fig. 6. While increasing the disorder strength, the $\mathbb{Z}_2$ invariant is seen to take the quantized and non-fluctuating value of -1 until the mobility gap closes. From there on, the values fluctuate between ± 1, and the $\mathbb{Z}_2$ stabilizes once again when the path enters the trivial
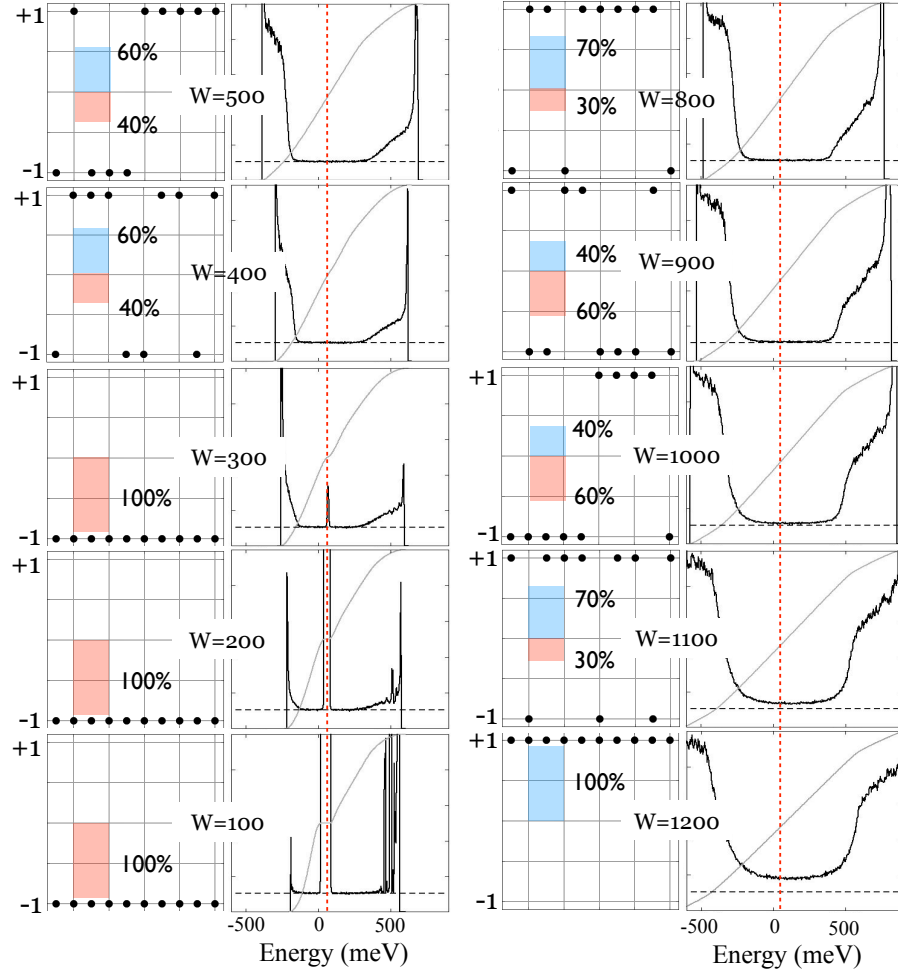
Figure 6.6: This figure reports the results of a computation of the strong $\mathbb{Z}_2$ invariant along the path (2) of Fig. 6.4, completed on a $8\times8\times8$ unit cells lattice via twisted boundary conditions. The disorder strength was increased from $W = 100$ to 1200 meV, as indicated in the figure. Each $\mathbb{Z}_2$ the calculation was repeated for 10 random disorder configurations and the output is shown by the full dots, exactly how it occur in the actual calculation. The percentages of the $\mathbb{Z}_2 = \pm1$ occurrences are displayed in each panel. The accompanying panels show the variance of the level spacings at the corresponding W's, from where we can determine when the Fermi level is in a region of localized/delocalized spectrum. The Fermi level, represented by the dotted vertical line, was kept at 68 meV during these calculations.

insulating state where it assumes the value $+1$.

6.7   Summary

A previously introduced gauge independent formulation of the strong $\mathbb{Z}_2$ invariant was found to bring significant numerical advantages, allowing direct computations of the invariant for large supercells with twisted boundary conditions. The numerical algorithm was applied to a disordered model of Bi_2Se_3 topological material and maps of the strong invariant were given as function of either Fermi level or disorder strength. The behavior of the strong $\mathbb{Z}_2$ invariant seen in our calculations is exactly what we will expect if this invariant was indeed robust to disorder. We observed the strong $\mathbb{Z}_2$ invariant taking quantized and non-fluctuating values whenever the Fermi level was in an energy region of localized states, and fluctuating values (between the only two possible values of ± 1) whenever the Fermi level was in an energy region of delocalized states. The fact that our numerical maps of the strong $\mathbb{Z}_2$ invariant were in good agreement with the phase diagram constructed from the level statistics analysis leaves little doubt that the strong topological phase survives beyond the point where the spectral gap closes, and that it extends all the way to the point where the mobility gap closes.

Our algorithm, combined with accurate tight binding models that can be applied to any material either via first principles calculations or by simple empirical means [57], providing accurate quantitative simulations of the real experimental samples. Recently, twisted boundary conditions were successfully used to compute the Chern invariant of an interacting two dimensional fractional Chern insulator [93]. Since the algorithm for computing the $\mathbb{Z}_2$ invariants is less demanding than the algorithm for the Chern invariant, we have high hopes that we will soon be able to map the $\mathbb{Z}_2$ invariants in the presence of electron interaction for accurate complex models of topological materials. Both disorder and electron interactions

are expected to strongly influence the phase diagram of a topological material.

The results of our study may be of interest for experimentalists. So far, all topological materials fabricated in the labs display metallic bulk properties, a feature that is attributed to the imperfections of the materials. Our study has revealed the interesting fact that, due to the very topological nature of the materials, the disorder pulls the valance and the conduction mobility edges closer to each other. In fact, within our tight-binding model for Be_2Se_3, we saw a rapid reduction of the mobility gap with disorder and the closing of the mobility gap when the disorder strength reached about 350 meV. This suggests that the topological materials have to be much "cleaner" than their trivial counterparts in order to see an insulating phase.

Appendix A

Lemmas and proofs

A.1 Proof of the theorem

Proof. The conditions of the Theorem together with Lemma 4 (see below), assure that, with probability one in ω, the operator $[\hat{D}_{\boldsymbol{x}_0}, \pi_\omega(p)]$ belongs to the q-Shatten class, for any $q > 2n$. This in turn, implies that the operators:

$$\pi_\omega^\mp(p) - \pi_\omega^\mp(p)\hat{D}_{\boldsymbol{x}_0}\pi_\omega^\pm(p)\hat{D}_{\boldsymbol{x}_0}\pi_\omega^\mp(p) = \pi_\omega^\mp(p)[\hat{D}_{\boldsymbol{x}_0}, \pi_\omega(p)]^2\pi_\omega^\mp(p) \qquad \text{(A.1)}$$

are in the q-Shatten class for any $q > n$. As such, $\pi_\omega^-(p)\hat{D}_{\boldsymbol{x}_0}\pi_\omega^+(p)$ belongs to the Fredholm class and its Fredholm index is well-defined for all $\omega \in \Omega$, except for a possible zero-measure subset.

Next, we establish three key properties of the Fredholm index of $\pi_\omega^-(p)\hat{D}_{\boldsymbol{x}_0}\pi_\omega^+(p)$: 1) it is, with probability one, independent of ω, 2) it is independent of $\boldsymbol{x}_0$, and 3) it is independent of what exactly is inserted at the second line of Eq. 4.9. Indeed, for 1), since the translations act ergodically on Ω, it is enough to investigate what happens when we replace ω with an arbitrarily translated $\mathsf{t}_{\boldsymbol{a}}\omega$. And since the Fredholm index is invariant to unitary transformations, and due to the covariance of π_ω, we only need to compare the indices of $\pi_\omega^-(p)\hat{D}_{\boldsymbol{x}_0}\pi_\omega^+(p)$ and $\pi_\omega^-(p)\hat{D}_{\boldsymbol{x}_0+\boldsymbol{a}}\pi_\omega^+(p)$. But these two operators differ by a compact operator so their Fredholm indices coincide. Property 2) follows from the same arguments and 3) is evident.

We now start the actual computation of the Fredholm index. We will use Connes' Chern characters [15] for the Fredholm module. Given that $[\pi_\omega(p), \hat{D}_{\boldsymbol{x}_0}]$ is in the q-Shatten class with $q > 2n$, the lowest Chern character we can use is τ_{2n+2}:

$$\text{Index}\left(\pi_\omega^-(p)\hat{D}_{\boldsymbol{x}_0}\pi_\omega^+(p)\right) = \tau_{2n+2}\big(\pi_\omega(p), \ldots, \pi_\omega(p)\big), \tag{A.2}$$

where the righthand side can be computed by the formula [15]:

$$\tau_{2n+2}\big(\pi_\omega(p), \ldots, \pi_\omega(p)\big) = \text{tr}\{\gamma_0\pi_\omega(p)[\hat{D}_{\boldsymbol{x}_0}, \pi_\omega(p)]^{2n+2}\}. \tag{A.3}$$

This formula can be processed to the following form:

$$-\int_{\mathbb{R}^{2n}} d\boldsymbol{x} \int_\Omega dP(\omega) \; \text{tr}\{\gamma_0\pi_\omega(p)[\hat{D}_{\boldsymbol{x}}, \pi_\omega(p)]^{2n}\chi_{\boldsymbol{0}}\}, \tag{A.4}$$

where it is understood that the equality holds for all $\boldsymbol{x}_0$ and all $\omega \in \Omega$, with possible exceptions that occur with zero probability. Since this last expression brings significant simplifications, it is worth presenting details of the derivation. First, using identities such as:

$$\left[\hat{D}_{\boldsymbol{x}_0}, [\hat{D}_{\boldsymbol{x}_0}, \pi_\omega(p)]^2\right] = 0, \quad \left[\pi_\omega(p), [\hat{D}_{\boldsymbol{x}_0}, \pi_\omega(p)]^2\right] = 0, \tag{A.5}$$

and generic properties of $\hat{D}_{\boldsymbol{x}_0}$ and γ matrices, we can write:

$$\text{tr}\{\gamma_0\pi_\omega(p)[\hat{D}_{\boldsymbol{x}_0}, \pi_\omega(p)]^{2n+2}\} = \frac{1}{2}\text{tr}\left\{\gamma_0[\hat{D}_{\boldsymbol{x}_0}, \pi_\omega(p)]^{2n+1}\hat{D}_{\boldsymbol{x}_0}\right\}. \tag{A.6}$$

Since, with probability one, the index is independent of ω, we can average over

this variable. Expanding the trace and using the translations:

$$\ldots = \frac{1}{2} \int_\Omega dP(\omega) \sum_{\boldsymbol{x} \in \mathbb{Z}^{2n}} \mathrm{tr}\left\{ \gamma_0 [\hat{D}_{\boldsymbol{x}+\boldsymbol{x}_0}, \pi_{\mathsf{t}_x \omega}(p)]^{2n+1} \hat{D}_{\boldsymbol{x}+\boldsymbol{x}_0} \chi_{\boldsymbol{0}} \right\}. \tag{A.7}$$

Since the sum over $\boldsymbol{x}$ is absolutely convergent, we can move the integration inside the sums. We then perform a change of variable $\omega \to \mathsf{t}_x \omega$ and use the invariance of the measure $P(\omega)$ to write:

$$\ldots = \frac{1}{2} \sum_{\boldsymbol{x} \in \boldsymbol{x}_0 + \mathbb{Z}^{2n}} \int_\Omega dP(\omega) \ \mathrm{tr}\left\{ \gamma_0 [\hat{D}_{\boldsymbol{x}}, \pi_\omega(p)]^{2n+1} \hat{D}_{\boldsymbol{x}} \chi_{\boldsymbol{0}} \right\}. \tag{A.8}$$

Since the index is independent of $\boldsymbol{x}_0$, we can integrate $\boldsymbol{x}_0$ over the unit cell and transform the discrete sum over $\boldsymbol{x}$ into an integral over the whole space. Next, we open one commutator and use the cyclic properties of the trace and the identities in Eqs. 4.10 and A.5 to arrive at Eq. A.4.

We continue the calculation from Eq. A.4. Let $\tilde{p} \in \mathcal{A}_0$ be an approximation of p (hence $\tilde{p}$ has compact support). Since $\mathcal{A}_0$ is dense in the Soboleev space, we can always find a sequence of such approximations that converges to p in the Sobolev norm $\| \ \|_W$. We will evaluate the righthand side of Eq. A.4 with p replaced by $\tilde{p}$. Eq. A.4 can be expended to:

$$-\int_{\mathbb{R}^{2n}} d\boldsymbol{x} \int_\Omega dP(\omega) \sum_{\boldsymbol{x}_i's \in \mathbb{Z}^{2n}} \mathrm{tr}\left\{ \gamma_0 \pi_\omega(\tilde{p}) \prod_{i=1}^{2n} \chi_{\boldsymbol{x}_i} [\hat{D}_{\boldsymbol{x}}, \pi_\omega(\tilde{p})] \chi_{\boldsymbol{x}_{i+1}} \right\}, \tag{A.9}$$

where $\boldsymbol{x}_{2n+1} = \boldsymbol{0}$. One important observation is that, due to the compact support of $\tilde{p}$, the sums over $\boldsymbol{x}_i$'s involve a finite number of zero elements. As such, we can interchange the sums and the integrals and, after the commutators are evaluated explictely, we obtain:

$$\ldots = - \sum_{\boldsymbol{x}_i's \in \mathbb{Z}^{2n}} \int_{\mathbb{R}^{2n}} d\boldsymbol{x} \; \mathrm{tr}_\gamma \Big\{ \gamma_0 \prod_{i=1}^{2n} \Big(\widehat{\boldsymbol{x}_i + \boldsymbol{x}} - \widehat{\boldsymbol{x}_{i+1} + \boldsymbol{x}} \Big) \cdot \boldsymbol{\gamma} \Big\}$$

$$\times \int_\Omega dP(\omega) \; \mathrm{tr} \Big\{ \pi_\omega(\tilde{p}) \prod_{i=1}^{2n} \chi_{\boldsymbol{x}_i} \pi_\omega(\tilde{p}) \chi_{\boldsymbol{x}_{i+1}} \Big\}, \qquad (\text{A.10})$$

Using the key identity from Lemma 3, this is the same as:

$$\ldots = -\frac{(2\pi i)^n}{n!} \sum_{\boldsymbol{x}_i's \in \mathbb{Z}^{2n}} \sum_\sigma (-1)^\sigma \prod_{i=1}^{2n} (x_i^{\sigma_i}) \int_\Omega dP(\omega) \; \mathrm{tr} \Big\{ \pi_\omega(\tilde{p}) \prod_{i=1}^{2n} \chi_{\boldsymbol{x}_i} \pi_\omega(\tilde{p}) \chi_{\boldsymbol{x}_{i+1}} \Big\},$$

where σ's denote permutations of $1, \ldots, 2n$. This can be conveniently written as:

$$\ldots = -\frac{(2\pi i)^n}{n!} \int_\Omega dP(\omega) \sum_\sigma (-1)^\sigma \mathrm{tr} \Big\{ \pi_\omega(\tilde{p}) \prod_{i=1}^{2n} [X_{\sigma_i}, \pi_\omega(\tilde{p})] \chi_{\boldsymbol{0}} \Big\}, \qquad (\text{A.11})$$

and using the rule of calculus from Eq. 2.24, we finally obtain:

$$\ldots = -\frac{(2\pi i)^n}{n!} \sum_\sigma (-1)^\sigma \mathcal{T} \left(\tilde{p} \prod_{i=1}^{2n} \partial_{\sigma_i} \tilde{p} \right). \qquad (\text{A.12})$$

We now can take the limit of $\tilde{p}$ towards p in the Sobolev space and the statement follows. Regarding the homotopy invariance, we only need to observe that if p is varied continuously with respect to the Sobolev norm $\| \; \|_W$, then the right-hand side of Eq. 4.13 varies continuously and, as a consequence, it cannot jump from one quantized value to another. $Q.E.D.$

A.2 Lemma 1

Lemma 2. Let $\boldsymbol{x}_1, \ldots, \boldsymbol{x}_{2n+1}$ be points of $\mathbb{R}^{2n}$ with $\boldsymbol{x}_{2n+1} = \boldsymbol{0}$. Then the following identity holds:

$$\int_{\mathbb{R}^{2n}} d\boldsymbol{x} \ \mathrm{tr}_\gamma \Big\{ \gamma_0 \prod_{i=1}^{2n} \Big(\widehat{\boldsymbol{x}_i + \boldsymbol{x}} - \widehat{\boldsymbol{x}_{i+1} + \boldsymbol{x}} \Big) \cdot \boldsymbol{\gamma} \Big\} = -\frac{(2\pi)^n}{i^n n!} \sum_\sigma (-1)^\sigma \prod_{i=1}^{2n} x_i^{\sigma_i}. \quad (A.13)$$

Proof. The proof of this key identity relies on the well known geometric interpretation of the following trace:

$$\mathrm{tr}_\gamma \{ \gamma_0 (\boldsymbol{y}_1 \cdot \boldsymbol{\gamma}) \dots (\boldsymbol{y}_{2n} \cdot \boldsymbol{\gamma}) \} = -i^{-n} 2^{n+1} \mathrm{Vol}[\boldsymbol{0}, \boldsymbol{y}_1, \dots, \boldsymbol{y}_{2n}], \quad (A.14)$$

where $[\boldsymbol{y}_0, \boldsymbol{y}_1, \dots, \boldsymbol{y}_{2n}]$ is the simplex with vertices at $\boldsymbol{y}_0$, $\boldsymbol{y}_1$, ..., $\boldsymbol{y}_{2n}$. Vol denotes the oriented volume of the simplex. Note that $\boldsymbol{y}_0 = \boldsymbol{0}$ in Eq. A.14. Expanding the lefthand side of Eq. A.13, we obtain:

$$\dots = -i^{-n} 2^{n+1} \int_{\mathbb{R}^{2n}} d\boldsymbol{x} \sum_{j=1}^{2n+1} (-1)^{j+1} \mathrm{Vol}[\boldsymbol{0}, \widehat{\boldsymbol{x}_1 - \boldsymbol{x}}, \dots, \underline{\widehat{\boldsymbol{x}_j - \boldsymbol{x}}}, \dots, \widehat{\boldsymbol{x}_{2n+1} - \boldsymbol{x}}],$$

$$(A.15)$$

where the underline means the term is omitted. In Eq. A.15, it is convenient to translate the simplexes and move the first vertex to the proper place. As such, we will work with:

$$\mathfrak{S}_j(\boldsymbol{x}) = [\boldsymbol{x} + \widehat{\boldsymbol{x}_1 - \boldsymbol{x}}, \dots, \boldsymbol{x}, \dots, \boldsymbol{x} + \widehat{\boldsymbol{x}_{2n+1} - \boldsymbol{x}}], \ j = 1, \dots, 2n+1, \quad (A.16)$$

where $\boldsymbol{x}$ is located at the j-th position. We will also denote by $\mathfrak{S}$ the simplex:

$$\mathfrak{S} = [\boldsymbol{x}_1, \dots, \boldsymbol{x}_{2n+1}], \quad (A.17)$$

where we recall that $\boldsymbol{x}_{2n+1}$ coincides with the origin. To summarize, we arrived at:

$$\int_{\mathbb{R}^{2n}} d\boldsymbol{x} \; \mathrm{tr}_\gamma \Big\{ \gamma_0 \prod_{i=1}^{2n} \big(\widehat{\boldsymbol{x}_i - \boldsymbol{x}} - \widehat{\boldsymbol{x}_{i+1} - \boldsymbol{x}} \big) \cdot \boldsymbol{\gamma} \Big\} = -2(-2i)^n \int_{\mathbb{R}^{2n}} d\boldsymbol{x} \sum_{j=1}^{2n+1} \mathrm{Vol}\{\mathfrak{S}_j(\boldsymbol{x})\}.$$

(A.18)

Note that the sign factor $(-1)^{j+1}$ disappeared because we changed the order of the vertices. Furthermore, if $\boldsymbol{x}$ is located inside $\mathfrak{S}$, then the orientations of the simplexes $\mathfrak{S}_j$ $(j = \overline{1, 2n+1})$ are the same as that of $\mathcal{S}$. This is the case because each $\mathfrak{S}_j$ can be continuously deformed into $\mathfrak{S}$ without sending its volume to zero. Such deformation can be achieved by moving $\boldsymbol{x}$ at $\boldsymbol{x}_j$ and $\boldsymbol{x} + \widehat{\boldsymbol{x}_i - \boldsymbol{x}}$ at $\boldsymbol{x}_i$ $(i \neq j)$, along straight paths. One such deformation process is illustrated in Fig. 1(a) for the 2-dimensional case.

If we look closer at the simplexes $\mathfrak{S}_j(\boldsymbol{x})$, we see that all vertices that are different from $\boldsymbol{x}$ are located on the unit sphere centered at $\boldsymbol{x}$. As such, for any given simplex $\mathfrak{S}_j(\boldsymbol{x})$, the facets stemming from $\boldsymbol{x}$ define a sector of the unit ball $\boldsymbol{\mathcal{B}}_{2n}(\boldsymbol{x})$ centered at $\boldsymbol{x}$. This sector will be denoted by $\mathcal{B}_j(\boldsymbol{x})$. This construction is illustrated in Fig. 1(b) for the 2-dimensional case. The orientation of $\mathcal{B}_j(\boldsymbol{x})$'s are considered to be the same as that of $\mathfrak{S}_j(\boldsymbol{x})$'s. Now, one important observation is that:

$$\mathrm{Vol}\{\mathfrak{S}_j(\boldsymbol{x})\} - \mathrm{Vol}\{\mathcal{B}_j(\boldsymbol{x})\} \sim |\boldsymbol{x}|^{-(2n+1)}$$

(A.19)

in the asymptotic regime $|\boldsymbol{x}| \to \infty$. Consequently, we can write:

$$\int_{\mathbb{R}^{2n}} d\boldsymbol{x} \sum_{i=1}^{2n+1} \mathrm{Vol}\{\mathfrak{S}_j(\boldsymbol{x})\} = \int_{\mathbb{R}^{2n}} d\boldsymbol{x} \sum_{i=1}^{2n+1} \mathrm{Vol}\{\mathcal{B}_j(\boldsymbol{x})\}$$

(A.20)

$$+ \sum_{i=1}^{2n+1} \int_{\mathbb{R}^{2n}} d\boldsymbol{x} \big(\mathrm{Vol}\{\mathfrak{S}_j(\boldsymbol{x})\} - \mathrm{Vol}\{\mathcal{B}_j(\boldsymbol{x})\} \big),$$

with the integrals in the second line being absolutely convergent. There are two
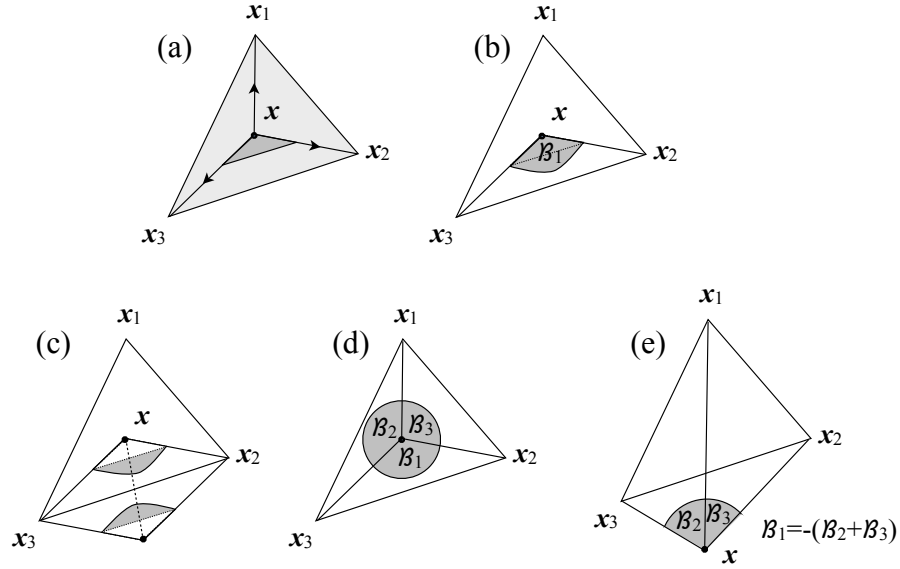
Figure A.1: (a) Illustration of the simplexes $\mathfrak{S} = (\boldsymbol{x}_1, \boldsymbol{x}_2, \boldsymbol{x}_3)$ (light gray) and $\mathfrak{S}_1(\boldsymbol{x}) = (\boldsymbol{x}, \boldsymbol{x} + \widehat{\boldsymbol{x}_2 - \boldsymbol{x}}, \boldsymbol{x} + \widehat{\boldsymbol{x}_3 - \boldsymbol{x}})$ (darker gray), together with the interpolation process that takes $\mathfrak{S}_1(\boldsymbol{x})$ into $\mathfrak{S}$. (b) Illustration of the ball sector $\mathcal{B}_1(\boldsymbol{x})$ corresponding to the simplex $\mathfrak{S}_1(\boldsymbol{x})$. (c) Illustration of the inversion operation on $\boldsymbol{x}$ relative to the center of the segment $(\boldsymbol{x}_2, \boldsymbol{x}_3)$. The volume of $\mathcal{B}_1(\boldsymbol{x}) - \mathfrak{S}_1(\boldsymbol{x})$ (shaded in gray) changes sign after this operation because $\boldsymbol{x}$ crosses the segment $(\boldsymbol{x}_2, \boldsymbol{x}_3)$ (the volume becomes zero at the crossing and changes sign after that). (d) The ball sectors $\mathcal{B}_1(\boldsymbol{x})$, $\mathcal{B}_2(\boldsymbol{x})$ and $\mathcal{B}_3(\boldsymbol{x})$ have same orientation and they add up to the full unit disk when $\boldsymbol{x}$ is inside $\mathfrak{S}$. (e) When $\boldsymbol{x}$ is outside of $\mathfrak{S}$, the ball sector $\mathcal{B}_1(\boldsymbol{x})$ has the opposite orientation of $\mathcal{B}_2(\boldsymbol{x})$ and $\mathcal{B}_3(\boldsymbol{x})$ (because $\boldsymbol{x}$ crossed the segment $(\boldsymbol{x}_2, \boldsymbol{x}_3)$) and, as a consequence, $\mathcal{B}_1(\boldsymbol{x})$, $\mathcal{B}_2(\boldsymbol{x})$ and $\mathcal{B}_3(\boldsymbol{x})$ add up to zero.

extraordinary facts taking place, simultaneously:

$$\int_{\mathbb{R}^{2n}} d\boldsymbol{x} \left(\text{Vol}\{\mathfrak{S}_j(\boldsymbol{x})\} - \text{Vol}\{\mathcal{B}_j(\boldsymbol{x})\} \right) = 0, \text{ for all } j = \overline{1, 2n+1}, \qquad (\text{A.21})$$

and

$$\sum_{i=1}^{2n+1} \text{Vol}\{\mathcal{B}_j(\boldsymbol{x})\} = \begin{cases} \text{Vol}(\mathcal{B}_{2n}) \text{ if } \boldsymbol{x} \text{ inside } \mathfrak{S}, \\ \\ 0 \text{ if } \boldsymbol{x} \text{ outside } \mathfrak{S}. \end{cases} \qquad (\text{A.22})$$

Eq. A.21 follows from the fact that the integrand is odd under the inversion of $\boldsymbol{x}$ relative to the center of the facet $\{\boldsymbol{x}_1, \dots, \underline{\boldsymbol{x}_j}, \dots, \boldsymbol{x}_{2n+1}\}$ of the simplex $\mathfrak{S}$. This property is illustrated in Fig. 1(c) for the 2-dimensional case. Eq. A.22 is a simple geometric fact. It is illustrated in Figs. 1(d) and 1(e) for the 2-dimensional case. Then Eq. A.18 reduces to:

$$\int_{\mathbb{R}^{2n}} d\boldsymbol{x} \ \text{tr}_\gamma \Big\{ \gamma_0 \prod_{i=1}^{2n} \Big(\widehat{\boldsymbol{x}_i - \boldsymbol{x}} \cdot \boldsymbol{\gamma} - \widehat{\boldsymbol{x}_{i+1} - \boldsymbol{x}} \cdot \boldsymbol{\gamma} \Big) \Big\} = -2(-2i)^n \text{Vol}\{\mathcal{B}_{2n}\} \text{Vol}\{\mathfrak{S}\}, \qquad (\text{A.23})$$

and the statement follows. $Q.E.D.$

A.3 Lemma 2

Lemma 3. Let p be an element from the Sobolev space $W(\mathcal{A}, \mathcal{T})$ and let Tr_{Dix} denote the Dixmier trace [17]. Then, with probability one in ω, the following identity holds:

$$\text{Tr}_{\text{Dix}} \Big\{ \big(i[\hat{D}_{\boldsymbol{x}_0}, \pi_\omega(p)] \big)^{2n} \Big\} = \frac{1}{2n} \int_{\mathcal{S}_{2n-1}} d\hat{\boldsymbol{x}} \ \mathcal{T} \otimes \text{tr}_\gamma \Big\{ \big(\boldsymbol{\gamma}(\hat{\boldsymbol{x}}) \cdot \boldsymbol{\nabla} p \big)^{2n} \Big\}. \qquad (\text{A.24})$$

In particular, the Dixmier trace of $(i[\hat{D}_{\boldsymbol{x}_0}, \pi_\omega(p)])^{2n}$ is finite for any $p \in W(\mathcal{A}, \mathcal{T})$, a fact that follows immediately from the noncommutative version of the Holder inequality [51, 92]. In Eq. A.24, $\hat{\boldsymbol{x}}$ is the unit vector in $\mathbb{R}^{2n}$ which is integrated over the $(2n\text{-}1)$-sphere $\mathcal{S}_{2n-1}$, and

$$\gamma_i(\hat{\boldsymbol{x}}) = \gamma_i - \hat{x}_i(\hat{\boldsymbol{x}} \cdot \boldsymbol{\gamma}), \ i = 1, \ldots, 2n, \tag{A.25}$$

are the generators of the Clifford algebra:

$$\{\gamma_i(\hat{\boldsymbol{x}}), \gamma_j(\hat{\boldsymbol{x}})\} = 2(\delta_{ij} - \hat{x}_i\hat{x}_j). \tag{A.26}$$

Remark. From a standard property of the Dixmier trace [9], it follows that $\left(i[\hat{D}_{\boldsymbol{x}_0}, \pi_\omega(p)]\right)^{2n}$ belongs to the qth-Schatten classes with $q > 2n$, whenever $p \in W(\mathcal{A}, \mathcal{T})$.

Proof. We will derive the identity in Eq. A.24 for an element p from $\mathcal{A}_0$ (hence with compact support). Since $\mathcal{A}_0$ is dense in the Sobolev space $W(\mathcal{A}, \mathcal{T})$, the identity extends by continuity over this space. First, it is easy to establish that any translation of ω leads to a trace-class perturbation and, as such, the Dixmier trace remains unchanged. Since the translations act ergodically on Ω, this tells that the Dixmier trace in Eq. A.24 is independent of ω, except for cases that occur with zero probability. Using the arguments from Ref. [9], we only need to consider the diagonal part of the operator:

$$\text{Diag} \left(i[\hat{D}, \pi_\omega(p)]\right)^{2n} = (-1)^n \sum_{\boldsymbol{x} \in \mathbb{Z}^{2n}} \sum_{\alpha=1}^{Q} \text{tr}_\gamma \left\{ \langle \boldsymbol{x}, \alpha | [\hat{D}, \pi_\omega(p)]^{2n} | \boldsymbol{x}, \alpha \rangle \right\} \chi_{\boldsymbol{x},\alpha}, \tag{A.27}$$

where $\chi_{\boldsymbol{x},\alpha} = |\boldsymbol{x}, \alpha\rangle\langle\boldsymbol{x}, \alpha|$. We expand the righthand side in the following way:

$$\cdots = (-1)^n \sum_{\boldsymbol{x}\in\mathbb{Z}^{2n}} \sum_{\alpha=1}^{Q} \sum_{\boldsymbol{x}_i's\in\mathbb{Z}^{2n}} \mathrm{tr}_\gamma\big\{\langle \boldsymbol{0},\alpha|\prod_{i=1}^{2n}\chi_{\boldsymbol{x}_{i-1}}[\hat{D}_{\boldsymbol{x}},\pi_{\mathrm{t}_{\boldsymbol{x}}\omega}(p)]\chi_{\boldsymbol{x}_i}|\boldsymbol{0},\alpha\rangle\big\}\chi_{\boldsymbol{x},\alpha},$$

(A.28)

where $\boldsymbol{x}_0 = \boldsymbol{x}_{2n} = \boldsymbol{0}$ and the summation over these variables is omitted. The commutators can be evaluated explicitly and note that, since p has a compact support, there are only a finite number of non-zero terms in the sums over $\boldsymbol{x}_i$ variables. We have:

$$\cdots = (-1)^n \sum_{\boldsymbol{x}\in\mathbb{Z}^{2n}} \sum_{\alpha=1}^{Q} \sum_{\boldsymbol{x}_i's\in\mathbb{Z}^{2n}} \langle \boldsymbol{0},\alpha|\prod_{i=1}^{2n}\chi_{\boldsymbol{x}_{i-1}}\pi_{\mathrm{t}_{\boldsymbol{x}}\omega}(p)\chi_{\boldsymbol{x}_i}|\boldsymbol{0},\alpha\rangle$$

(A.29)

$$\times\,\mathrm{tr}_\gamma\big\{\prod_{i=1}^{2n}\big(\widehat{\boldsymbol{x}_{i-1}+\boldsymbol{x}} - \widehat{\boldsymbol{x}_i+\boldsymbol{x}}\big)\cdot\boldsymbol{\gamma}\big\}\chi_{\boldsymbol{x},\alpha}.$$

In the asymptotic limit $|\boldsymbol{x}|\to\infty$, we have:

$$\big(\widehat{\boldsymbol{x}_{i-1}+\boldsymbol{x}} - \widehat{\boldsymbol{x}_i+\boldsymbol{x}}\big)\cdot\boldsymbol{\gamma} = \frac{1}{|\boldsymbol{x}|}(\boldsymbol{x}_{i-1}-\boldsymbol{x}_i)\cdot\boldsymbol{\gamma}(\hat{\boldsymbol{x}}) + O(|\boldsymbol{x}|^{-2}).$$

(A.30)

Hence, apart from terms that are in the trace-class and don't count for the Dixmier trace [9], the diagonal part of our operator is:

$$\mathrm{Diag}\,\big(i[\hat{D},\pi_\omega(p)]\big)^{2n} = \sum_{\alpha=1}^{Q}\sum_{\boldsymbol{x}\in\mathbb{Z}^{2n}}\mathrm{tr}_\gamma\big\{\langle\boldsymbol{0},\alpha|\big(\boldsymbol{\gamma}(\hat{\boldsymbol{x}})\cdot i[\boldsymbol{X},\pi_{\mathrm{t}_{\boldsymbol{x}}\omega}(p)]\big)^{2n}|\boldsymbol{0},\alpha\rangle\big\}\frac{\chi_{\boldsymbol{x},\alpha}}{|\boldsymbol{x}|^{2n}}.$$

(A.31)

Then the statement follows from the following Lemma. *Q.E.D.*

A.4 Lemma 3

Lemma 4. Let $f : \Omega \to \mathbb{C}$ and $\varphi : \mathcal{S}_{2n-1} \to \mathbb{C}$ be bounded measurable functions. Consider the operator:

$$\sum_{\boldsymbol{x} \in \mathbb{Z}^{2n}} f(\mathsf{t}_{\boldsymbol{x}}\omega)\varphi(\hat{\boldsymbol{x}})\frac{\chi_{\boldsymbol{x},\alpha}}{|\boldsymbol{x}|^{2n}}, \tag{A.32}$$

and assume that any translation of ω in Eq. A.32 leads to a trace-class perturbation. Then:

$$\mathrm{Tr}_{\mathrm{Dix}} \sum_{\boldsymbol{x} \in \mathbb{Z}^{2n}} f(\mathsf{t}_{\boldsymbol{x}}\omega)\varphi(\hat{\boldsymbol{x}})\frac{\chi_{\boldsymbol{x},\alpha}}{|\boldsymbol{x}|^{2n}} = \frac{1}{2n} \int_{\Omega} dP(\omega)\, f(\omega) \int_{\mathcal{S}_{2n-1}} d\hat{\boldsymbol{x}}\, \varphi(\hat{\boldsymbol{x}}). \tag{A.33}$$

Proof. One of the main ingredients of the proof is Lemma 3 of Ref. [9], which says:

$$\mathrm{Tr}_{\mathrm{Dix}} \sum_{\boldsymbol{x} \in \Sigma} \frac{\chi_{\boldsymbol{x},\alpha}}{|\boldsymbol{x}|^{2n}} = \frac{s_{2n-1}}{2n}\mathrm{Dens}\,\Sigma, \tag{A.34}$$

where s_{2n-1} is the area of the ($2n$-1)-sphere, and the density of a set $\Sigma \in \mathbb{Z}^{2n}$ is defined as:

$$\mathrm{Dens}\,\Sigma = \lim_{N \to \infty} \frac{1}{N^{2n}} \sum_{\boldsymbol{x} \in \Sigma \cap \mathfrak{C}_{2n}} 1, \tag{A.35}$$

with $\mathfrak{C}_{2n}$ being the cube $\left[-\frac{N}{2}, \frac{N}{2}\right]^{2n}$. To use this general result, we partition the space according to the level sets of φ and f. First, let us partition the configuration space Ω:

$$\Omega_j = \{\omega \in \Omega \mid f_{j-1} \leq f(\omega) < f_j\}, \tag{A.36}$$

where $f_j = (j + \frac{1}{2})\delta$ and δ is a small positive number. Since f is bounded, only a

finite number of Ω_j's are non-empty. Then let $\Sigma_j(\omega)$ be the sets in $\mathbb{Z}^{2n}$, defined as:

$$\Sigma_j(\omega) = \{\boldsymbol{x} \in \mathbb{Z}^{2n} \mid \mathsf{t}_x \omega \in \Omega_j\}. \tag{A.37}$$

These sets have finite densities in $\mathbb{Z}^{2n}$, and in fact Birckhoff's theorem tells us that, with probability one:

$$\mathrm{Dens}\, \Sigma_j(\omega) = P(\Omega_j). \tag{A.38}$$

The unit vector $\hat{\boldsymbol{x}}$ takes values on the $\mathcal{S}_{2n-1}$ unit sphere in $\mathbb{R}^{2n}$, and we partition the sphere into level sets of φ:

$$S_k = \{\hat{\boldsymbol{x}} \in \mathcal{S}_{2n-1} \mid \varphi_{k-1} \leq \varphi(\hat{\boldsymbol{x}}) < \varphi_k\}, \tag{A.39}$$

where $\varphi_k = (k + \frac{1}{2})\delta$. Since φ is bounded, there are a finite number of non-empty such sets. We then refine our partition of $\mathbb{Z}^{2n}$ to:

$$\Sigma_{j,k}(\omega) = \Sigma_j(\omega) \cap \{\boldsymbol{x} \in \mathbb{R}^{2n} \mid \hat{\boldsymbol{x}} \in S_k\}. \tag{A.40}$$

This partition is still finite, hence we can write:

$$\mathrm{Tr}_{\mathrm{Dix}} \sum_{\boldsymbol{x} \in \mathbb{Z}^{2n}} f(\mathsf{t}_{\boldsymbol{x}}\omega)\varphi(\hat{\boldsymbol{x}})\frac{\chi_{\boldsymbol{x},\alpha}}{|\boldsymbol{x}|^{2n}} = \sum_{j,k} \mathrm{Tr}_{\mathrm{Dix}} \sum_{\boldsymbol{x} \in \Sigma_{j,k}(\omega)} f(\mathsf{t}_{\boldsymbol{x}}\omega)\varphi(\hat{\boldsymbol{x}})\frac{\chi_{\boldsymbol{x},\alpha}}{|\boldsymbol{x}|^{2n}}. \tag{A.41}$$

Furthermore, from the definition of the partition:

$$\mathrm{Tr}_{\mathrm{Dix}} \sum_{\boldsymbol{x} \in \Sigma_{j,k}(\omega)} f(\mathsf{t}_{\boldsymbol{x}}\omega)\varphi(\hat{\boldsymbol{x}})\frac{\chi_{\boldsymbol{x},\alpha}}{|\boldsymbol{x}|^{2n}} = f_j \phi_k \, \mathrm{Tr}_{\mathrm{Dix}} \sum_{\boldsymbol{x} \in \Sigma_{j,k}(\omega)} \frac{\chi_{\boldsymbol{x},\alpha}}{|\boldsymbol{x}|^{2n}}, \tag{A.42}$$

plus corrections that are of second order in δ. We arrive at:

$$\mathrm{Tr}_{\mathrm{Dix}} \sum_{\boldsymbol{x} \in \Sigma_{j,k}(\omega)} f(\mathsf{t}_{\boldsymbol{x}} \omega) \varphi(\hat{\boldsymbol{x}}) \frac{\chi_{\boldsymbol{x},\alpha}}{|\boldsymbol{x}|^{2n}} = f_j \phi_k \, \frac{s_{2n-1}}{2n} \mathrm{Dens}\, \Sigma_{j,k}(\omega), \qquad \text{(A.43)}$$

plus the corrections we mentioned. Our next task will be to compute the density of $\Sigma_{j,k}(\omega)$. However, instead of working directly with $\Sigma_{j,k}(\omega)$, we recall that the original Dixmier trace remains unchanged when we translate ω. As such, we can replace $\mathrm{Dens}\, \Sigma_{j,k}(\omega)$ with the average $M^{-2n} \sum_{\boldsymbol{m} \in \mathfrak{C}_M} \mathrm{Dens}\, \Sigma_{j,k}(\mathsf{t}_{\boldsymbol{m}} \omega)$. The latter can also be written as:

$$M^{-2n} \sum_{\boldsymbol{m} \in \mathfrak{C}_M} \mathrm{Dens}\, \left\{ [\boldsymbol{m} + \Sigma_j(\omega)] \cap \{\boldsymbol{x} \in \mathbb{R}^{2n} \mid \hat{\boldsymbol{x}} \in S_k\} \right\}. \qquad \text{(A.44)}$$

We will work in the limit $M \to \infty$, where we consider the following measure on the sphere:

$$\nu(S \subset \mathcal{S}_{2n-1}) = \lim_{M \to \infty} \frac{M^{-2n}}{P(\Omega_j)} \sum_{\boldsymbol{m} \in \mathfrak{C}_M} \mathrm{Dens}\, \left\{ [\boldsymbol{m} + \Sigma_j(\omega)] \cap \{\boldsymbol{x} \in \mathbb{R}^{2n} \mid \hat{\boldsymbol{x}} \in S\} \right\}. \qquad \text{(A.45)}$$

From this expression, one can derive two immediate properties. First, $\nu(\mathcal{S}_{2n-1}) = 1$, hence ν is a probability measure, and second, ν is invariant to rotations. Hence ν must be equal to:

$$\nu(S \subset \mathcal{S}_{2n-1}) = \frac{|S|}{s_{2n-1}}, \qquad \text{(A.46)}$$

where $|S|$ denotes the area of S. Consequently:

$$\lim_{M \to 0} M^{-2n} \sum_{\boldsymbol{m} \in \mathfrak{C}_M} \mathrm{Dens}\, \Sigma_{j,k}(\mathsf{t}_{\boldsymbol{m}} \omega) = \frac{P(\Omega_j)|S|}{s_{2n-1}}. \qquad \text{(A.47)}$$

Putting everything together, we demonstrated that, apart from corrections that vanish as $\delta \to 0$:

$$\text{Tr}_{\text{Dix}} \sum_{\boldsymbol{x} \in \mathbb{Z}^{2n}} f(\mathsf{t}_{\boldsymbol{x}}\omega)\varphi(\hat{\boldsymbol{x}})\frac{\chi_{\boldsymbol{x},\alpha}}{|\boldsymbol{x}|^{2n}} = \frac{1}{2n} \sum_{j,k} f_j \phi_k P(\Omega_j)|S_k|, \tag{A.48}$$

and the statement follows by taking the limit of δ goes to zero. $Q.E.D.$

A.5 Proof of proposition 1

We will use the bound on the fractional powers of the Green's function in the following way. First, let us note that, under the localization assumption, the projector onto the occupied states can be written as:

$$p = \frac{i}{2\pi} \int_{\mathcal{C}} d\xi \ (h - \xi)^{-1}, \tag{A.49}$$

where $\mathcal{C}$ is a contour in the complex plane surrounding the energy spectrum below the zero-energy level. This is the case because, even though the spectrum is dense near the origin, with probability one, the contour $\mathcal{C}$ will miss the point spectrum of h. Since the resolvent $(h - \xi)^{-1}$ decay exponentially when ξ is away from the real axis, we can always extend the bound to the entire $\mathcal{C}$:

$$\int_{\Omega} dP(\omega) \ |(h - \xi)^{-1}(\omega, \boldsymbol{x})|^s \le C_s e^{-s\beta|\boldsymbol{x}|}, \text{ for all } \xi \in \mathcal{C}. \tag{A.50}$$

Proof. We will use the following simple estimate: If f_1, ..., f_{2n} are elements from the algebra $\mathcal{A}$, then:

$$|\text{tr}\{(f_{2n} * \ldots * f_1)(\omega, \boldsymbol{0})\}| \le Q \sum_{\boldsymbol{x}'_j s \in \mathbb{Z}^{2n}} \prod_{j=1}^{2n} |f_j(\mathsf{t}_{\boldsymbol{x}_j}^{-1}\omega, \boldsymbol{x}_{j-1} - \boldsymbol{x}_j)|, \tag{A.51}$$

with $\boldsymbol{x}_0$ and $\boldsymbol{x}_{2n}$ fixed at the origin (which is imposed throughout this section).

(i) We consider only the terms of the Sobolev norm that contain derivations,

because the remaining term can be treated similarly. We take for all j's $f_j = \partial_i p$ in Eq. A.51, and observe that:

$$|f_j(\omega, \boldsymbol{x})| \leq \frac{|\boldsymbol{x}|}{2\pi} \int_{\mathcal{C}} |d\xi| \ |\mathrm{Im} \ \xi|^{-1+s} |(h - \xi)^{-1}(\omega, \boldsymbol{x})|^s. \tag{A.52}$$

Then:

$$\mathcal{T}\left(|\partial_i p|^{2n}\right) \leq \left(\frac{1}{2\pi}\right)^{2n} Q \int_{\mathcal{C}} |d\xi_1| \ |\mathrm{Im} \ \xi_1|^{-1+s} \ldots \int_{\mathcal{C}} |d\xi_{2n}| \ |\mathrm{Im} \ \xi_{2n}|^{-1+s}$$

$$\times \sum_{\boldsymbol{x}'_j s \in \mathbb{Z}^{2n}} \int_{\Omega} dP(\omega) \prod_{j=1}^{2n} |\boldsymbol{x}_{j-1} - \boldsymbol{x}_j| |(h - \xi_j)^{-1}(\mathsf{t}_{\boldsymbol{x}_j}^{-1}\omega, \boldsymbol{x}_{j-1} - \boldsymbol{x}_j)|^s.$$

Holder inequality enables us to continue:

$$\ldots \leq \left(\frac{1}{2\pi}\right)^{2n} Q \int_{\mathcal{C}} |d\xi_1| \ |\mathrm{Im} \ \xi_1|^{-1+s} \ldots \int_{\mathcal{C}} |d\xi_{2n}| \ |\mathrm{Im} \ \xi_{2n})|^{-1+s} \tag{A.53}$$

$$\times \sum_{\boldsymbol{x}'_j s \in \mathbb{Z}^{2n}} \prod_{j=1}^{2n} |\boldsymbol{x}_{j-1} - \boldsymbol{x}_j| \left[\int_{\Omega} dP(\omega) |(h - \xi_j)^{-1}(\mathsf{t}_{\boldsymbol{x}_j}^{-1}\omega, \boldsymbol{x}_{j-1} - \boldsymbol{x}_j)|^{2ns}\right]^{\frac{1}{2n}}.$$

If we take $s < \frac{1}{2n}$, we can use the bound in Eq A.50 on the fractional powers of the resolvent. Noting that the remaining integrals over ξ_j's are convergent, the inequality reduces to:

$$\mathcal{T}\left(|\partial_i p|^{2n}\right) \leq ct. \sum_{\boldsymbol{x}'_j s \in \mathbb{Z}^{2n}} \prod_{j=1}^{2n} |\boldsymbol{x}_{j-1} - \boldsymbol{x}_j| e^{-s\beta|\boldsymbol{x}_{j-1} - \boldsymbol{x}_j|},$$

and the remaining sums are evidently convergent.

(ii) For all j's, we take

$$f_j = \partial_i(p' - p) = \frac{i}{2\pi} \int_{\mathcal{C}} d\xi \; \partial_i\big((h' - \xi)^{-1} - (h - \xi)^{-1}\big) \tag{A.54}$$

in Eq. A.51, and observe again that:

$$\big|f_j(\omega, \boldsymbol{x})\big| \leq \frac{|\boldsymbol{x}|}{2\pi} \int_{\mathcal{C}} |d\xi| \; |\text{Im } \xi|^{-1+s} \big|\big((h' - \xi)^{-1} - (h - \xi)^{-1}\big)(\omega, \boldsymbol{x})\big|^s. \tag{A.55}$$

Using the resolvent identity, the condition $|\delta h(\omega, \boldsymbol{x})| \leq \overline{\delta h} \; \chi_R(\boldsymbol{x})$, and the generic inequality $|a1 + a_2 + \dots|^s \leq |a_1|^s + |a_2|^s \dots$, we can continue:

$$\dots \leq \frac{(\overline{\delta h})^s}{2\pi} |\boldsymbol{x}| \sum_{\boldsymbol{y}, \boldsymbol{z}} \chi_R(\boldsymbol{y} - \boldsymbol{z}) \int_{\mathcal{C}} |d\xi| \; |\text{Im } \xi|^{-1+s} \tag{A.56}$$
$$\times \big|(h' - \xi)^{-1}(\omega, \boldsymbol{y})\big|^s \big|(h - \xi)^{-1}(\mathsf{t}_{\boldsymbol{z}}^{-1}\omega, \boldsymbol{x} - \boldsymbol{z})\big|^s.$$

Then, from Eq. A.51 we obtain:

$$\mathcal{T}\Big(\big|\partial_i(p' - p)\big|^{2n}\Big) \leq \frac{(\overline{\delta h})^{2ns}}{(2\pi)^{2n}} \int_{\mathcal{C}} |d\xi_1| \; |\text{Im } \xi_1|^{-1+s} \dots \int_{\mathcal{C}} |d\xi_{2n}| \; |\text{Im } \xi_{2n}|^{-1+s}$$
$$\times \sum_{(\boldsymbol{x}_j, \boldsymbol{y}_j, \boldsymbol{z}_j)'s} \int_{\Omega} dP(\omega) \prod_{j=1}^{2n} |\boldsymbol{x}_{j-1} - \boldsymbol{x}_j| \chi_R(\boldsymbol{y}_j - \boldsymbol{z}_j) \tag{A.57}$$
$$\times \big|(h' - \xi_j)^{-1}(\mathsf{t}_{\boldsymbol{x}_j}^{-1}\omega, \boldsymbol{y}_j)\big|^s \big|(h - \xi_j)^{-1}(\mathsf{t}_{\boldsymbol{x}_j + \boldsymbol{z}_j}^{-1}\omega, \boldsymbol{x}_{j-1} - \boldsymbol{x}_j - \boldsymbol{z}_j)\big|^s.$$

Holder inequality enables us to continue as:

$$\ldots \leq \frac{(\overline{\delta h})^{2ns}}{(2\pi)^{2n}} \int_{\mathcal{C}} |d\xi_1| \; |\mathrm{Im}\; \xi_1|^{-1+s} \ldots \int_{\mathcal{C}} |d\xi_{2n}| \; |\mathrm{Im}\; \xi_{2n}|^{-1+s}$$

$$\times \sum_{(\boldsymbol{x}_j, \boldsymbol{y}_j, \boldsymbol{z}_j)'s} \prod_{j=1}^{2n} |\boldsymbol{x}_{j-1} - \boldsymbol{x}_j| \chi_R(\boldsymbol{y}_j - \boldsymbol{z}_j) \qquad (A.58)$$

$$\times \left[\int_{\Omega} dP(\omega) \; |(h' - \xi_j)^{-1} (\mathsf{t}_{\boldsymbol{x}_j}^{-1} \omega, \boldsymbol{y}_j)|^{4ns} \right]^{\frac{1}{4n}}$$

$$\times \left[\int_{\Omega} dP(\omega) |(h - \xi_j)^{-1} (\mathsf{t}_{\boldsymbol{x}_j + \boldsymbol{z}_j}^{-1} \omega, \boldsymbol{x}_{j-1} - \boldsymbol{x}_j - \boldsymbol{z}_j)|^{4ns} \right]^{\frac{1}{4n}}$$

If $s < \frac{1}{4n}$, then we can use the bound in Eq A.50 on the fractional powers of the resolvent, in which case:

$$\ldots \leq ct. \left(\overline{\delta h} \right)^{2ns} \sum_{(\boldsymbol{x}_j, \boldsymbol{y}_j, \boldsymbol{z}_j)'s} \prod_{j=1}^{2n} |\boldsymbol{x}_{j-1} - \boldsymbol{x}_j| \chi_R(\boldsymbol{y}_j - \boldsymbol{z}_j) e^{-s\beta(|\boldsymbol{y}_j| + |\boldsymbol{x}_{j-1} - \boldsymbol{x}_j - \boldsymbol{z}_j|)}, \quad (A.59)$$

and the remaining sums are evidently convergent. The statement follows. $Q.E.D.$

Bibliography

[1] M. Aizenman, "Localization at weak disorder: Some elementary bounds," *Rev. Math. Phys.*, vol. **Special Issue**, p. 1163, 1994.

[2] M. Aizenman, A. Elgart, S. Naboko, J. H. Schenker, and G. Stolz, "Moment analysis for localization in random schroedinger operators," *Invet. Math.*, vol. **163**, p. 343, 2006.

[3] M. Aizenman and G. M. Graf, "Localization bounds for an electron gas," *J. Phys. A: Math. Gen.*, vol. **31**, p. 6783, 1998.

[4] M. Aizenman and S. Molvhanov, "Localization at large disorder and extreme energies: an elementary derivation," *Comm. Math. Phys.*, vol. **157**, p. 245, 1993.

[5] Y. Ando, "Topological insulator materials," *J. Phys. Soc. Jpn.*, vol. **82**, p. 102001, 2013.

[6] J. E. Avron, L. Sadun, J. Segert, and B. Simon, "Chern numbers, quaternions, and berry's phases in fermi systems," *Comm. Math. Phys.*, vol. **124**, p. 595, 1989.

[7] J. Bellissard, *K-theory of C*-Algebras in solid state physics.* Springer-Verlag, 1986, vol. **257**, pp. 99–156.

[8] J. Bellissard, *Geometry and Topological Methods for Quantum Field Theory.* River Edge, NJ: World Sci. Publ., 2003.

[9] J. Bellissard, A. van Elst, and H. Schulz-Baldes, "The noncommuative geometry of the quantum hall effect," *J. Math. Phys.*, vol. **35**, p. 5373, 1994.

[10] B. A. Bernevig, T. L. Hughes, and S. C. Zhang, "Quantum spin hall effect and topological phase transition in hgte quantum wells," *Science*, vol. **314**, p. 1757, 2006.

[11] K. T. Chen and P. A. Lee, "Unified formalism for calculating polarization, magnetization, and more in a periodic insulator," *Phys. Rev. B*, vol. **84**, p. 205137, 2011.

[12] V. Chua and G. A. Fiete, "Exactly solvable topological chiral spin liquid with random exchange," *Phys. Rev. B*, vol. **84**, p. 195129, 2011.

[13] S. Coh, D. Vanderbilt, A. Malashevich, and I. Souza, "Chern-simons orbital magnetoelectric coupling in generic insulators," *Phys. Rev. B*, vol. **83**, p. 085108, 2011.

[14] A. Connes, "Non-commutative differential geometry," *Publications Mathematiques de l'I.H.E.S.*, vol. **62**, pp. 257–360, 1985.

[15] A. Connes, *Noncommutative Geometry.* Academic Press, San Diego, CA, 1994.

[16] A. Connes and H. Moscovici, "The local index formula in noncommutative geometry," *Geom. Funct. Anal.*, vol. **5**, p. 174, 1995.

[17] J. Dixmier, "Existence de traces non normales," *C. R. Acad. Schi. Paris*, vol. **262**, p. A1107, 1966.

[18] K. B. Efetov, "Statistics of the levels in small metallic particles," *Zh. Eksp. Teor. Fiz. 83, 833 (1982)*, vol. **83**, p. 833, 1982.

[19] K. B. Efetov, *Supersymmetry in Disorder and Chaos.* Cambridge University Press, Cambridge, UK, 1997.

[20] A. E. Essin and J. E. Moore, "Topological insulators beyond the brillouin zone via chern parity," *Phys. Rev. B*, vol. **76**, p. 165307, 2007.

[21] A. M. Essin, J. E. Moore, and D. Vanderbilt, "Magnetoelectric polarizability and axion electrodynamics in crystalline insulators," *Phys. Rev. Lett.*, vol. **102**, p. 146805, 2009.

[22] A. M. Essin, A. M. Turner, J. E. Moore, and D. Vanderbilt, "Orbital magnetoelectric coupling in band insulators," *Phys. Rev. B*, vol. **81**, p. 205104, 2010.

[23] W. Feng, D. Xiao, J. Ding, and Y. Yao, "Three-dimensional topological insulators in i-iii-vi$_2$ and ii-iv-v$_2$ chalcopyrite semiconductors," *Phys. Rev. Lett.*, vol. **106**, p. 016402, 2011.

[24] W. Feng, D. Xiao, Y. Zhang, and Y. Yao, "Half-heusler topological insulators: A first-principles study with the tran-blaha modified becke-johnson density functional," *Phys. Rev. B*, vol. **82**, p. 235121, 2010.

[25] M. Fiebig, "Revival of the magnetoelectric effect," *J. Phys. D: Appl. Phys.*, vol. **38**, pp. R123–R152, 2005.

[26] L. Fu and C. L. Kane, "Time reversal polarization and a z$_2$ adiabatic spin pump," *Phys. Rev. B*, vol. **74**, p. 195312, 2006.

[27] L. Fu and C. L. Kane, "Topological insulators with inversion symmetry," *Phys. Rev. B*, vol. **76**, p. 045302, 2007.

[28] L. Fu, C. L. Kane, and E. J. Mele, "Topological insulators in three dimensions," *Phys. Rev. Lett.*, vol. **98**, p. 106803, 2007.

[29] T. Fukui, Y. Hatsugai, and H. Suzuki, "Chern numbers in discretized brillouin zone: Efficient method of computing (spin) hall conductances," *J. Phys. Soc. Jpn.*, vol. **74**, p. 1674, 2005.

[30] I. C. Fulga, F. Hassler, and A. R. Akhmerov, "Scattering theory of topological insulators and superconductors," *Phys. Rev. B*, vol. **85**, p. 165409, 2012.

[31] C. Gonzalez-Ballestero, L. M. Robledo, and G. F. Bertsch, "Numeric and symbolic evaluation of the pfaffian of general skew-symmetric matrices," *Computer Physics Communications*, vol. **182**, p. 2213, 2011.

[32] G. W. Groth, M. Wimmer, A. R. Akhmerov, J. Tworzydlo, and C. W. J. Beenakker, "Theory of the topological anderson insulator," *Phys. Rev. Lett.*, vol. **103**, p. 196805, 2009.

[33] H. M. Guo, "Topological invariant in three-dimensional band insulators with disorder," *Phys. Rev. B*, vol. **82**, p. 115122, 2010.

[34] H. M. Guo, G. Rosenberg, G. Refael, and M. Franz, "Topological anderson insulator in three dimensions," *Phys. Rev. Lett.*, vol. **105**, p. 216601, 2010.

[35] D. Haldane, "Model for a quantum hall effect without landau levels: condensed-matter realization of the parity anomaly," *Phys. Rev. Lett.*, vol. **61**, p. 2015, 1988.

[36] B. I. Halperin, "Quantized hall conductance, current-carrying edge states, and the existence of extended states in a two-dimensional disordered potential," *Phys. Rev. B*, vol. **25**, p. 2185, 1982.

[37] M. Z. Hasan and C. L. Kane, "Colloquium: topological insulators," *Rev. Mod. Phys.*, vol. **82**, p. 3045, 2010.

[38] M. Z. Hasan and J. E. Moore, "Three-dimensional topological insulators," *Ann. Rev. Cond. Mat. Phys.*, vol. **2**, p. 55, 2011.

[39] M. B. Hastings and T. A. Loring, "Topological insulators and c*-algebras: Theory and numerical practice," *Ann. Phys.*, vol. **326**, p. 1699, 2011.

[40] I. Hatsugai, "Quantized berry phases for a local characterization of spin liquids in frustrated spin systems," *J. Phys.: Condens. Matter.*, vol. **19**, p. 145209, 2007.

[41] T. Highes, E. Prodan, and B. A. Bernevig, "Inversion-symmetric topological insulators," *Phys. Rev. B*, vol. **83**, p. 245132, 2011.

[42] D. Hsieh, D. Qian, L. Wray, Y. Xia, Y. S. Hor, R. J. Cava, and M. Z. Hasan, "A topological dirac insulator in a quantum spin hall phase," *Nature*, vol. **452**, p. 970, 2008.

[43] H. Jiang, L. Wang, Q. F. Sun, and X. C. Xie, "Numerical study of the topological anderson insulator in hgte/cdte quantum wells," *Phys. Rev. B*, vol. **80**, p. 165316, 2009.

[44] C. L. Kane and E. Mele, "Quantum spin hall effect in graphene," *Phys. Rev. Lett.*, vol. **95**, p. 226801, 2005.

[45] C. L. Kane and E. Mele, "Z_2 topological order and the quantum spin hall effect," *Phys. Rev. Lett.*, vol. **95**, p. 146802, 2005.

[46] R. D. King-Smith and D. Vanderbilt, "Theory of polarization of crystalline solids," *Phys. Rev. B*, vol. **47**, p. 1651, 1993.

[47] A. Kitaev, "Periodic table for topological insulators and superconductors," *AIP Conf. Proc.*, vol. **1134**, p. 22, 2009.

[48] S. Kivelson, D. H. Lee, and S. C. Zhang, "Global phase diagram in the quantum hall effect," *Phys. Rev. B*, vol. **46**, p. 2223, 1992.

[49] K. Klitzing, G. Dorda, and M. Pepper, "New method for high-accuracy determination of the fine-structure constant based on quantized hall resistance," *Phys. Rev. Lett.*, vol. **45**, p. 494, 1980.

[50] M. Koenig, S. Wiedmann, C. Bruene, A. Roth, H. Buhmann, L. W. Molenkamp, X. L. Qi, and S. C. Zhang, "Quantum spin hall insulator state in hgte quantum wells," *Science*, vol. **318**, p. 766, 2007.

[51] H. Kosaki, "Applications of the complex interpolation method to a von neumann algebra: Non-commutative l^p-spaces," *J. Func. Analysis*, vol. **59**, p. 123, 1984.

[52] R. B. Laughlin, "Levitation of extended-state bands in a strong magnetic field," *Phys. Rev. Lett.*, vol. **52**, p. 2304, 1984.

[53] B. Leung and E. Prodan, "Effect of strong disorder in a three-dimensional topological insulator: Phase diagram and maps of the z$_2$ invariant," *Phys. Rev. B*, vol. **85**, p. 205136, 2012.

[54] B. Leung and E. Prodan, "A non-commutative formula for the isotropic magneto-electric response," *J. Phys. A: Math. Theor.*, vol. **46**, p. 085205, 2013.

[55] J. Li, R. L. Chu, J. K. Jain, and S. Q. Shen, "Topological anderson insulator," *Phys. Rev. Lett.*, vol. **102**, p. 136806, 2009.

[56] R. Li, J. Wang, X. L. Qi, and S. C. Zhang, "Dynamical axion field in topological magnetic insulators," *Nature Phys.*, vol. **6**, pp. 284–288, 2010.

[57] C. X. Liu, X. L. Qi, H. Zhang, X. Dai, Z. Fang, and S. C. Zhang, "Model hamiltonian for topological insulators," *Phys. Rev. B*, vol. **82**, p. 045122, 2010.

[58] T. A. Loring and M. B. Hastings, "Disordered topological insulators via c*-algebras," *Europhys. Lett.*, vol. **92**, p. 67004, 2010.

[59] A. Malashevich, I. Souza, S. Coh, and D. Vanderbilt, "Theory of orbital magnetoelectric response," *New J. Phys.*, vol. **12**, p. 053032, 2010.

[60] J. E. Moore and L. Balents, "Topological invariants of time-reversal-invariant band structures," *Phys. Rev. B*, vol. **75**, p. 121306, 2007.

[61] M. Nakahara, *Geometry, Topology and Physics.* Taylor & Francis, 2003.

[62] G. Nenciu, "Linear adiabatic theory. exponential estimates," *Comm. Math. Phys.*, vol. **152**, p. 479, 1993.

[63] Q. Niu, D. J. Thouless, and Y. S. Wu, "Quantized hall conductance as a topological invariant," *Phys. Rev. B*, vol. **31**, p. 3372, 1985.

[64] H. Obuse, A. Furusaki, S. Ryu, and C. Mudry, "Two-dimensional spin-filtered chiral network model for the z_2 quantum spin-hall effect," *Phys. Rev. B*, vol. **76**, p. 075301, 2007.

[65] H. Obuse, A. Furusaki, S. Ryu, and C. Mudry, "Boundary criticality at the anderson transition between a metal and a quantum spin hall insulator in two dimensions," *Phys. Rev. B*, vol. **78**, p. 115301, 2008.

[66] M. Onoda, Y. Avishai, and N. Nagaosa, "Localization in a quantum spin hall system," *Phys. Rev. Lett.*, vol. **98**, p. 076802, 2007.

[67] G. Panati, H. Spohn, and S. Teufel, "Effective dynamics for bloch electrons: Peierls substitution and beyond," *Commun. Math. Phys.*, vol. **242**, p. 547, 2003.

[68] R. E. Peierls, "Zur theorie des diamagnetismus von leitungelectronen," *Z. fur Phys.*, vol. **80**, p. 763, 1933.

[69] R. E. Prange and S. M. Girvin, *The quantum Hall effect.* Springer-Verlag, 1987.

[70] E. Prodan, *In preparation.*

[71] E. Prodan, "Robustness of the spin-chern number," *Phys. Rev. B*, vol. **80**, p. 125327, 2009.

[72] E. Prodan, "Topological quantization of ensemble averages," *J. Phys. A: Math. Theor.*, vol. **42**, p. 065207, 2009.

[73] E. Prodan, "Disordered topological insulators: a non-commutative geometry perspective," *J. Phys. A: Math. Theor.*, vol. **44**, p. 113001, 2011.

[74] E. Prodan, "Manifestly gauge-independent formulations of the z_2 invariants," *Phys. Rev. B*, vol. **83**, p. 235115, 2011.

[75] E. Prodan, "Three-dimensional phase diagram of disordered hgte/cdte quantum spin-hall wells," *Phys. Rev. B*, vol. **83**, p. 195119, 2011.

[76] E. Prodan, "Quantum transport in disordered systems under magnetic fields: A study based on operator algebras," *Appl. Math. Res. Express*, vol. **abs017**, 2012.

[77] E. Prodan, T. L. Hughes, and B. A. Bernevig, "Entanglement spectrum of a disordered topological chern insulator," *Phys. Rev. Lett.*, vol. **105**, p. 115501, 2010.

[78] E. Prodan, B. Leung, and J. Bellissard, "The noncommutative n^{th} chern number," *arXiv:1305.2425 (2013).*

[79] X. L. Qi, T. L. Hughes, and S. C. Zhang, "Topological field theory of time-reversal invariant insulators," *Phys. Rev. B*, vol. **78**, p. 195424, 2008.

[80] X. L. Qi and S. C. Zhang, "The quantum spin hall effect and topological insulators," *Physics Today*, vol. **63**, p. 33, 2010.

[81] X. L. Qi and S. C. Zhang, "Topological insulators and superconductors," *Rev. Mod. Phys.*, vol. **83**, p. 1057, 2011.

[82] R. Rammal and J. Bellissard, "An algebraic semiclassical approach to bloch electrons in a magnetic field," *J. Phys. France*, vol. **51**, p. 1803, 1990.

[83] R. Resta, "Quantization of particle transport," *Ferroelectrics*, vol. **136**, p. 51, 1992.

[84] M. J. Rice and E. J. Mele, "Elementary excitations of a linearly conjugated diatomic polymer," *Phys. Rev. Lett.*, vol. **49**, p. 1455, 1982.

[85] T. Richter and H. Schulz-Baldes, "Homotopy arguments for quantized hall conductivity," *J. Math. Phys.*, vol. **42**, p. 3439, 2001.

[86] Z. Ringel and E. Kraus, "Determining topological order from a local ground-state correlation function," *Phys. Rev. B*, vol. **83**, p. 245115, 2011.

[87] S. Roche, "Quantum transport by means of o(n) real-space methods," *Phys. Rev. B*, vol. **59**, p. 2284, 1999.

[88] R. Roy, "Topological phases and the quantum spin hall effect in three dimensions," *Phys. Rev. B*, vol. **79**, p. 195322, 2009.

[89] S. Ryu, J. Moore, and A. W. W. Ludwig, "Electromagnetic and gravitational responses and anomalies in topological insulators and superconductors," *Phys. Rev. B.*, vol. **85**, p. 045105, 2012.

[90] A. P. Schnyder, S. Ryu, A. Furusaki, and A. W. W. Ludwig, "Classification of topological insulators and superconductors in three spatial dimensions," *Phys. Rev. B.*, vol. **78**, p. 195125, 2008.

[91] H. Schulz-Baldes and S. Teufel, "Orbital polarization and magnetization for independent particles in disordered media," *Comm. Math. Phys.*, vol. **157**, p. 649, 2012.

[92] I. E. Segal, "A non-commutative extension of abstract integration," *Ann. Math.*, vol. **57**, p. 401, 1953.

[93] D. N. Sheng, Z. C. Gu, K. Sun, and L. Sheng, "Fractional quantum hall effect in the absence of landau levels," *Nature Comm.*, vol. **2**, p. 389, 2011.

[94] D. N. Sheng, Z. Y. Weng, L. Sheng, and F. D. M. Haldane, "Quantum spin-hall effect and topologically invariant chern numbers," *Phys. Rev. Lett.*, vol. **97**, p. 036808, 2006.

[95] H. Shulman and E. Prodan, "Robust extended states in a topological bulk model with even spin-chern invariant," *arXiv:1011.5456 (2010)*.

[96] A. Soluyanov and D. Vanderbilt, "Computing topological invariants without inversion symmetry," *Phys. Rev. B*, vol. **83**, p. 235401, 2011.

[97] A. Soluyanov and D. Vanderbilt, "Wannier representation of z_2 topological insulators," *Phys. Rev. B*, vol. **83**, p. 035108, 2011.

[98] J. Song, B. Leung, I. Mondragon-Shem, T. Hughes, and E. Prodan, "Does quantized polarization imply extended states under disorder?" *In preparation.*

[99] N. A. Spaldin and M. Fiebig, "The renaissance of magnetoelectric multiferroics," *Science*, vol. **309**, p. 391, 2005.

[100] W. P. Su, J. R. Schrieffer, and A. J. Heeger, "Solitons in polyacetylene," *Phys. Rev. Lett.*, vol. **42**, p. 1698, 1979.

[101] D. J. Thouless, "Quantization of particle transport," *Phys. Rev. B*, vol. **27**, p. 6083, 1983.

[102] D. J. Thouless, "Theory of the electric polarization in crystals," *Phys. Rev. B*, vol. **27**, p. 6083, 1983.

[103] D. J. Thouless, M. Kohmoto, M. P. Nightingale, and M. den Nijs, "Quantized hall conductance in a two-dimensional periodic potential," *Phys. Rev. Lett.*, vol. **49**, p. 405, 1982.

[104] A. M. Turner, Y. Zhang, R. S. K. Mong, and A. Vishwanath, "Quantized response and topology of magnetic insulators with inversion symmetry," *Phys. Rev. B*, vol. **85**, p. 165120, 2012.

[105] M. Wada, S. Murakami, F. Freimuth, and G. Bihlmayer, "Localized edge states in two-dimensional topological insulators: Ultrathin bi films," *Phys. Rev. B*, vol. **83**, p. 121310, 2011.

[106] Z. Wang, X. L. Qi, and S. C. Zhang, "Equivalent topological invariants of topological insulators," *New J. Phys.*, vol. **12**, p. 065007, 2010.

[107] D. Xiao, Y. Yao, W. Feng, J. Wen, W. Zhu, X. Q. Chen, G. M. Stocks, and Z. Zhang, "Half-heusler compounds as a new class of three-dimensional topological insulators," *Phys. Rev. Lett.*, vol. **105**, p. 096404, 2010.

[108] Z. Xu, L. Sheng, D. Y. Xing, E. Prodan, and D. N. Sheng, "Topologically protected extended states in disordered quantum spin-hall systems without time-reversal symmetry," *Phys. Rev. B*, vol. **85**, p. 075115, 2012.

[109] Y. Xue and E. Prodan, "Noncommutative kubo formula: Applications to transport in disordered topological insulators with and without magnetic fields," *Phys. Rev. B*, vol. **86**, p. 155445, 2012.

[110] A. Yamakage, K. Nomura, K. I. Imura, and Y. Kuramoto, "Disorder-induced multiple transition involving z_2 topological insulator," *J. Phys. Soc. Jpn.*, vol. **80**, p. 053703, 2011.

[111] K. Yang and R. N. Bhatt, "Quantum hall insulator transitions in lattice models with strong disorder," *Phys. Rev. B*, vol. **59**, p. 8144, 1999.

[112] R. Yu, X. L. Qi, A. Bernevig, Z. Fang, and X. Dai, "Equivalent expression of z_2 topological invariant for band insulators using the non-abelian berry connection," *Phys. Rev. B*, vol. **84**, p. 075119, 2011.